Μελέτη της κινητικής ενέργειας σκεδαζόμενων ηλεκτρονίων παραγόμενα από ασύμμετρο παλμό λέιζερ.

Αθανασόπουλος Αθανάσιος

ΠΑΝΕΠΙΣΤΗΜΙΟ ΙΩΑΝΝΙΝΩΝ

Υπο την επίβλεψη του επίκουρου καθηγητή *Σοφικίτη Δημήτριου*

2021

Περίληψη

Όταν ένας ισχυρός παλμός λέιζερ ιονίζει ένα άτομο ή ένα μόριο, το απελευθερωμένο ηλεκτρόνιο μπορεί να οδηγηθεί πίσω στο πατρικό ιόν λόγω της αλληλεπίδρασης του με το ηλεκτρικό πεδίο του παλμού. Όταν το ηλεκτρόνιο επιστρέφει στον πυρήνα του ιόντος, μπορεί να αλληλεπιδράσει μαζί του σε μια διαδικασία γνωστή ως επανασκέδαση ηλεκτρονίων (electron rescattering). Μελετάμε την κινητική ενέργεια του ηλεκτρονίου που παράγεται από έναν ισχυρό, ασύμμετρο παλμό $\omega/2\omega$ τη στιγμή της επανασκέδασης. Η κινητική ενέργεια των επιστρεφόμενων ηλεκτρονίων είναι συνάρτηση των παραμέτρων του ασύμμετρου παλμού, δηλαδή του λόγου των πλατών των ηλεκτρικών πεδίων $\omega/2\omega$ (παράμετρος γ) και της σχετικής φάσης τους (παράμετρος φ). Βρίσκουμε συνθήκες για τις οποίες τα περισσότερα από τα ηλεκτρόνια που επιστρέφουν στον πυρήνα των ιόντων έχουν παρόμοιες κινητικές ενέργειες, δημιουργώντας έτσι ένα μονοχρωματικό φάσμα για την κινητική ενέργεια αυτών των επανασκεδαζόμενων ηλεκτρονίων. Εξερευνούμε την εφαρμογή αυτών των μονοχρωματικών ηλεκτρονίων στη δημιουργία υψηλών αρμονικών (High-Harmonic-Generation) και βρίσκουμε παρόμοια μονοχρωματικότητα στο φάσμα των υψηλών αρμονικών. Αυτά τα μονοχρωματικά επανασκεδαζόμενα ηλεκτρόνια μπορούν να βρουν ένα ευρύ φάσμα εφαρμογής σε διαδικασίες όπως η παραγωγή υψηλών αρμονικών, ο μη-διαδοχικός διπλός ιονισμός (non-sequential double ionization) και άλλες.

Abstract

When a strong laser pulse ionizes an atom or molecule, the ejected electron can be driven back to the ion due to the interaction with the electric field of the pulse. When the electron returns to the ion core, it can interact with it, in a process known as electron rescattering. We study the kinetic energy of the electron generated by a strong, asymmetric, $\omega/2\omega$ pulse at the moment of rescattering. The kinetic energy is a function of the asymmetric pulse parameters, namely the ratio of the $\omega/2\omega$ electric field amplitudes (γ parameter) and their relative phase (φ parameter). We find conditions for which most of the electrons return to the ion core with similar kinetic energies, thus generating a monochromatic spectrum for the kinetic energy of these rescattering electrons. We explore the application of these monochromatic electrons in the generation of high harmonics and find a similar monochromaticity in the high-harmonic spectrum. These monochromatic rescattering electrons can find a wide range of application in processes like high harmonic generation, non-sequential double ionization and more.

Contents

1 Introduction **5**

1.1 The Keldysh parameter 6

1.1.1 Simple man's model 9

1.1.2 The context of this thesis 10

2 Tunnelling ionization of atoms **13**

2.1 A.D.K. theory of tunneling ionization 13

2.1.1 Brief description of the derivation of the $A.D.K.$ formula 14

2.1.2 Over the barrier ionization 20

3 Propagation of the electron in an oscillating electric field **22**

3.1 Dynamics of one colour field 23

3.1.1 Equations of motion 23

3.1.2 Kinetic energy of the returning electrons 24

3.1.3 Calculation of the Kinetic energy of the Returning/rescattering electrons 26

3.1.4 Kinetic energy distribution of the returning electrons, $E.D.R.E.$ 29

3.2 Dynamics in a two-colour field 34

3.2.1 Equations of motion and cycle average kinetic energy 34

3.2.2 Kinetic energy and of the returning electrons and $E.D.R.E.$ 36

3.2.3 Optimization for generation of the narrowest kinetic energy distribution of the returning electrons distribution 39

3.2.4 Advantages and robustness of the optimized fields 44

3.2.5 From continuous waves to pulses 47

4 High (-order) Harmonic Generation **52**

4.1 HHG theory 53

4.1.1 *Strong Field Approximation* (SFA) 54

4.1.2 Time dependent-dipole moment 55

4.1.3 Expansion of the time dependent dipole moment as a *Fourier series* 58

4.1.4 Relation to the simple man's model 58

4.2 Generation of spectra with the use of Lewenstein's model 59

4.2.1 Simple sinusoidal field 60

4.2.2 $\omega/2\omega$ asymmetric pulse 61

4.2.3 Energy density of the returning electrons in the high harmonics generation spectra and the modified semiclassical cutoff law 62

4.3 Phases of the Harmonic Component 65

5 Conclusions **73**
5.1 Deformation of the initial wavefunction of a particle 74
5.2 Volkov states 75
5.3 Saddle Point Approximation 77
5.4 Construction of the discrete dipole function 77
5.4.1 High (order) harmonic generation with the use of hydrogen like wavefunctions 78

Bibliography **80**

Chapter 1

Introduction

Quantum mechanics is one of the most successful theories ever created and it provides a description of the physical phenomena at the scale of atoms and subatomic particles. It is a theory in which the energy comes in small packages, *quanta*, and where the *wave–particle duality* (the fact that every particle or "quantum entity" may be described as either a particle or a wave) is embedded in it.

The idea that the energy is *quantized*, was something that revolutionized our view about nature. More specifically, the idea of the existence of quanta of light was introduced by *A. Einstein*, in his first paper "Lichquanten" in *"Annalen der Physik"* in the year of 1905. In the same paper, *Einstein* mentioned that when strong radiating fields are interacting with atoms (and molecules), a single- and a multi-photon absorption may occur. But in order for this idea to be tested in the laboratory, the invention of the first laser in 1960 by *T. H. Maiman* at Hughes Research Laboratories (based on theoretical work by *C. H. Townes* and *A. L. Schawlow*[1]), had to be made. After five years from its invention, in the year 1965, the first experimental observation of the multi-photon absorption phenomenon was recorded by *Voronov* and *Delone*[2].

The wave-particle duality of matter is another very interesting aspect of quantum mechanics. It is a property of nature which makes the "*Quantum tunneling*" phenomenon possible. The Quantum tunneling phenomenon was first noticed theoretically in the late 30s by *F. Hund* and it describes a particle which propagates through a potential barrier. Combining the Quantum tunneling phenomenon and the fact that the high intensity light sources existed and could be used, the physicists of the day (around the 60s) introduced the idea of the *quantum tunneling ionization* phenomenon, in which the interaction of a system with an externally applied electric field would result in the liberation of an (initially bounded) electron.

Initially the fate of the liberated electron was never put in question, but three decades later, in the year 1993 *P. B. Corkum* took the idea of the tunneling ionization on the next step and introduced the "*Simple man's model*". A model which would qualitatively explain a wide variety of phenomena that make their appearance in intense electromagnetic fields, by examining the trajectories of those liberated electrons; some of which would return to the parent ion and interact with it (rescattering electrons). His model was used to qualitatively describe a wide range of phenomena from the production rate of doubly charged ions to the *generation of high-(order)-harmonics.*

The first observation of high harmonic generation was reported by *Burnett et al* [14] in the year 1977, where they investigated the interaction of intense CO_2 laser pulses with plasma generated from solid targets. The generation of high order harmonics is also accompanied with a surprising result. High harmonics were found to decrease in intensity at low orders, as expected, but then were observed to form a plateau, with the intensity of the harmonics remaining approximately constant over many orders. The first

[1]For more information: `https://www.aps.org/publications/apsnews/200312/history.cfm`

[2]Voronov, G. S. and Delone, N. B. [1965], 'Ionization of xenon atom by the electric field of ruby laser emission', Soviet Physics JETP 23(1), 66–68.

record of this characteristic of the high harmonics was recorded by *Huillier et al* [13] in 1989.

In general, since the invention of lasers, the interaction of high intensity electromagnetic radiation with matter became and still is a subject of great interest. Initially only one-colour fields were being studied but since the very beginning of the millennium the use of high intensity two-colour, asymmetric fields started taking their turn. The spatial asymmetry of the electromagnetic field profile is achieved by the combination of the fundamental and (in most cases) the second harmonic of the light source.

These asymmetric fields can be used for excitation of atoms to some particular atomic state as well as the production of atomic ions via the rescattering electrons; the selective dissociation of some molecular bonds [11, 12], controlling their electronic density, etc. Furthermore, with the dynamics of the rescattering electrons asymmetric pulses could be used for studying the scattering of electrons by positively charged atomic and molecular ions to record the corresponding differential and total, elastic (*electron diffraction* phenomenon) and inelastic cross sections (resulting in excitations or even in ionizations).

In the course of this thesis the dynamics of the rescattering electrons generated by asymmetric continuous waves and pulses were studied. The study of the dynamics of the rescattering electrons, necessitates the good understanding of the tunneling ionization theory and can used for the prediction of the production rate of doubly charges ions via the *sequential* and *non sequential double ionization* processes, as well as the generation of high order harmonics. Based on the understanding of these processes, this text was written with the hope of also being used as a good introduction material for the physics behind the phenomenon of high order harmonics generation.

To make every step in understanding this phenomenon clear, the most important characteristics of the tunneling ionization theory will be explained and emphasized, the trajectories of the liberated and (afterwards) propagating electrons will be "drawn" and their form will be clarified both qualitatively and quantitatively. For the qualitative description of the problem, some fundamental concepts from classical physics will be described, while for its quantitative description the steps of the procedure for attaining the results will be listed and explained and described. Moreover, in order for the results to be independent from the intensity of the external light source some new "units of measurement" will be presented. Finally, in Chapter 4 I will introduce a "rule of thumb" regarding the form of the spectra of the high order harmonic generations.

Last but not least, an "optimized" two colour field will be presented (or perhaps proposed) that (at least theoretically) presents some very interesting characteristics for some of the "rescattering" phenomena. These characteristics were found to be general and robust. Changing the parameters of problem slightly does not alter significantly the rescattering results. Throughout this text, the characteristics of the "optimized" fields will be presented and the reason behind their existence will also thoroughly be explained.

1.1 The Keldysh parameter

In laser ionization of atoms and molecules, there are two regimes: the semi-static regime and the multi-photon regime. In the multi-photon regime, the amplitude of the electromagnetic field is low enough so that the main cause of the ionization of the system is the effective combination of the energies of several photons. This case is schematically shown in Fig. 1.1. In this figure, the blue curve shows the potential energy of an electron in a Hydrogen atom, the horizontal lines depict the energy levels at which the electron is transferred to after the absorption of a number of photons (black arrows[3]) and the black horizontal line depicts the

[3]In this figure, the black arrows have deliberately not been drawn on the same vertical line. This is because as the electron energy level is increased, its mean distance from the nucleus is also increased.

energy level which separates the bound from the continuum eigenstates. The energy of each photon is much smaller than the ionization threshold of the system, and it is the successive absorption of photons[4] which transfer an initially bound electron (lowest red line) to the continuum. In this figure, the ionization energy of the system is equal with five times the energy of the photons.

In the semi-static regime, the laser intensity is even higher and the energy of the photons are still lower than the binding energy of the system. Under the influence of the strong electric field, the potential barrier of the system is drastically distorted to such extent that an electron has an important probability to propagate through or above the system's barrier. Shown in Fig. 1.2. In this figure, the orange and blue line depict the potential energy of the electron due to its interaction with the Coulomb and laser field respectively. The green line depicts the sum of these two potential energy factors. The green line shows that the potential energy is increased on the "left" and is decreased on the "right" side of the nucleus. The great values of the potential energy on the left result in the exponential decreasing form of the wavefunction of the electron (red line), while the potential energy scheme enables the propagation of the initially bound electron through or above the system's potential barrier. Assuming that the energy of the electron is less than the local maximum value of the potential energy, this is achieved by quantum tunnelling phenomenon which is characterised by the exponentially decreasing form of the wavefunction (see Fig. 1.2). When an electron manages to propagate through the system's potential barrier, then we are talking about the *Tunnelling Ionization* subregion. On the contrary if the amplitude of the electric field is strong enough or the energy level on which the electron was initially sitting on is high enough, the tunnelling barrier falls below electron's energy level, allowing it to escape over the barrier. This case is referred to in the literature as the *Over the Barrier Ionization* subregion.

In both of these two subregions, the electromagnetic fields are characterized by the not exceedingly fast rate of change of the fields' amplitude with respect to time. In general, in the *Tunneling Ionization* subregion, the rate of change of the potential barrier must be slow, so that the electron's "trajectory" through the barrier cannot be "delayed or interrupted", while on the later case, the slow variation of the potential barrier ensures that the electron's form of action can be adequately described by just one of the preciously mentioned subregions.

In order to make a distinction of the two aforementioned regions, the *Keldysh* parameter is

[4]The probability of such a phenomenon taking place is rapidly decreasing with the number of photons required.

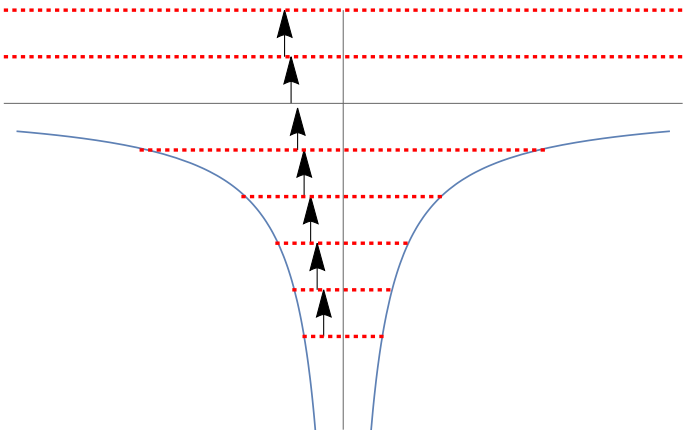

Figure 1.1: Qualitative scheme of the multi-photon ionization process. The initially bound electron is liberated by the absorption of many photons. The probability of such a process decreases as the number of photons that are needed is increased. Note that the black arrows have not been drawn on the same vertical line deliberately. As the energy of the electron is increased, its mean value of its distance from the nucleus is also increased.

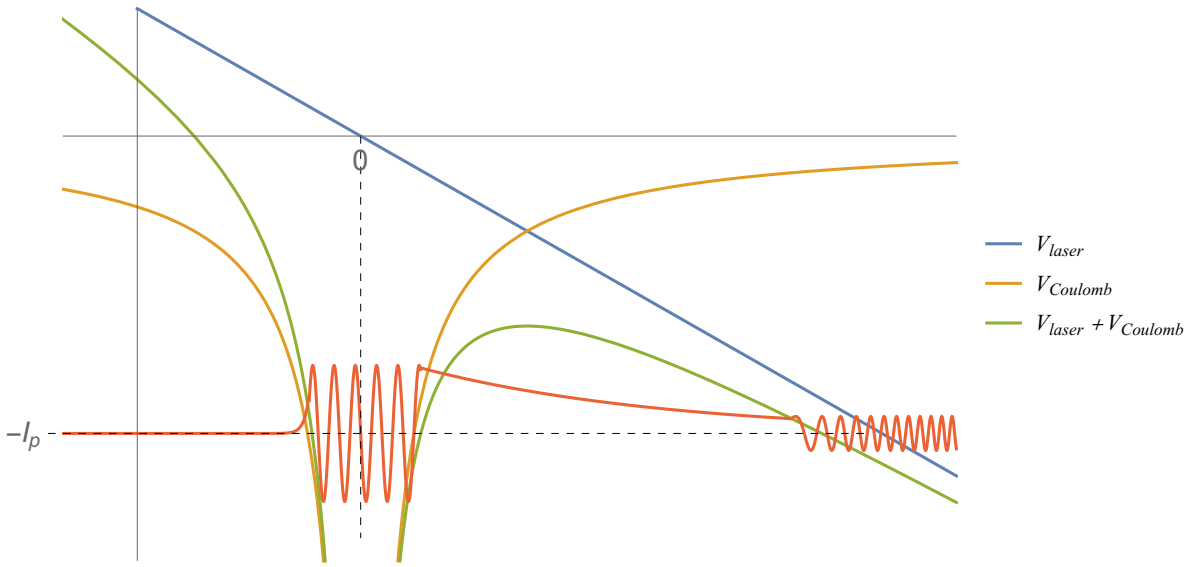

Figure 1.2: Qualitative potential energy scheme. The orange and blue line depict the potential energy of the electron due to its interaction with the parent ion and laser field respectively, whereas the green line depicts the sum of these two potential energy factors. The red line depicts the qualitative picture of the electron's wave-function. Due to the monotonically increasing form of the potential energy on the left, the wavefunction is exponentially decreasing with respect to the distance from its centre. On the contrary, on the right hand side, the potential energy of the electron has a local maximum value. This characteristic enables the facilitated pass of the electron through (quantum tunnelling) or above the barrier.

used.

$$\gamma_k = \sqrt{\frac{2m_e I_p \omega^2}{q^2 \mathcal{E}^2}}, \tag{1.1}$$

which depends on the characteristic and on the parameters of the system: field strength $\mathcal{E}$, frequency of the laser ω as well as the ionization energy of the atomic or molecular system I_p. The Keldysh parameter can be derived and translated into a physical, intuitive picture via the following consideration.

Consider the case of a sinusoidal laser with time period T_{period}. The difficulty in which the electron manages to pass through the potential barrier can be expressed as the ratio between the equivalent classical time it takes for the electron to tunnel through the potential barrier $T_{tunneling}$(classical time of flight of an electron through a potential barrier), divided by half of the laser cycle, $T_{laser}/2$. The devision is carried out with half the laser period because only during half a cycle, the potential barrier is being bent down since during the other half of a cycle, the potential barrier is being fortified

$$\gamma_k \equiv \frac{T_{tunneling}}{\frac{1}{2}T_{laser}} \sim 2\frac{L_{tunneling}/\langle u \rangle}{T_{laser}}, \tag{1.2}$$

where $L_{tunneling}$ is the distance the electron has to cross under the barrier in order to be liberated and $\langle u \rangle$ is the mean value of the electron's velocity under the barrier. This ratio is a measure of how fast the barrier oscillates compared to the time it takes for the electron to tunnel ionize.

It is assumed that the electron in the classical Coulomb potential well moves back and forth along the width of the barrier with a kinetic energy equal to the binding energy, I_p, before the external field is applied. The $L_{tunneling}$ can vaguely be set to be the distance for which the work due to the Coulomb force F_C is equal with the ionization energy $F_C L_{tunneling} = q\mathcal{E}L_{tunneling} \sim I_p$, while the mean velocity of the

electron can also vaguely be set to be determined from its maximum kinetic energy, $\langle u \rangle^2 \sim 2I_p/m_e$. Under these considerations, the Keldysh parameter is brought to the final form:

$$\gamma_k = \frac{T_{tunneling}}{\frac{1}{2}T_{laser}} \sim \sqrt{\frac{2m_e I_p}{q^2\mathcal{E}^2}} \frac{1}{T_{laser}} \sim \sqrt{\frac{2m_e I_p \omega^2}{q^2\mathcal{E}^2}} \tag{1.3}$$

In the limiting cases where $\gamma_k \gg 1$ or $\gamma_k \ll 1$, the ionization of the system is accurately characterized by the photoionization processes and by the effect of the electric field, respectively. These can be understood with respect to the tunnelling time. The former case, at high laser frequencies and low intensities, the tunnelling time is larger than the laser period, so that the electric field's direction will change while a propagating electron is still confined within the barrier. The direction towards which the electron was initially heading to, has now been inverted. Therefore, tunnel ionization is completely suppressed and the ionization of the system can be achieved only via the absorption of multiple photons. It should be noted that *Ilkov et al.* [2] have found that the condition $\gamma_k < 0.5$ is necessary for the tunnelling process to be dominant. In the intermediate region $\gamma \approx 1$, both the tunnelling and multi-photon processes contribute to the ionization.

For the subsequent parts of this thesis, it is important to note that in strong field theory, there is another widely used quantity which in the literature is referred to as the *ponderomotive energy*, U_p and it corresponds to the cycle-averaged oscillatory energy of the charged particle in an oscillating electromagnetic field. The ponderomotive energy depends on the square of the wavelength, is linearly dependent on the intensity $\mathcal{I}$ and in the simplest case of a-one-colour field, it takes the form

$$U_p \equiv \langle K_{osc} \rangle = \frac{q^2\mathcal{E}^2}{4m\omega^2} \approx 9.33 \times 10^{-14} \mathcal{I}(W/cm^2)\lambda^2(\mu m), \tag{1.4}$$

and so, by using eqs. (1.3), (1.4) the Keldysh parameter can be written as

$$\gamma_k = \sqrt{\frac{I_p}{2U_p}}. \tag{1.5}$$

1.1.1 Simple man's model

In the early 1980s, there were some experimental results regarding the production rate of doubly charged ions, that failed to be accurately described by models which considered the first and second ionization events to take place independently. Such a process is known in the literature as the sequential double ionization. In these models, both events were thought to be occurring due to the distorted potential surface of the system by the electric field. However, approaching the problem in this manner, resulted in the underestimation of the production rate by nearly 2 orders of magnitude.

In 1993 a new process was proposed by *P. B. Corkum* [4] in order to explain these results. The main difference from most models used at the time, was that the liberation of the second electron from the system is dependent on the emission of the first one, the so called *non-sequential double ionization N.S.D.I.*. In this work, a simple model was introduced which is referred to in the literature as the *simple man's model* or *the three step model*.

The simple man's model conveys an intuitive understanding of interpreting and explaining the experimental results of not only the production rate of doubly charged ions but also of various other phenomena that make their appearance in intense electromagnetic fields. In Fig. 1.3, the simple man's

model is being depicted. In it, I_p denotes the ionization energy of the system and the blue vertical lines depicts the gain energy of the electron after the process described in this model has finished. The relevant dynamics of this model can be broken down in a three step process:

1. **First the system is ionized by the field.** This is achieved by the tunnelling effect. In an intense electric field, the drastically distorted potential barrier of the system leads to the facilitated pass of an electron through or above the system's potential barrier and its escape from it (second panel of Fig. 1.3). By increasing the electric field amplitude of the laser field, the length of the barrier that the electron has to pass decreases, and thus the electron can escape from the atom's potential more easily.

2. **The liberated electron propagates in the electric field of the laser.** In this stage of the process, the electron having escaped from the parent ion, is being accelerated by the the external electromagnetic field and it acquires a high velocity and momentum, (third panel of Fig. 1.3). As a result, the attractive force exerted by the parent ion does not strongly affect the trajectory of the electron and therefore the interaction with the parents ion's potential can be neglected (In Fig. 1.3 this is depicted by the fact that the potential energy of the system (red line) is approximately equal to the potential energy due to the external field.).

3. **The freed electron might be driven back to the parent ion.** Under the influence of a sinusoidal electromagnetic field, the local electric field amplitude exerted to the system is not constant in time but quite on the contrary, it heavily depends on it. As times passes, the form of the potential energy of the system changes and the electron is driven back to its original position. Whether an electron will be driven back to the parent ion or away from it depends on certain conditions. Some of the them are, the shape of the electromagnetic field after the electron has spawned and its initial velocity. By returning to the parent ion (fourth panel in Fig. 1.3), the electron can

   i) scatter elastically to increase its kinetic energy,

   ii) recombine with the parent ion and emit a high energy photon. This phenomenon is known as high harmonics generation[5], and it was demonstrated for the first time in 1987 [8].

   iii) or scatter inelastically to excite a second electron or even to ionize the ion for a second time. The production of a doubly charged ion in this way is known as the *non-sequential double ionization*, NSDI[6].

   However, the exact mechanisms governing the recollision-induced ionization are not yet fully understood. One of the reasons is that in multi-cycle laser pulses, N.S.D.I. may involve multiple recollisions. Not only of the parent ion with the free electrons but also of aforementioned with one another. A mechanism like this represents a great challenge for the theoretical description and interpretation of experimental results.

1.1.2 The context of this thesis

The layout of the thesis is organized as follows:

- **Chapter 1** is the introduction, presenting the two primary regimes being used in the bibliography regarding the laser facilitated ionization of atoms. In this chapter, there is also a brief presentation

[5] high-order harmonics of the fundamental (linearly-polarized) laser field

[6] The production of the a di-cation can also be achieved by the successful tunneling of the excited electron (this mechanism is referred to as the recollision-excitation-tunneling-ionization mechanism, *RESI*)

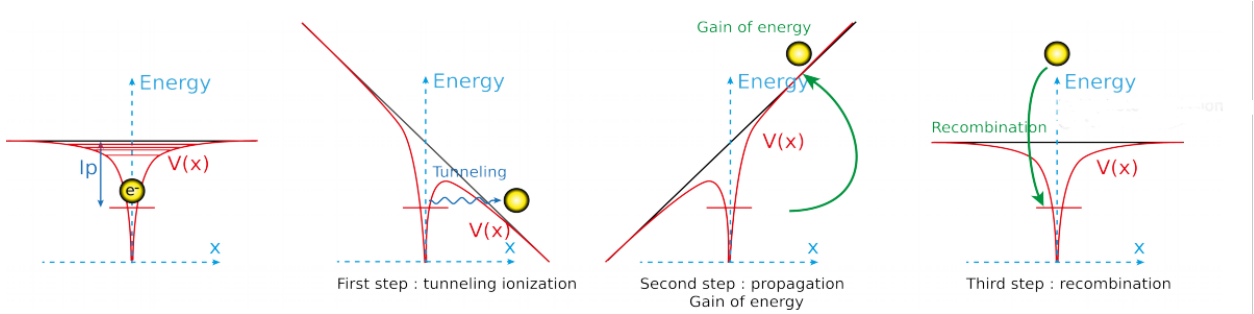

Figure 1.3: Qualitative presentation of the *simple man's model*. In each panel, the red line depicts the total potential energy of the system and the black line depicts the potential energy due to the external electric field. In the first panel, the potential energy of the system without the interaction of it with the external field is depicted. In the second panel, the external field distorts the potential energy surface of the system and facilitates the transition of an initially bound electron to the continuum. In the third panel, the propagation of the electron in the external field results in some energy gain in the electron's kinetic energy. The energy gain of the liberated electron makes the influence of the parent ion insignificant and it can thus be neglected (the potential energy due to the parent ion does not change significantly the potential energy due to the external field.). In the fourth panel, the electron's propagation in the external field has resulted in its return to its parent ion. When the electron returns to its original position, it can recombine with the parent ion.

of the so called *Simple man's model*, the simplest model being used to explain a variety of physical phenomena that appear in strong laser physics; two of which are going to be examined in this thesis.

- **Chapter 2** presents the fundamental ideas behind the tunnelling ionization theory and the most important steps for the derivation of the most widely used tunneling ionization formula, i.e. the ADK ionization formula.. Moreover there is discussion on the *single ionization process*, *the sequential double ionization*, as well as a brief mention of the physics regarding the *over the barrier ionization.*

- **Chapter 3** is dedicated to the study of the dynamics (motion and kinetic energy) of liberated electrons that are interacting with an externally applied, oscillating electric field. The liberated electrons are propagating in the laser field and at some moment in time, some of them, return to their original position. The kinetic energy of the retuning electron at that moment will be calculated and a thorough explanation of it will be given. Moreover, an "optimized" laser field will be introduced, which presents some advantages over all the other laser pulses regarding the kinetic energy of the returning electrons. For the optimized laser field, the electron return with a narrow kinetic energy distribution whose form does not change significantly for small variation of the pulse parameters Nevertheless, the "optimized" pulse has some other advantages that cannot be examined in this section and will be further studied in Chapter 4. This characteristic has to do with the intrinsic phases of the harmonics.

- **Chapter 4** describes the theoretical framework behind the calculation of the probability of the high harmonics generation, due to the interaction of a system with low frequency radiation fields. In order to do so, the *Strong Field Approximation* will be introduced and the *Time dependent- and laser induced dipole moment* of the system will be calculated. The dipole moment will be *Fourier* transformed to yield the harmonic spectrum and the characteristics that are in common with the results presented in Chapter 3 will be pointed out. Based on these characteristics, a "rule of thumb" that has not been presented anywhere in the literature will be presented. Moreover, the "optimized" pulse introduced in Chapter 3 will be studied in order to compute its corresponding harmonic spectrum. The harmonic

spectrum of the "optimized" pulse presents some advantages that could not be studied using the *Simple Man's Model*, and an application of it is being proposed.

Chapter 2

Tunnelling ionization of atoms

As it has been briefly discussed in the introduction, in strong laser field physics, there are two regimes that result in the liberation of electrons from the system. In general, in the semis-static regime, the potential barrier of the system is being distorted, and the initially bound electron gains a significant probability of propagating through (*tunnelling ionization*) or above the potential barrier (*over the barrier ionization*). In this section of the thesis, the two aforementioned subdivisions of the semi-static regime will be discussed.

In section 2.1, the fundamental ideas behind the tunnelling ionization theory will be listed. The tunnelling ionization theory derived by *Ammosov-Delone-Krainov* is widely being mentioned in the literature and its application is widely spread. The *ADK* formula is going to be used in the forthcoming chapters: 3 and 4 to take into account the tunneling ionization step in the electron rescattering processes.

The *ADK* formula can be used to calculate the probability rate of a single electron being liberated from the system of interest for any given electromagnetic wave interacting with it. In 2.1.1.1, the behaviour of the *ADK* formula with respect to the applied external electric field and the form of the incident wave's profile will be studied. In addition, single ionization processes are being discussed, in which an electron is being liberated from the system to produce a parent ion.

Nevertheless, in the presence of a strong incident electromagnetic field, there is a probability of not only one but two electrons being liberated. The tunnelling ionization of two initially bound electrons results in the production of doubly charged ions. If the first and second ionization events are uncorrelated, we are referring to the *sequential double ionization:*. In 2.1.1.2, the behaviour of the *A.D.K.* formula with respect to the initial state of the forthcoming liberated electron will be examined. To make a clear discussion about it, the ionization probability rate of the neutral helium atom and the ionization probability rate of the helium cation will be compared.

As the incident intensity is increased, there is a smooth transition from the *tunnelling ionization* regime to the *over the barrier Ionization regime*. In this regime, the deformation of the atom's Coulomb's potential results in an initially bound electron escaping classically over the barrier without the need to tunnel through it. We are going to make a brief discussion about it in 2.1.2 and present the modified *ADK* formula proposed *Tong and Lin* in [15] to extend the use of the original *ADK* model to higher intensities.

2.1 A.D.K. theory of tunneling ionization

Nowadays, the most widely used tunnelling model is the one introduced by *Ammosov-Delone-Krainov* [21], A.D.K. model, in 1986. The ADK model describes the tunnel ionization of complex atoms and of atomic ions in an alternating electromagnetic field. This model is the extension of the tunnelling ionization rate in a static, electric field for a hydrogen-like atom [7] to an arbitrary asymptotic Coulomb-like potential. The

derivation, presented in [21], is based on three key assumptions.

i) First, only the initial state and final states (continuous or free states) of the electron play an important role in the tunnelling process while the intermediate states place no role.

ii) Second, the emitted-photons' energy is much smaller than the ionization potential of the initial state, $\hbar\omega \ll I_p$, and the electric field amplitude of the laser is not exceedingly larger than the atomic field strength.

iii) Third, it is assumed that the potential that acts on the valence electron varies rather slowly with respect to the radial distance from the nucleus. Basically this assumption implies that the wavelength of the applied field is larger than the effective radius of the atom. Assuming that the laser period is much larger than the time scale that an electron needs to be set free, the ionization probability rate for an alternating field are to be sufficiently well approximated by the ionization probability rate of a constant field.

All these allow the derivation of an analytic expression for the tunnelling-ionization probability rate.

2.1.1 Brief description of the derivation of the $A.D.K.$ formula

To make the theory of the tunnelling ionization probability as clear as possible, the basic steps in the derivation of the ADK formula will be described. [1] Consider the case of a constant electric field $\mathcal{E}$ along the z-direction, $\vec{\mathcal{E}} = \mathcal{E}\hat{z}$ and an atom which is placed on the axis origin. The starting point in the derivation of the tunnelling theory for an atom in an external field is the observation that during the tunnelling-ionization by a strong constant electric field, the atom's binding potential overshadows the external electric field in very short distances from the nucleus, whereas it is greatly suppressed at large distances from it and competes with it somewhere in between. Thus, the potential energy region of the valence electron, the one that is the most likely one to to escape from the atom, can be divided in three main regions (see the dashed lines in Fig. 2.1).

In more detail, in the cases in which the external electric field amplitude is below a certain threshold, the first region (interior region) can also be divided in two subregions. In the first one, the nucleus' potential is enormously strong and cannot be approximated by a Coulomb potential (screened Coulombic potential) due to the presence of all the other electrons (interior region) and the second one where the field acting on the valence electron reduces to a Coulomb's "tail" field with effective atomic number $\mathcal{Z}$ (interior region). This is happening due to the screening by the presence of all the other electrons. In the interior region, even though the atomic-residue field is already relatively weak, the external field can still be neglected [2]. and thus the wavefunction of the active electron can sufficiently well be approximated with the wavefunction of the free atom:

$$\psi(\vec{r}) = C_{n^\star l} r^{n^\star - 1} e^{-\mathcal{Z}r/n^\star} Y_l^m(\Omega), \tag{2.1}$$

[1] A good presentation of the derivation of the ADK formula is given in [30]

[2] For example, in the simplest case scenario, of a helium atom in which one of the electrons is assumed to be in the ground state and the other one is assumed to be in a state with large principal and azimuthal quantum numbers, the effective potential experienced by the valence electron can be approximated by the use of Gauss'es law in electrostatics:

$$V_{eff} = -\frac{1}{r} - e^{-4r}\left(\frac{1}{r} + 2\right).$$

In a radial distance, let's say, three times the Bohr radius ($r = 3\alpha_0$), the value of the electric field coming from the Coulomb-like potential is approximately $10^{11} V/m$ while the electric field coming from the second term is approximately $10^7 V/m$.

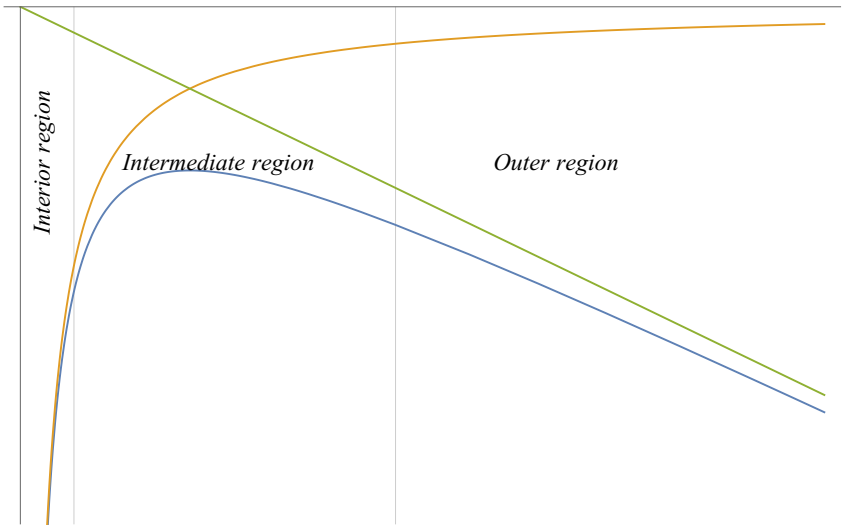

Figure 2.1: Qualitative potential energy of a valence electron of an atom which is exposed to a strong external electric field. In short distances from the nucleus, the atom's binding potential overshadows the external electric field (interior region) while in large distances from it, the atom's binding potential is suppressed (outer region).

where $n^\star = \mathcal{Z}/\sqrt{2I_p}$, l are the effective principal and orbital quantum number. The constant C_{nl} is known analytically for arbitrary states of the hydrogen atom and its values for the ground states of complex atoms and single ions can be obtained from numerical calculations.

On the other hand, in the most outer region of the potential energy surface, where the influence of the Coulomb-like potential is negligible compared to the potential energy of the external electric field, the wave-function of the system is primarily molded by the characteristics of the external source. In this region (outer region), by making use of the *Wentzel–Kramers–Brillouin* approximation [3], the wave-function of the system, in parabolic coordinates [4], takes the form

$$\psi(\vec{r}) \propto \xi^{|m|/2} e^{-\xi\kappa/2} \frac{e^{im\phi}}{\sqrt{2\pi}} \frac{1}{\sqrt{|\eta\, p(\eta)|}} e^{i\int p(\eta)d\eta}, \tag{2.2}$$

where $p(\eta)$ is one of the components of the "semi-classical momentum":

$$p(\eta) = \sqrt{-I_p + \frac{\mathcal{Z}}{\eta} + \frac{1}{4}\mathcal{E}\eta - \frac{|m|+1}{2\eta}\left(\kappa + \frac{|m|-1}{2\eta}\right)}. \tag{2.3}$$

In the expression above m is the magnetic number of the initial state, I_p is the ionization potential, $\mathcal{Z}$ is the degree of ionization of the atomic ion of interest and $\kappa = (2I_p)^{-1/2}$.

Finally, the basic premise is to match the atomic wavefunction in the interior region, eq. (2.1), with the one in the exterior region. In the exterior region the solution is an outgoing WKB solution [5], eq.

[3] For more information, see Appendices

[4] $x = \sqrt{\eta\xi}\cos\phi, \quad y = \sqrt{\eta\xi}\sin\phi, \quad z = (\xi-\eta)/2 \Rightarrow \xi = r+z, \quad \eta = r-z, \quad \phi = \arctan(y/x)$

[5] Of course doing so is not very easy. Depending on the value of the η coordinate, the semi-classical momentum can be real or imaginary. In a classically allowed region, where the ionization energy of the system is greater than its potential energy the momentum is real valued function, while for a non-classical region, the momentum becomes imaginary. As a result, in a classical region, the wavefunction is but an oscillating function whereas, in a non-classical region, the wavefunction of the system, eq. (2.2), becomes a real and exponentially decreasing function; just like the asymptotic form of the Coulomb-wavefunction. In the end, there is not just one matching, but two! The first matching, has to do with matching the $W.K.B.$ solution in the non classical area with the asymptotic form of the Coulomb-wavefunction and the second matching is done for the continuity of the $W.K.B.$ solutions in the classical and non-classical regions.

Effective principal quantum number list, for noble gases			
Atom	$n^\star$	Ion	$n^\star$
He	0.74	He^+	1.00
Ne	0.79	Ne^+	1.15
Ar	0.93	Ar^+	1.40
Kr	0.99	$Kr^\star$	1.44
Xe	1.06	$Xe^\star$	1.60

Table 2.1: Effective principal quantum number list for noble gases and the corresponding cations. [21]

(2.2), and then calculate the probability current density along the direction in which the electron is most likely to be liberated ($(-z)-$ direction), $\mathcal{J}_z$. The ionization probability rate near the $z-$axis is given by the surface integral of probability current density, $\mathcal{J}_z$, over surface orthogonal to it. Having used the *W.K.B.* solution, it is takes the form

$$\mathcal{W} \approx -\iint \mathcal{J}_z dS_z = \cdots = \frac{1}{\kappa^{2n^\star-1}} \frac{|B(l,m)|^2}{2^m\,|m|!} \left(\frac{2\kappa^3}{\mathcal{E}}\right)^{2n^\star-|m|-1} e^{-2\kappa^3/3\mathcal{E}}, \tag{2.4}$$

$$B(l,m) = C_{n^\star l}(-1)^{(m+|m|)/2} \sqrt{\frac{(2l+1)(l+|m|)!}{2(l-|m|)}}, \tag{2.5}$$

$$C^2_{n^\star l^\star} = \frac{1}{2\pi n^\star} \left(\frac{4e}{n^{\star 2}-l^{\star 2}}\right)^{n^\star} \left(\frac{n^\star+l^\star}{n^\star-l^\star}\right)^{l^\star+1/2}. \tag{2.6}$$

The only unknown quantity in this equation is the term $B(l,m)$ which can be determined by the normalization constant $C_{n^\star l^\star}$, which in its turn can be determined by matching the quantum mechanical wavefunction of the atom to the asymptotic Coulomb form. The expression for C_{nl} in eq 2.6 is the one given in ref. [21] (eq. (20)), where $n^\star$ and $l^\star$ denote the effective principal and orbital quantum numbers[6]

In the case of an alternating electromagnetic field, the potential that acts on the valence electron varies rather slowly with respect to the radial distance from the nucleus (in other words, we are assuming the validity of the adiabatic approximation. Then the instantaneous ionization rate can be obtained by inserting the time-dependent magnitude of the electric field in the formula for the static field, eq. (2.4),

$$\mathcal{W}(t;I_p) \propto \frac{|B(m)|^2}{2^m\,|m|!} \left(\frac{2\kappa^3}{\mathcal{E}(t)}\right)^{2n^\star-|m|-1} e^{-2\kappa^3/3\mathcal{E}(t)}. \tag{2.7}$$

2.1.1.1 Single ionization process:

In the simplest case scenario, the external electric field results in the emission of a single electron and the appearance of a parent ion. In the panels α) and γ) of Fig. 2.2 we have plotted the electric field shape of one colour sinusoidal electromagnetic wave and the electric field shape of a $\cos-$enveloped one colour field [7] respectively. In panels β) and δ) of Fig. 2.2 their corresponding normalized (the maximum value in these

[6]The effective orbital quantum number is defined as

$$l^\star = n^\star - 1$$

in [21]. $n^\star$ is the effective principal quantum number of the lowest state for a given orbital quantum number.

[7]For a $\cos-$enveloped one colour field, the mathematical formula expressing its form at any moment in time is

$$\mathcal{E}_{tot} = \mathcal{E}_0 \times \underbrace{H\left(\pi\mathcal{N} - \omega|t+t_0|\right)\cos^2\left(\frac{\omega(t+t_0)}{2\mathcal{N}}\right)}_{\text{envelope form}} \times \underbrace{\left\{\cos\left(\omega\left(t+t_0\right)+\Phi\right)\right\}}_{\text{carrier wave}}. \tag{2.8}$$

graphs is one [8]) instantaneous ionization probability rates have been plotted in a logarithmic scale. The periodic form of the one colour sinusoidal electromagnetic wave (panel α) 2.2) results in a periodic form of the instantaneous ionization probability rate (panel β) 2.2). The envelope shape of the cos −enveloped one colour field in panel γ) 2.2, results in an enveloped-instantaneous ionization probability rate (see panel δ) 2.2).

In order to make these graphs, the ionization potential was set to be equal to $I_p = 24.6\ eV$ while the intensity of the electromagnetic field was set to be equal with $\mathcal{I} = 3 \times 10^{14}\ W/cm^2$. The instantaneous ionization rates depend exponentially on the electric field amplitude of the incident wave and thus there are some preferable at which the valence electron is being emitted. It should be noted that, the choice of the incident intensity was not chosen for a particular reason, but was only restricted to be below the saturation ionization level. The ionization potential corresponds to the ionization potential of helium's ground state. What we want to emphasize is that in general (no matter the model) the ionization probability rate is a function which depends exponentially on the strength of the electric field (another well known model is the PPT-model [3]).

To make this a little bit clearer, in panel γ) of Fig. 2.2, two black bullets have been added which correspond to the second largest local maximum of the electric field, $E \approx \frac{3}{4}E_{max}$, and the second lowest local minimum of the electric field, $E \approx \frac{1}{2}E_{max}$. For these candidate ionization moments, the instantaneous ionization probability rate is of the order of 10^{-1} $a.u.$ and 10^{-3} $a.u.$ (arbitrary units). For half of the value of the maximum electric field amplitude, the instantaneous ionization probability rate has been decreased by more than orders of magnitude.

2.1.1.2 Sequential double ionization:

Eq. 2.7 can be used, not only for calculating the ionization probability rate of a neutral atom but also to calculate the ionization probability rate of an ion ($n^\star = \mathcal{Z}/\sqrt{2I_p}$). It can be used to calculate the production rate of doubly charged ions; assuming that the first and second ionization steps are two independent procedures. This mechanism is known in the literature as the sequential double ionization. It is a process of forming a doubly charged ions consisting of two single-electron ionization events: the first electron is removed from a neutral atom/molecule (leaving a singly charged ion in its ground state) followed by the detachment of the second electron from the ion [9]. Due to the fact that the first and second ionization are considered to be uncorrelated, the production rate of a doubly charged ion is given by the product of the ionization probability f the neutral atom times the ionization probability of the cation.

In Fig. 2.3, the electric field from of a cos-enveloped one colour field (panel α)) and the corresponding production rates of a cation (blue curve) and di-cation (red curve) are depicted (panel β)) in a logarithmic scale. In order to make these graphs, the ionization potential for the creation of the cation was set to be equal to $I_p = 24.6\ eV$ (ground state of He atom) and the ionization potential for the creation of the di-cation was set to be equal to $I_p = 54.4\ eV$ (ground state of cation of He). The maximum values of the ionization probability rates were mutually normalized, and the intensity of the electromagnetic field was set

Where

$$H(x) = \begin{cases} 1, & x \geq 0 \\ 0, & x < 0 \end{cases}$$

And $\mathcal{N}$ denotes the total number of cycles in the pulse.

[8] This is something which is not physically important. Since we are talking about ionization probability **rates**, the normalization of the graphs can be translated as working in different units of time.

[9] This process is to be distinguished for the *non-sequential double ionization* ($NSDI$) process. The $NSDI$ process involves the rescattering of a returning electron from the parent ion. An extensive discussion about the rescattering process will be made in the forthcoming chapters.

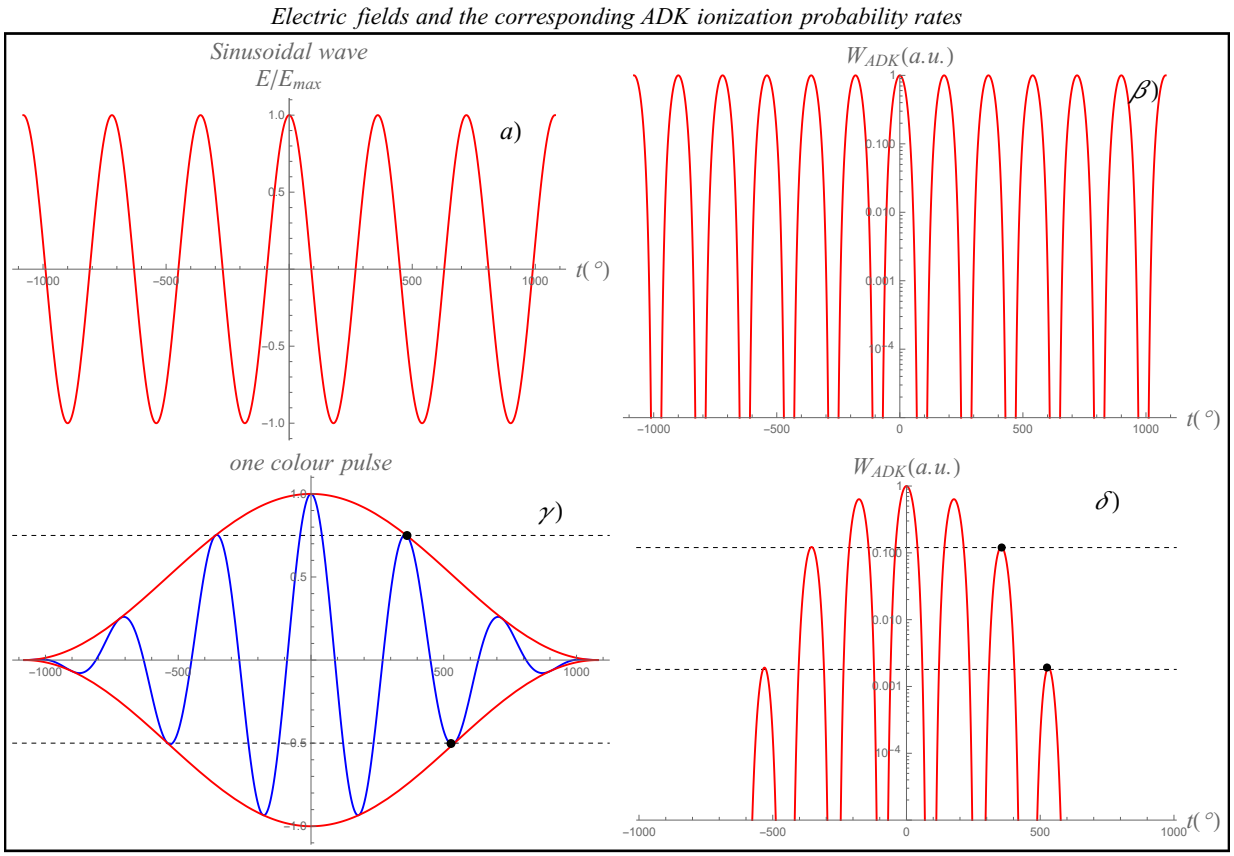

Figure 2.2: In panels α) and β) the the electric field shape of one colour sinusoidal electromagnetic wave and the corresponding instantaneous ionization probability rate are depicted. In panels γ) and δ) the electric field shape of $\cos-$enveloped one colour field and the corresponding instantaneous ionization probability rate are depicted. For these graphs, the ionization potential was set to be equal to $I_p = 24.6\ eV$, ground state of helium, while the intensity of the incident electromagnetic field was set to be equal with $\mathcal{I} = 3 \times 10^{14}\ W/cm^2$.

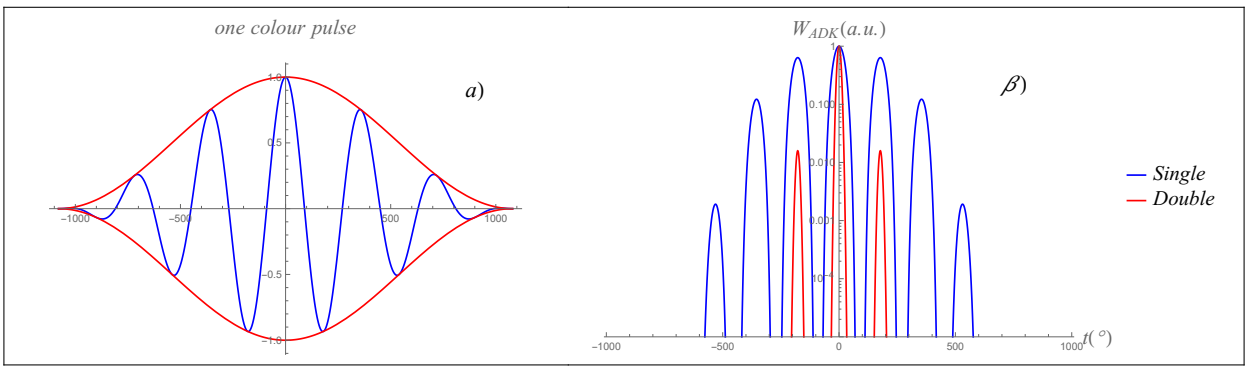

Figure 2.3: In panels α) and β) the the electric field shape of one colour sinusoidal electromagnetic wave and the corresponding instantaneous ionization probability rate are depicted. The envelope contains 6 cycles of the carrier wave, the carrier-envelope-phase is set to zero, $\Phi = 0$ and the maximum intensity due to the fundamental harmonic of the laser field was set to be equal with $\mathcal{I} = 10^4\ W/cm^2$. For the single ionization the ionizaiton potential was set to be equal with $I_p = 24.6\ eV$ and for the double ionization $I_p = 54.6\ eV$.

to be equal with $\mathcal{I} = 3 \times 10^{14}\ W/cm^2$.

The probability of a double sequential ionization process is a function which decreases much

more rapidly than the single ionization probability rate, with the decreasing values of the external field is. For the second greatest local maximum of the electric field's strength, the single ionization probability rate is close to its maximum value. On the contrary for double ionization the corresponding ionization probability rate has dropped by approximately two orders of magnitude. For the third greatest local maximum of the electric field's strength, the single ionization probability rate has dropped by approximately one order of magnitude while the corresponding ionization probability rate of the double ionization has dropped more than five orders of magnitude.

Now since the typical frequencies of the external light source correspond to wavelengths in the infrared region, the observed ionization rate (in a laboratory) will be proportional of the integral of the instantaneous ionization rate over the duration of the field.

$$\mathcal{W} \propto \int_{t_i}^{t_f} \mathcal{W}(t; I_p) dt. \tag{2.9}$$

From the equation above, we can understand that the observed ionization rate is a function which crucially depends on both the amplitude of the external electric field as well as the ionization potential of the system.

To examine the validity of the theory presented above, in Fig. 2.4, the ionization probability rates for a single and double ionization process have been plotted as a function of intensity of a Gaussian envelope, 0.6 μm one colour field interacting with helium. The characteristics of the field were chosen so

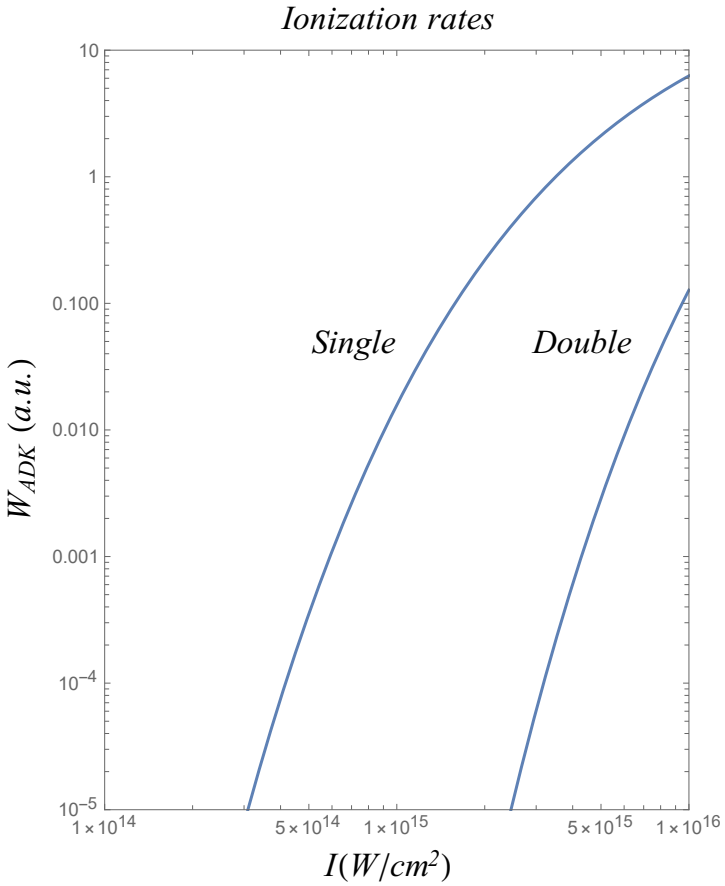

Figure 2.4: Observed ionization probability rate for a single a sequential double ionization process as a function of intensity of a Gaussian envelop, 0.6 μm one colour field interacting with helium. These results can be compared with the experimental results published in [5] and the theoretical results in [4].

that the results could be compared with the experimental results published in [5]. The theoretical results are in excellent agreement with the experimental ones. In this figure, we notice that the due to the large value of the ionization potential of the cation of helium, the corresponding calculated ion yields [10] do not take significant values until high light intensities are being reached.

2.1.2 Over the barrier ionization

In the previous paragraphs of this chapter, we have discussed the theory behind the tunnelling ionization mechanisms and we have examined how the ionization probability rate depends on both the intensity as well as the ionization potential of the system. However, the discussion was limited to working below a certain threshold value for the external electric field. As the external field's strength is increased the dominant ionization mechanism of some systems might change. Given that specific laser frequencies are being used (infrared region), the tunnelling regime gives its place to the over-the-barrier regime, which is also known as barrier-suppression ionization (B.S.I.).

In this regime, the deformation of the atom's electrostatic potential is so great that it results to an initially bound electron escaping classically over the barrier without the need to tunnel through it. Consider the picture in Fig. 1.2 of the potential energy of the valence electron as the strength of the external electric field is increased. As the light intensity is being continuously increased, the potential barrier of the initially bound electron becomes more and more narrow. This results in the decrease of the barriers width and thus smoothly enhancing the tunnelling ionization probability rate. At the same time, the height of the potential barrier is also being reduced and for a given critical value of the external electric field, called *threshold field strength*, the height of the potential barrier is in the same level with the energy level of the initially bound electron. In this limit, the width of the potential barrier is brought to zero and thus after this point, the ionization of the system is not happening due to the quantum tunnelling effect but due to the classical propagation of the electron over the barrier.

To determine the critical field strength of the system and obtain the barrier suppression intensity, BSI, we are going to follow a classical approach. Consider the case of a static electric field along the positive z-direction. The potential energy of an active electron in this static electric field is given by:

$$V(\rho, z) = -\frac{\mathcal{Z}}{\sqrt{\rho^2 + z^2}} + \mathcal{E}z. \tag{2.10}$$

In the equation above, we have used cylindrical coordinates due to the axial symmetry of the problem. ρ is the radial coordinate, z is the height and $\mathcal{Z}$ denotes the charge of the residual ion. The maximum of the potential energy is equal to,

$$V_{max} = -2\sqrt{\mathcal{Z}\mathcal{E}}, \tag{2.11}$$

and it corresponds to the point

$$\rho_{max} = 0 \quad \text{and} \quad z_{max} = -\sqrt{\frac{\mathcal{Z}}{\mathcal{E}}}. \tag{2.12}$$

The range of field strengths which correspond to the $B.S.I.$ regime is found by requiring the maximum potential energy to be lower or equal to the sum of the kinetic and potential energy, $I_p = K + V \geq V_{max}$. By setting the maximum of the potential energy equal to ionization potential, i.e. by assuming that the initial velocity of the liberated electron is zero, the minimum field strength at which the electron may escape over

[10] The calculated ion yields are proportional to the observed ionization probability rate

the barrier is equal to

$$\mathcal{E}_c = \frac{I_p^2}{4\mathcal{Z}}. \tag{2.13}$$

For a monochromatic colour field, the corresponding critical value of the intensity threshold is equal to

$$I_c(W/cm^2) \approx 4 \times 10^9 \frac{I_p^4(eV)}{\mathcal{Z}^2}. \tag{2.14}$$

At this point we should stress out that for the determination of critical electric field strength we have made two silent assumptions. First of all, we have assumed that the applied field does not change the ionization potential significantly (we have not taken into account a *Stark effect*[11]) and second we have not taken into account the centrifugal term who is inversely proportional to the square of the distance from the nucleus, $\propto 1/z^2$. Thus, aside from the fact that we refer to the case of an unperturbed atomic energy level, we also refer to the case when the angular momentum barrier, which repels the electron from z-axis, is set to be zero.

At the critical threshold field, $\mathcal{E}_c$, the unperturbed atomic energy level lies at the top of the potential barrier. Above this critical field, we enter the barrier-suppression regime and then the ionization rate that depends on the perturbation theory has been found experimentally to significantly overestimate the ionization rate [15]. Tong and Lin in their paper [15] have modified the original ADK model to extend the ADK rates from the tunnelling ionization region to the near- and over-the-barrier regime. This was done by introducing an empirical correction factor α_c, which brings the modified ADK formula to the form:

$$W_{modified} = W_{A.D.K.} e^{-\frac{2\kappa^3}{3}\alpha_c \mathcal{E}(t)} \tag{2.15a}$$

$$\propto \frac{|B(m)|^2}{2^m\,|m|!} \left(\frac{2\kappa^3}{\mathcal{E}(t)}\right)^{2n^\star - |m| - 1} \exp\left\{-\frac{2\kappa^3}{3}\left(\frac{1}{\mathcal{E}(t)} + \alpha_c \mathcal{E}(t)\right)\right\}. \tag{2.15b}$$

In the formula above, we can see that the empirical factor has been used in order to place and exponential decreasing term for high incident electromagnetic fields. For high values of the incident intensity, the $1/\mathcal{E}(t)$ term has no serious effect on the ionization probability rate, while the $\alpha_c \mathcal{E}(t)$ term, given the appropriate value α_c, adds the saturation behaviour that is found experimentally.

[11] Perhaps it should be noted that for high intensities, we are not talking about the linear *Stark effect*

Chapter 3

Propagation of the electron in an oscillating electric field

An atomic (or molecular) system that is interacting with a strong electromagnetic field has a probability of being ionized (for example through the tunnelling ionization mechanism). Afterwards, the liberated electron propagates in the external field and might be driven back to the parent ion. On its return to its original position, rescattering phenomena might occur. The shape of the electromagnetic field after the electron has spawned is crucial in selecting the electrons that return to the parent ion with some "returning (final) kinetic energy". In this chapter, the motion of electrons in alternating electromagnetic fields are studied. Initially we will study continuous electromagnetic fields, carrying one and two frequencies (3.1.1, 3.2.1). The kinetic energy of the electrons that returns to their initial position are calculated(3.1.2, 3.2.2) and the corresponding kinetic energy distribution (spectra) (3.1.4, 3.2.2). From all of the spectra being evaluated, the one which results in the most narrow kinetic energy distribution of the returning electrons will be searched for (3.2.3).

The search for a narrow kinetic energy distribution is described and the "optimized" laser field which is responsible for is being put under some tests 3.2.4, to check its reliability and robustness, as well as its advantages over other electromagnetic field shapes. The tests deal with the parameters that define the optimized electromagnetic field and the case in which the returning electrons fail to interact with the parent ion on their first return to it. The electrons that are not interacting with the parent ion when they return to their original position, will continue propagating in the laser field and perhaps, at some later time some of them might "re-return" back to it. But having propagated in the laser field after not interacting with the parent ion will result in changing the final kinetic energy of these electrons and thus altering their contribution to the spectra and thus affecting their monochromaticity. All these questions are going to be examined.

Yet, the electromagnetic fields that are used in strong laser field physics are not continuous waves but pulses, brief bursts of electromagnetic energy. The continuous optimized electromagnetic field is then enclosed in an envelope. The envelope results in the deformation of the continuous electromagnetic field shape, and consequently to the deformation of its spectrum. The spectrum is also tested based on the number of cycles in the envelope 3.2.5 .

The method with which the spectra are evaluated is presented in 3.1.3. The numerical method which was used is analytically explained and the choice of using it was made so that the program could also be used even for the propagation of electron in an arbitrary pulse.

With a classical picture in our minds, the electronic cloud density of the valence electron can be thought of as a distribution that informs us about the time that a classically orbiting electron spends in a particular position around the parent ion. During the interaction with the laser field, the electron spends

most of its time (relatively) away from the parent ion. At these distances, the electron's potential energy is relatively small, and so is the corresponding force exerted by the parent ion to the electron. Under this consideration, the electric field of the parent ion will be neglected. Moreover, due to the fact that that applied force due to the magnetic component of an electromagnetic wave is approximately eight orders of magnitude lower than the corresponding electric field, we shall ignore it as well.

3.1 Dynamics of one colour field

The simplest case scenario is the case of a monochromatic or one colour field without envelope, (i.e a CW field) will be used for two primary reasons. Firstly, to present an introduction to this complex problem by noting the basic characteristics and emphasising on the ones that are most important. Secondly, the dynamics in a sinusoidal electromagnetic field have been studied extensively in the biography [4, 9, 10]. These studies were used as a criterion for the verification of the results produced by our calculations.

3.1.1 Equations of motion

The trajectory of the charged particle can be found solving *Newton*'s second law of motion in one spatial dimension (1D):

$$m\ddot{x} = q\mathcal{E}_0 \cos\left(\omega\left(t + t_0\right)\right). \tag{3.1}$$

ω denotes the angular frequency of the laser, $\mathcal{E}_0$ denotes the electric field amplitude and ωt_0 is an initial phase. The t_0 can be used to express the moment of ionization, which is the moment that the charged particle starts experiencing the force of the electric field.

Under the initial conditions that the charged particle starts its journey from the nucleus (where we set the Cartesian axis origin in our problem) with almost zero velocity, the position of it at any given time, is given by:

$$x = -\frac{q\mathcal{E}}{m\omega^2}\Bigg[\underbrace{\cos\left(\omega\left(t + t_0\right)\right)}_{\text{Oscillating term}} + \underbrace{\sin\left(\omega t_0\right)\omega t}_{\text{Linear term}} - \underbrace{\cos\left(\omega t_0\right)}_{\text{Constant term}}\Bigg] \tag{3.2}$$

The equation of motion (3.2) consists of three terms. The **oscillating term** indicates that the motion of the electron is not linear but rather that the electron is constantly pulled towards the direction of a specific point (the equilibrium position). This point is not fixed in time but it is moving with a constant velocity which is is equal to

$$u_{dr} = -\frac{q\mathcal{E}}{m\omega}\sin\left(\omega t_0\right). \tag{3.3}$$

In the literature the constant part of the velocity is called "drift velocity" and it comes from the **linear term**. Last but not least, the **constant term** appears in the equation (3.2) to ensure that the initial position of the electron is on the axes origin. To be more specific, its appearance cancels the contribution of the oscillatory term in the equation of motion of the electron the moment the electron was spawned.

Under this perspective, the trajectory of an electron (see Fig 3.1) can roughly be thought of as an oscillatory motion taking place on top of a line, which passes through the origin and whose angle with respect to the positive horizontal axis is $\arctan(u_{dr})$ (dashed line). In Fig. 3.1, the black dots indicate the returning time for some of the trajectories. As it can be seen, for some ionization moments, t_0, the emitted electron never returns to its original position. Last but not least, the displacement of the electron is measured in "ponderomotive length units".

$$L_p \equiv \sqrt{\langle x_{osc}^2 \rangle|_t} = \frac{q\mathcal{E}}{\sqrt{2}m\omega^2}. \tag{3.4}$$

This quantity is the Root Mean Square of the oscillating displacement, x_{rms}^{osc}, and it has been introduced, in order to separate the form of the trajectory of the electron from the magnitude of the maximum displacement.

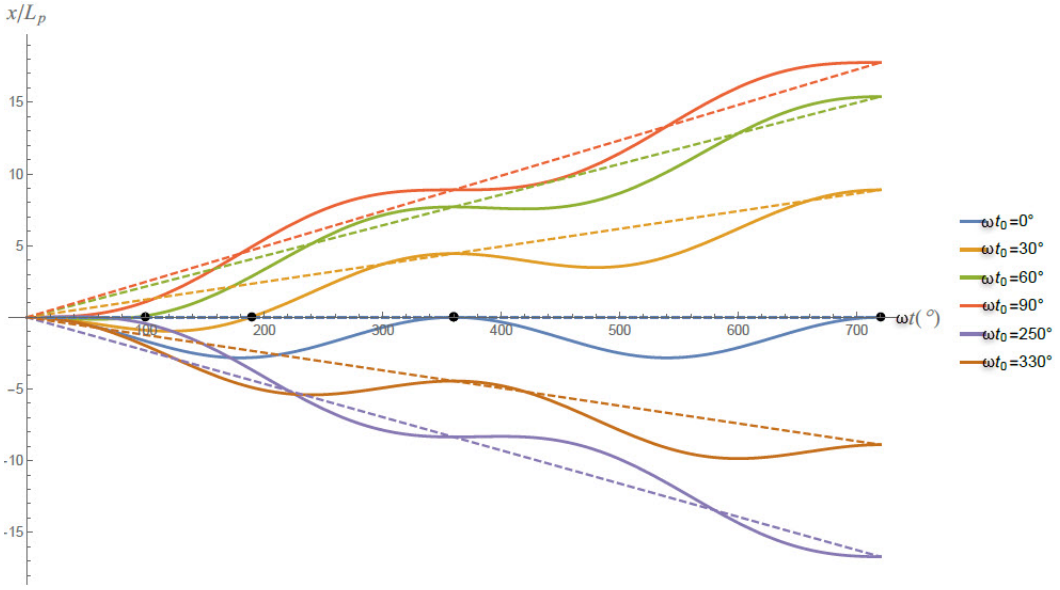

Figure 3.1: Trajectories of electrons generated at different times, t_0, in the presence of a cos −like electromagnetic field of angular frequency ω. The dashed lines indicate the uniform part of the displacement of the electron. For a quantitative understanding, L_p is the ponderomotive length and for example, in the case of $\mathcal{E}_0 = 10^8 V/cm$ and $\lambda = 1500nm$, $L_p \approx 0.8nm$ and $1^\circ \to 5 \times 10^{-15}$ s.

3.1.2 Kinetic energy of the returning electrons

In this subsection, we are going to study the kinetic energy of the electrons at the moment that return to their initial position. In order to study the quantitative side of this problem, the results will be expressed in terms of the ponderomotive potential. The ponderomotive potential is a characteristic energy quantity of the system that is widely used in the literature. Furthermore, the electrons that are driven back to their original position in the case of cos −like electromagnetic wave will be listed in two categories. This categorization of the electrons is based on the amount of time that they propagated under the influence of the external field and are the long and short trajectories.

To define the ponderomotive energy, it is important to mention that due to the oscillating term in eq. 3.2, the kinetic energy of the electron is not constant but it is a periodic function with respect to time. Using the equation of motion (eq.(3.2)), the **cycle averaged kinetic energy** of the charged particle over an optical cycle is equal to:

$$\frac{1}{2}m\langle \dot{x}^2 \rangle\Big|_t = \underbrace{\frac{q^2\mathcal{E}^2}{2m\omega^2}\sin^2(i\omega t_0)}_{\frac{1}{2}mu_{dr}^2 \leftarrow \text{Linear term of eq.(3.2}} + \underbrace{\frac{q^2\mathcal{E}^2}{4m\omega^2}}_{U_p \leftarrow \text{Oscillatory term of eq.(3.2)}} \tag{3.5}$$

The charged particle's kinetic energy is composed of two terms. The first term depends on the initial conditions and by comparing eq. (3.5) and eq. (3.2), we notice that it comes from the linear term of

eq. (3.2). This term is the net drift kinetic energy due to the drift momentum (the constant part of the momentum) of the charged particle. As a result, we can deduce that the second term, which is unaffected by the initial conditions (absence of t_0), corresponds to the average kinetic energy due to the oscillating term in the equation of the motion. This term is the definition of the **ponderomotive potential**

$$U_p = \frac{1}{2} m \langle \dot{x}_{osc}^2 \rangle = \frac{q^2 \mathcal{E}^2}{4 m \omega^2}. \tag{3.6}$$

In figure (fig. 3.2), the kinetic energy of the returning electrons as a function of the ionization time $K(t_0)$ as well as the *recombination time* $t_R = t_0 + t_r$ $K(t_R)$ have been plotted. t_r is the time interval that the electron needed to return to its parent ion. In the plot, $\omega t_0 \in [0°, 180°]$ and this is because of the symmetric form of the sinusoidal wave. In $\omega t_0 \in [180°, 360°]$ the kinetic energy of the returning electrons is exactly the same as the kinetic energy in the $\omega t_0 \in [0°, 180°]$. What differs is only the direction of the position and momentum of the electron, $x(t_r; t_0) = -x(t_r; t_0 + 180°)$, $p(t_r; t_0) = -p(t_r; t_0 + 180°)$.

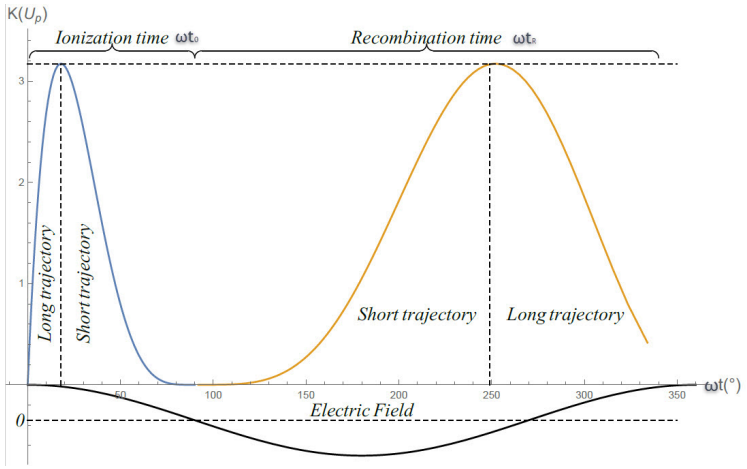

Figure 3.2: Plot of the kinetic energy of the returning electron in a single colour sinusoidal electric field. The graph has been plotted with respect to two parameters, the time in which the electron starts experiencing the electric field(ωt_0, blue curve) and the time in which the electron returned to its parent ion (ωt_R, orange curve). In the same graph, the electric field has been included in order to give a clearer picture of the process. The vertical dashed lines mark the local maximum of the function being plotted whereas the horizontal line indicates the zero value of the electric field. As an example, for $\mathcal{E}_0 = 10^8$ V/cm and $\lambda = 1500$ nm, $K_p \approx 3$ eV and $1° \rightarrow 5 \times 10^{-15}$ s.

The kinetic energy of the returning electron in the case of a $\cos -$like field, is characterized by a single local maximum. In the literature, this single local maximum has been used to split the plot in two parts. The second part is attributed to the returning electrons which travelled within a *short trajectory* to return to the parent ion while the first part is attributed to the returning electrons that travelled a *long trajectory*. The words short and long refer to the time duration that the electron spend, making an oscillatory trajectory, before returning to its starting position [1].

In order to understand which part of the $K(t_R)$ plot correspond to which part of the $K(t_0)$ plot, let us examine the physical picture of the problem, for $t \approx 90°$. For $t_0 = 90° - \delta t$, where δt has a relative small value (with respect to the period of the sinusoidal wave), the electron return to their initial position with very low kinetic energy. This can be understood with the help of the electric field amplitude plotted

[1] This is because in quantum mechanics, an electron has an uncertainty in its position and the uncertainty in its position increases as time passes. This phenomenon is called quantum diffusion and its significance has to do with the indirect parameters in the dynamics of the returning electrons. For more information see 4.1.2

in the same graph. For $t_0 = 90^\circ - \delta t$, the electric field exerts a relative small force[2] on the electron making it move in the negative $x-$axis. After a small period of time δt, the direction of the force changes and the electron is driven back to the parent ion. Thus, the force that was exerted on the electron is not very strong, and the time duration for which the electron was accelerated back to its initial position is very short. As a result, the kinetic energy of these returning electrons must be very low. This means that, even though the $K(t_0)$ and $K(t_R)$ functions provide us with the same physical information, the two parts of its graph are not "read" in the same way. The first part of the $K(t_0)$ function corresponds to the long trajectories whereas the second part corresponds to the short ones. For $K(t_R)$ function, the two branches are reversed.

For the time interval $t_0 \in [0, 18^\circ],\ t_R \in [250^\circ, 360^\circ]$, the kinetic energy of the returning electron increases monotonically and reaches its maximum value, $K_{max} \approx 3.17U_p$ and it is found for the ionization time, $t_0 \approx 18^\circ$ and the recombination time, $t_R \approx 250^\circ$. For the time interval $t_0 \in [18^\circ, 90^\circ),\ t_R \in [90^\circ, 250^\circ]$ the kinetic energy of the returning electron is a monotonically decreasing function and for the time interval $t_0 \in (90^\circ, 180^\circ)$ none of the electrons which initiated with zero momentum return to the parent ion.

3.1.3 Calculation of the Kinetic energy of the Returning/rescattering electrons

In this paragraph, an explanation of the way in which kinetic energy of the returning electrons is calculated, at the time when they return to their initial position (the position of the parent ion) , is presented. The procedure that was used was the same for the case of one- and of two- colour fields. The program was written in such a way so that it could be used even for the propagation of electron in an arbitrary pulse and not only for a sinusoidal wave. Briefly speaking, for every ionization time t_0, the corresponding returning time t_R will be found and with it the kinetic energy of the electrons at the moment that they return to their initial position will be evaluated.

The trajectory of a charged particle interacting with an oscillating electric field is given by the solution of Newton's 2nd law of motion

$$m\ddot{x} = q\mathcal{E}(t). \tag{3.7}$$

In general, given the initial conditions of this problem (the initial position of the electron is at the origin and its initial velocity is equal to zero) the solution of this differential equation cannot be solved analytically for an arbitrary pulse but it can be solved numerically. By finding the trajectory of the charged particle, the time at which the electron returns to its initial position and its corresponding kinetic energy can be found.

As a first step, the differential equation 3.7, was solved for every ionization time $t_0 \in [0^\circ, 360^\circ]$. Using the numerical solutions, a $3-$dimensional list was constructed at which the first column gave the ionization time t_0 of the charged particle, the second column gave the time duration that the electron was propagating in the laser field t and the third column gave its corresponding position. By dividing the time period of the laser in N equally separated time intervals, $\Delta t = 360^\circ/N$

$$t_0 = 0,\ \Delta t,\ 2\Delta t,\ 3\Delta t,\ \cdots,\ (N-2)\Delta t,\ (N-1)\Delta t, \tag{3.8}$$

$$t = \Delta t,\ 2\Delta t,\ 3\Delta t,\ \cdots,\ (N-2)\Delta t,\ (N-1)\Delta t,\ 360^\circ \tag{3.9}$$

a two dimensional list was created, with any possible pair between the ionization and propagation time. In

[2]The force is analogous to the absolute magnitude of the field.

a matrix representation, the data took the form,

$$\left(\begin{array}{ccc} t_0 & t & x(t_0,t) \\ \hline 0 & \Delta t & x(0,\Delta t) \\ 0 & 2\Delta t & x(0,2\Delta t) \\ \vdots & \vdots & \vdots \\ \Delta t & \Delta t & x(\Delta t,\Delta t) \\ \Delta t & 2\Delta t & x(\Delta t,2\Delta t) \\ \vdots & \vdots & \vdots \\ (N-1)\Delta t & (N-1)\Delta t & x((N-1)\Delta t,(N-1)\Delta t) \\ (N-1)\Delta t & 360^\circ & x((N-1)\Delta t,360^\circ) \end{array}\right). \tag{3.10}$$

Using of this list, we can construct an interpolated function $x(t,t_0)$. In the following figure, Fig. 3.3 , the $3D$-plot of the interpolated function $x(t,t_0)$ is depicted. To locate the moment in time at which the electron returns to its initial position, $x=0$, we take a projection of the $x(t,t_0)$ function on the $x(t,t_0)=0$ plane (blue plane in Fig. 3.3). This projection is the intersection of two surfaces, surface $x(t,t_0)$ and the surface $x=0$. The intersection of the two surfaces is the curve depicted with a red colour which gives the *the recollision temporal coordinates*. The *recollision temporal coordinates* are the pairs of the ionization times

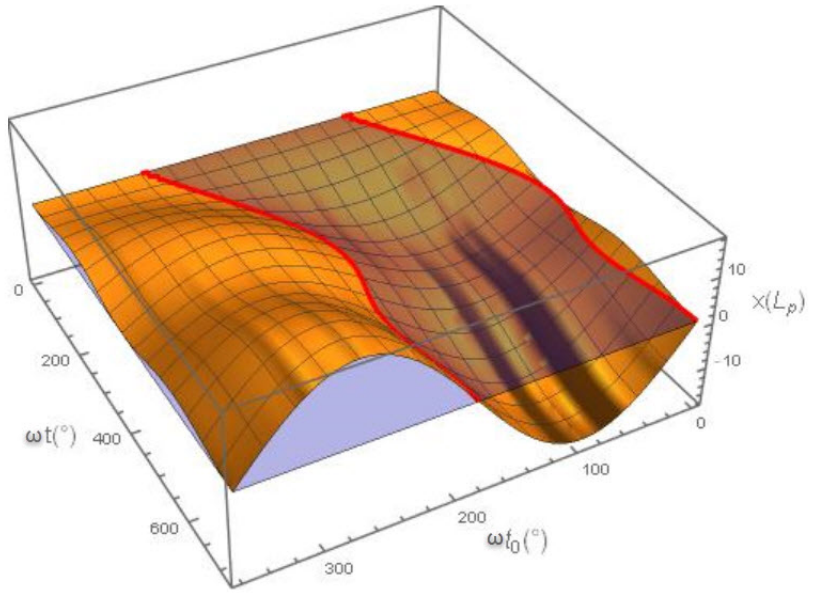

Figure 3.3: 3D-plot of the trajectories of the electrons $x(t,t_0)$ in one colour field under the initial conditions that its initial velocity and distance from the axis origin are zero. The blue plane corresponds to $x=0$, i.e. the distance of the electron from its initial position is zero. The red line corresponds to the recollision temporal coordinates, the moments in time in which the electron returns to its initial position. For $\mathcal{E}_0 = 10^8 V/cm$ and $\lambda = 1500nm$, $L_p \approx 0.8nm$ and $1^\circ \rightarrow t = 10^{-17}s$.

with the corresponding times at which the electron returned to its initial position t_R. In the following figure, Fig. 3.4, the recollision temporal coordinates of an electron in one colour field are shown. From this figure

it is clear that, there are moments in time in which the electron returns to the parent ion for a second, third time, etc. By changing the range of values for the propagating time of the electron, t_r, the second, third and

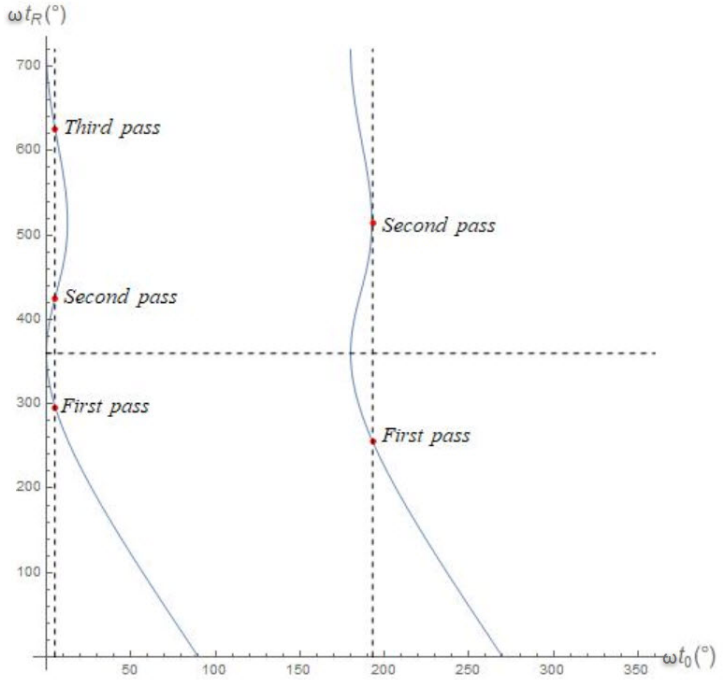

Figure 3.4: Plot of the recollision temporal coordinates of an electron in one colour field under the initial conditions that its initial velocity and distance from the origin are zero. The horizontal axis corresponds to the ionization time of an electron and the vertical axis corresponds to the returning time of the electron to its initial position. For every ionization time, the maximum number of times that an electron can return to the parent ion after one laser period, is one (vertical dashed line corresponds to $t_R = 360°$). If the electron does not interact with the parent ion, then the number of times that an electron can return to it in the next period of the laser, depends on the ionization moment. For $\mathcal{E}_0 = 10^8 V/cm$ and $\lambda = 1500nm$, $1° \rightarrow t = 10^{-17}s$.

so fourth time that an electron returned to its initial position can be computed. But, by changing the range of the propagating time, a different number of passes of the electron from its initial position are calculated for each ionization moment. In Fig. 3.4 two vertical lines have been drawn. The first one shows that in the $t_R \in (0°, 720°]$ range, an electron liberated at time $t_0 = 5°$ returns to its initial position three times while an electron liberated at time $t_0 = 193°$ returns to its initial position 2 times.

Later, the points on the Fig. 3.4 were extracted and put in a different list. The first column hold the information on the ionization time, the second column hold the information on the first time that the electron returned to its initial position, the third one hold the information on the second time that the electron returned to it, the forth column hold the information on the third pass of the electron from its initial position and so on. In a matrix representation, the new list took the form,

$$\left(\begin{array}{cccc} t_0 & t_r(1^{st}\ pass) & t_r(2^{nd}\ pass) & \cdots \\ \hline 0 & t_r|_1 & t_r|_2 & \cdots \\ \Delta t & t_r|_1 & t_r|_2 & \cdots \\ \vdots & \vdots & \vdots & \ddots \end{array}\right). \tag{3.11}$$

Finally, this list was used in order to calculate the kinetic energy of the returning electrons. This was done

by inserting the returning times to the numerical solution for the velocity of the electron.

3.1.4 Kinetic energy distribution of the returning electrons, $E.D.R.E.$

In the previous subsections, we have calculated t_r, and have presented the method through which it is evaluated. Initially the electron was assumed to be emitted from the parent ion at time t_0 (ionization moment), with zero initial velocity on the axis origin. After that, it propagated in the laser field, gained some kinetic energy and later on, at time t_R, returned to the parent ion. But the kinetic energy of the returning electrons, with respect to a time parameter (ionization or recombination moment), cannot give us sufficient information for the analysis of some experimental results. In a realistic experiment, several trajectories lead to rescattering of the electron from the ionic core. Additionally, every kinetic energy above a threshold will contribute to rescattering ionization. Thus, it is useful to calculate the kinetic energy spectrum of the electrons at the moment of their return to their initial position. To do so, the kinetic energy of the returning electrons ($m\dot{x}^2/2$) should be calculated.

The spectrum of the returning electrons is given by the kinetic Energy Distribution of the Returning Electron, $E.D.R.E.$. $E.D.R.E.(K) \times dK$ informs us about the "probability" of an electron returning to the parent ion with kinetic energy in the range, $[K, K + dK]$ and it is affected by two factors. The first factor has to do with the probability of an electron being emitted by the system at some particular time(s) while the second factor has to do with the shape of the electromagnetic field. The $E.D.R.E.$ can be derived via the following consideration.

Suppose that some electrons are liberated in a time interval Δt_0, propagate in the laser field and finally, return to their initial position with some kinetic energy in the range $[K, K+\Delta K]$. The probability of an electron returning to the parent ion with some kinetic energy in that range should be proportional to the **total** probability that the electron had of being liberated in the first place (in the time interval Δt_0).

Practically to numerically evaluate the $E.D.R.E.$ under this consideration, we discretize the returning kinetic energy vs time plot with a fixed time step δt_0 and sum all the ionization probabilities that correspond to a kinetic energy in the intervals $[K_i, K_i + \Delta K]$ to construct a weighted histogram[3]. The histogram is then smoothed out so that it becomes a function.

From a mathematical point of view, the above consideration is expressed through the following formula

$$E.D.R.E.(K) \times dK \;\propto \sum_{i=\text{Branches 1, 2}} \int_{t_0^{(i)}}^{t_0^{(i)}+dt_0^{(i)}} \mathcal{W}(t^{(i)})dt^{(i)}, \tag{3.12}$$

where W denotes the ionization probability rate. The $\sum_{i=\text{Branches}}$ has been used to take into account the fact that there are more than one time intervals from which the electron's returning kinetic energy is in the range $[K, K + dK]$ (long and short trajectories).

To make the form of the mathematical formula eq. 3.12 clear, in Fig. 3.5, two time intervals are highlighted. Both intervals correspond to electrons that return to their parent ion position with kinetic energy in the range $[0.5 \times U_p, U_p]$. Yet the two time intervals are not equal. The first time interval is approximately equal to $\Delta t_0^{(1)} \approx 1.5^\circ$ while the second time interval is approximately 4 times longer, $\Delta t_0^{(2)} \approx 7.5^\circ$. This is the reason that in eq. 3.12, two different differential time elements are being used $\left(dt_0^{(1)},\ dt_0^{(2)}\right)$. Thus, the two integrals are being used to take into account the total probability that the electrons had in being emitted in both time intervals.

Yet both time parameters $(t_0^{(1)},\ t_0^{(2)})$ are functions with respect to the returning kinetic energy.

[3]the sum of all the integral should be the $[0, K_{max}]$ interval

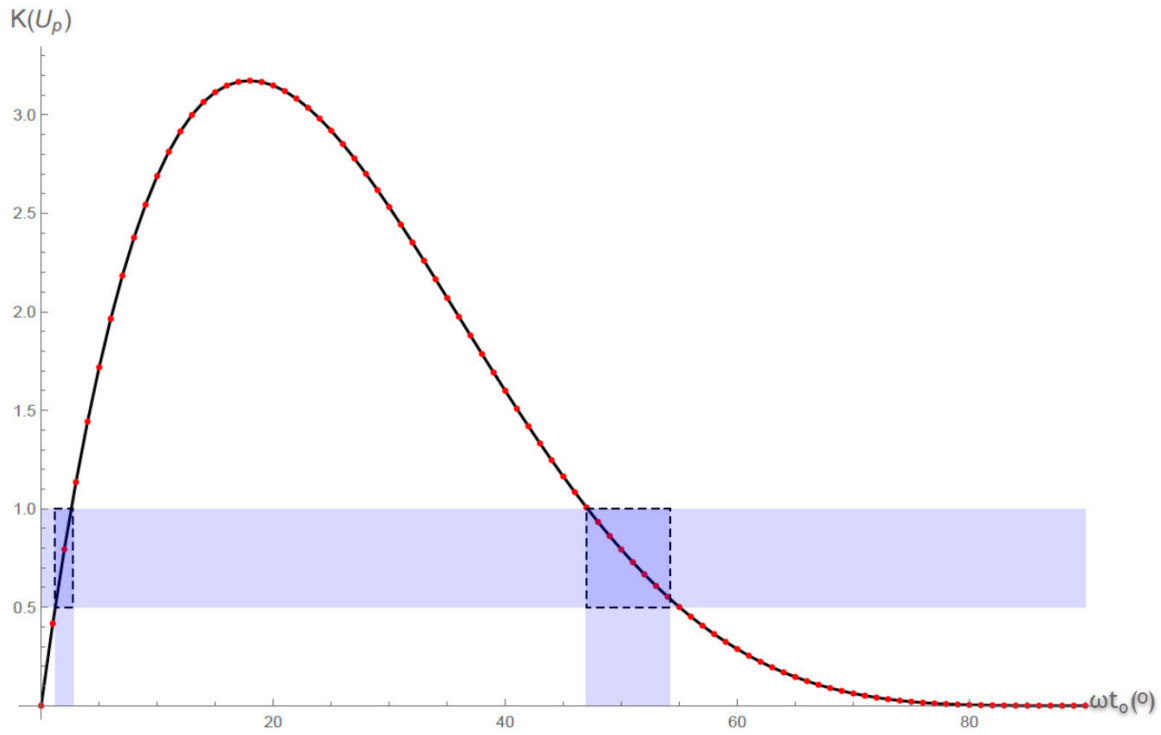

Figure 3.5: Plot of the Kinetic energy of the returning electrons as a function of the ionization moment. The red plot-markers correspond to some equally time spaced ionization moments. As you can see, more than one time intervals correspond to a given range of the kinetic energy of the returning electron and the density of the numerical data is not the same for each one. The mean value of the slope of the returning kinetic energy function in a given time interval is qualitatively inversely proportional to the density of the numerical data.

By denoting with " f " the function that gives us the kinetic energy of the returning electrons with respect to the ionization moment, i.e. $K = f(t_0)$, and by denoting with " f_i^{-1} " the function that gives us the $i-th$ ionization moment with respect to the kinetic energy of the returning electron, i.e. $t_0^{(i)} = f_i^{-1}(K)$, eq. 3.12 is brought to the final form:

$$E.D.R.E.(K) \times dK \propto \sum_{i=\text{Branches}} \int_{t_0^{(i)}}^{t_0^{(i)}+dt_0^{(i)}} \mathcal{W}(t^{(i)})dt^{(i)} \overset{dt_0^{(i)}\to 0}{\approx} \sum_{i=\text{Branches}} \mathcal{W}(t_0^{(i)})dt_0^{(i)} \tag{3.13a}$$

$$= \sum_{i=\text{Branches}} \mathcal{W}(f_i^{-1}(K))\frac{dt_0^{(i)}}{dK}dK = \sum_{i=\text{Branches}} \mathcal{W}(f_i^{-1}(K))\frac{df_i^{-1}}{dK}dK \tag{3.13b}$$

$$= \sum_{i=\text{Branches}} \frac{\mathcal{W}(f_i^{-1}(K))}{f'(f_i^{-1}(K))}dK = \sum_{i=\text{Branches}} \frac{\mathcal{W}(f_i^{-1}(K))}{K'(t_0^{(i)}(K))}dK \to \tag{3.13c}$$

$$\boxed{E.D.R.E.(K) \propto \sum_{i=\text{Branches}} \frac{\mathcal{W}(f_i^{-1}(K))}{f'(f_i^{-1}(K))}} \tag{3.13d}$$

Based on the formula above (and since $K = f(t_0)$,) the energy density of the kinetic electrons, $E.D.R.E.(K)$, can be thought as having the **qualitative** form:

$$E.D.R.E. \propto \frac{ionization\ probability}{|K'(t_0)|} \propto \frac{ionization\ probability}{|K'(t_R)|}. \tag{3.14}$$

This is a result, which give insight in the form of $E.D.R.E.(K)$. Due to the denominator, the local maxima of the $E.D.R.E.$ correspond to those values of the returning kinetic energy, for which the $K(t_0)$ and $K(t_R)$ plots have local extrema, $(K'(t_0) = K'(t_R) = 0$[4]$)$. By taking a look on Fig. 3.2, the maximum values of the $E.D.R.E.(K)$ for a one colour field, are anticipated for the values $K = 0$ and $K = 3.17 \times U_p$.

To make the procedure in which the $E.D.R.E.$ is evaluated clear, in Fig. 3.6 the steps of of the process for a simple sinusoidal wave are depicted. Below these steps are listed and explained.

1. Calculate the inverse function $t_0 = f^{-1}(K)$ of the kinetic energy of the returning electrons (panel (a) in Fig. 3.6).

2. Because (in this case) there are two branches, the inverse function is multivalued. To work with it, the inverse function has to be broken up in two single valued functions, $t_0^{(1)} = f_1^{-1}(K)$, $t_0^{(2)} = f_2^{-1}(K)$ (panel (β) in Fig. 3.6).

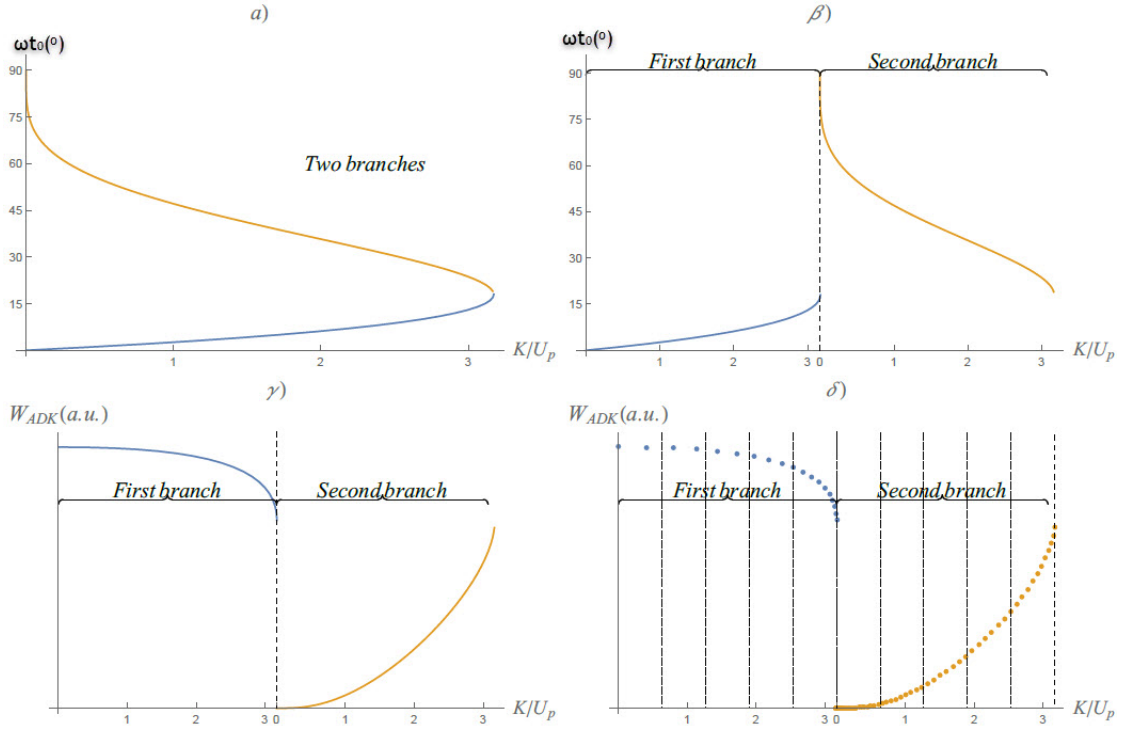

Figure 3.6: Steps of the procedure for evaluating the kinetic energy of the returning electrons, $E.D.R.E.$., in one colour electromagnetic field.

3. To take into account the fact that the probability of an electron being ionized at any moment in time is not a constant, the vertical axis should be changed into the ionization probability, $\mathcal{W}(t_0^{(1)})$, $\mathcal{W}(t_0^{(2)})$ (the weighting function) (panel (γ) in Fig. 3.6).

4. Since the kinetic energy of the returning electrons is a non analytical function, we only know the values for some specific ionization moments. If these ionization moments are equally separated in time and we divide the entire range of the arguments of the function into a series of equal intervals (panel δ) in Fig. 3.6 and Fig.3.5), the number of points in each interval will not be the same. This fact is reflected

[4]It is important to note that when $K'(t_0) \to 0$, we do not get $E.D.R.E. \to \infty$. This is happening since it is the $E.D.R.E. \times dK$ quantity which is being evaluated directly and not solely the $E.D.R.E.$. When $K'(t_0) \to 0$, $dK \to 0$ as well and this is what "normalizes" the $E.D.R.E.$ value.

in the term of the denominator, in eq. 3.13a . The total probability of an electron having a kinetic energy in the range $[K, K + \Delta K]$ is proportional to the sum of the values of the ionization probability function for each point in this interval.

The smaller the interval ΔK the more accurate the $E.D.R.E.(K)$ spectrum. As the kinetic energy interval is decreased, the total number of points needed to carry on this process is increased. This is done by decreasing the time interval between the ionization moments and thus the time needed for the evaluation of $E.D.R.E.$ is increased. To calculate the $E.D.R.E.$ in this thesis, the time interval between each ionization moment was equal to $0.001°$, i.e. a total of 36×10^4 returning kinetic energies have been evaluated.

Fig. 3.7, shows the *energy distribution of the returning electrons, E.D.R.E.*, for two cases. For the computation of the blue curve, the probability of an electron being liberated at any moment in time was approximated to be given by the formula 2.4 (ADK theory) , while for the orange curve, the probability of an electron spawned at any moment was taken to be the same (for example, $\mathcal{W} \to 1$). In this figure, both distributions have been plotted, in order to make an important comment.As it can be seen in this graph, , in both cases, the position in which there is a maximum is the same. Thus, we can deduce that, the qualitative form (position of the maximum of the spectrum) of the plot is heavily depended on the form of the kinetic energy distribution, which in its turn is moulded by the electromagnetic field of the external source. This characteristic of the $E.D.R.E.$ holds no matter the shape of the pulse (that produces the returning kinetic energy function).

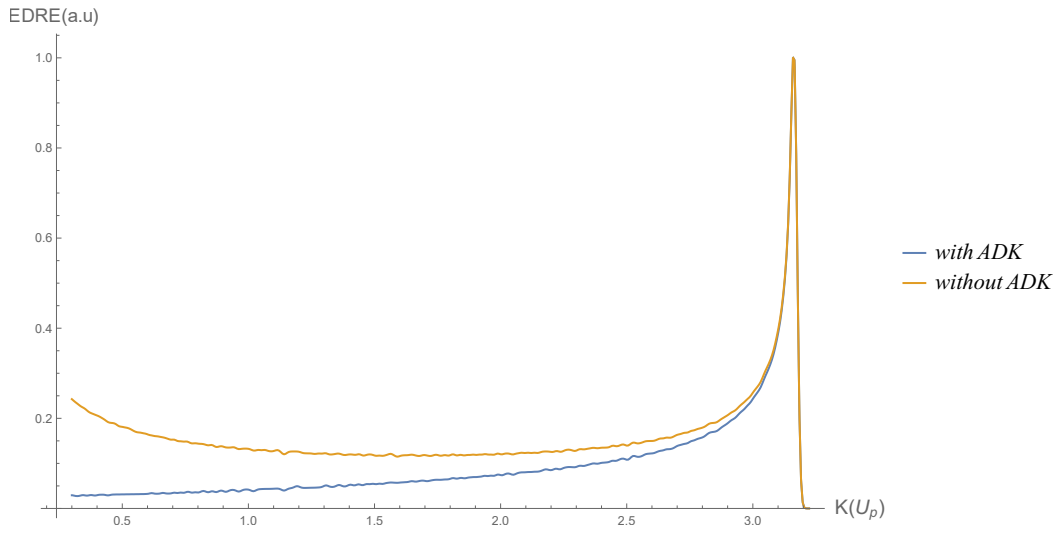

Figure 3.7: Kinetic energy distribution of the electrons when returning to their original positions, under the influence of a one-color field, assuming that α) the probability of an electron being spawned at any given moment is given by the ADK-theory (blue curve) and β) the probability of an electron being emitted at any given moment is one (1) (orange curve). Comparing the two curves, it is clear that the **qualitative** form of the $E.D.R.E.$ does not heavily depend on the ionization probability. It is the **quantitative** part of the $E.D.R.E.$ that depends on it. For the computation of both curves small values of the returning energy have been discarded ($K < 0.1 \times U_p$). Both distributions are rescaled so that its maximum value to be equal to one, $max(EDRE) = EDRE|_{K=3.17U_p} = 1$

To make the examination of the $E.D.R.E.$ for a one colour field complete, in Fig. 3.8, the ionization probability rate, $\mathcal{W}_{ADK}$, as a function of the candidate ionization moment t_0 has been plotted. In order to make this graph, the 2.4 formula was used, by setting the intensity of the electromagnetic field to be equal with $\mathcal{I} = 10^{14}\ W/cm^2$. The vertical axis has been normalized with respect to its maximum value, the vertical blue columns correspond to the ionization time intervals in which the kinetic of the returning electrons

lied in the range $[(1-\frac{1}{320})K_{max}, K_{max}]$ and the horizontal orange columns show the ionization probability rates that correspond to these ionization time intervals. As you can see, the ionization probability rate in the proximity of maximum returning kinetic energy is high enough, so that the quantitative form (blue line in Fig. 3.7) of the $E.D.R.E.$ does not differ significantly from its qualitative form (orange line in Fig. 3.7).

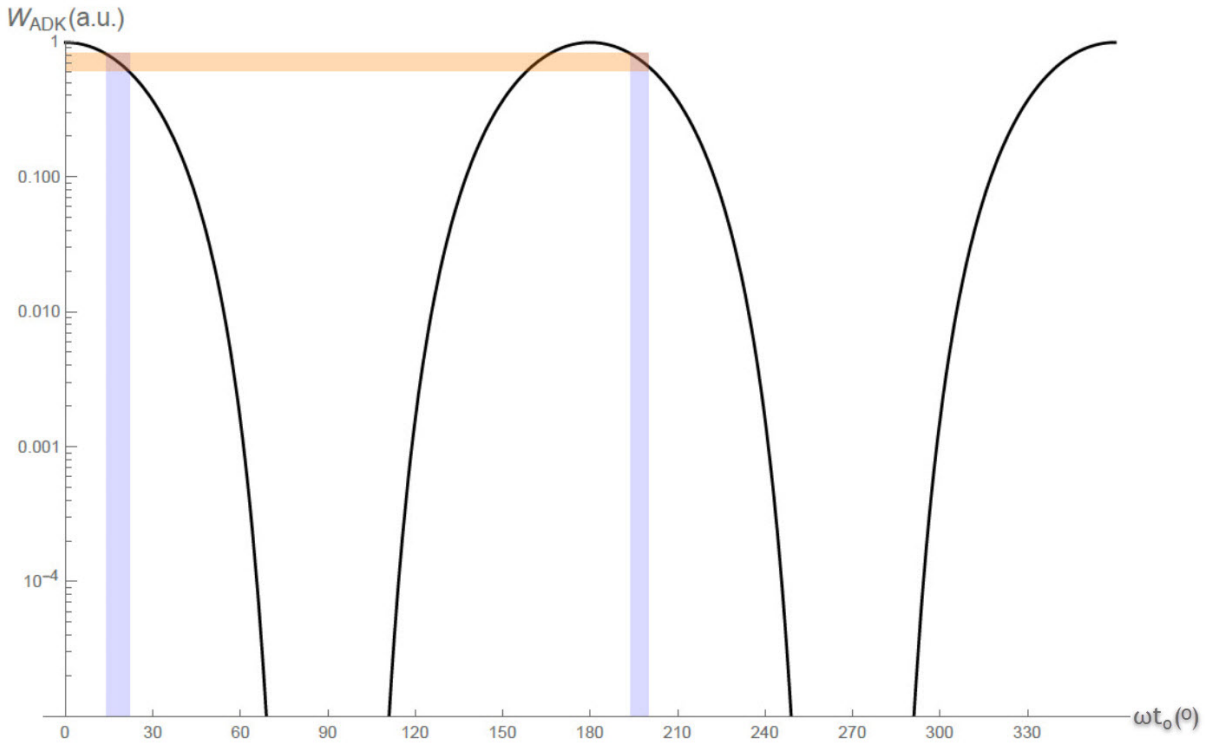

Figure 3.8: Ionization probability rate as a function of the ionization moments t_0 for a cos −like electromagnetic field. The vertical blue columns correspond to the ionization time intervals in which the kinetic of the returning electrons lied in the range $[(1-\frac{1}{320})K_{max}, K_{max}]$ and the horizontal orange columns show the ionization probability rates that correspond to these ionization time intervals. For the creation of this graph, the ionization probability rate given by the $ADK-$theory, $\mathcal{W}_{ADK}$, by setting the intensity of the laser field to be equal to $\mathcal{I} = 10^{14}\ W/cm^2$.

It has to be mentioned that in order to evaluate the distributions, the data regarding some small values of the Kinetic energy of the returning electrons were discarded. This was done because when small values of K were taken into account for the evaluation of the $EDRE$, the results exhibit a strong peak around zero kinetic energies. This is non-physical for most of the cases, since electrons that never return to the nucleus are erroneously counted as electrons with zero kinetic energy. Additionally, for the small number of electrons that indeed return to the nucleus with miniscule kinetic energies (our choice was to discard all the data with $K < 0.1 \times U_p$). Yet, this is not a problem since the returning electrons that have gained a small amount of kinetic energy (less than the energy ionization threshold), do not contribute to the rescattering process. The distributions have been normalized with respect to their maximum value which appears for the maximum kinetic energy value,

$$K_{max} \approx 3.17 U_p. \tag{3.15}$$

To qualitatively understand the reason that the maximum value of the $E.D.R.E.$ appears in that particular position, it is important to note that the value K_{max} corresponds to a point in the $K(t_0)$

function at which the first derivative approaches zero. This is because the probability of an electron having a kinetic energy in the range $[K, K + dK]$ is proportional to the corresponding time interval $[t_0, t_0 + dt_0]$ from which it came from[5].

In Fig. 3.5, the time interval, Δt, (ionization time interval) in which $K \in [U_p, U_p + \Delta K]$ is smaller than the time interval in which, for example, $K \in [0, \Delta K]$ (tail of the kinetic energy of the returning electrons, see Fig. 3.5). This is happening because for small energies, the $K(t_0)$ is practically a constant, i.e. $K'(t_0) \approx 0$ (eq. 3.14).

3.2 Dynamics in a two-colour field

The second step is to study the dynamics in a two-colour field. More specifically, in this part of the thesis, the dynamics of an electron in electric field composed of the fundamental and second harmonic of a laser around 800 nm will be studied.

In this case, the electric field amplitude, $\mathcal{E}_{tot}(t)$ takes the form

$$\mathcal{E}_{tot}(t) = \mathcal{E}_1 \cos\left(\omega\left(t + t_0\right)\right) + \mathcal{E}_2 \cos\left(2\omega\left(t + t_0\right) + \varphi\right) \tag{3.16a}$$

$$\equiv \mathcal{E}_0 \left\{\cos\left(\omega\left(t + t_0\right)\right) + \gamma \cos\left(2\omega\left(t + t_0\right) + \varphi\right)\right\}, \tag{3.16b}$$

where ω is the fundamental angular frequency, $\mathcal{E}_n$ denotes the electric field amplitude of each one of the sinusoidal waves, t_0 is the moment that the charged particle starts to experience the electric field and φ expresses the phase difference of the second harmonic component with respect to the fundamental harmonic at $t + t_0 = 0$.

In this case, the study of the dynamics of the electrons has two free parameters. The relative electric field strength of the 2ω-colour with respect the ω-colour, γ_2, and the phase difference of the second harmonic component with respect to the fundamental harmonic at time $t + t_0 = 0$, φ_2.

3.2.1 Equations of motion and cycle average kinetic energy

The trajectory of the charged particle can again be found by solving *Newton*'s second law of motion:

$$m\ddot{x} = q\mathcal{E}_{tot}(t), \tag{3.17}$$

Under the initial conditions that the charged particle starts its journey from the axes origin, with zero kinetic energy, the position of it at any given time, is given by:

$$x(t, t_0; \varphi, \gamma_2) = -\frac{q\mathcal{E}_0}{m\omega^2}\Bigg[\underbrace{\sum_{i=1}^{2}\left(\frac{\gamma_i}{i^2}\right)\cos\left(i\omega\left(t + t_0\right) + \varphi_i\right)}_{\text{Oscillating term}} + \underbrace{\sum_{i=1}^{2}\left(\frac{\gamma_i}{i}\right)\sin\left(i\omega t_0 + \varphi_i\right)\omega t}_{\text{Linear term}} - \underbrace{\sum_{i=1}^{2}\left(\frac{\gamma_i}{i^2}\right)\cos\left(i\omega t_0 + \varphi_i\right)}_{\text{Constant term}}\Bigg], \tag{3.18}$$

where $\gamma_1 = 1$, $\varphi_1 = 0$, $\varphi_2 \equiv \varphi$ and $\gamma_2 \equiv \gamma$.

The equation of motion (3.18) now consists of three terms. The oscillating term which indicates that the motion of the electron is not uniform, but rather that the electron is constantly pulled towards the

[5]The derivative of a function is nothing but the ratio of two differences. For the generation of the *E.D.R.E.*, the ratio that appears in the nominator is the difference between. By increasing the time interval which correspond to a particular fixed kinetic energy interval, the denominator increases and thus the derivative goes to zero.

direction of a point, which is moving with a constant velocity equal to (linear term)

$$u_{dr} = -\frac{q\mathcal{E}_0}{m\omega^2}\left\{\sin\left(\omega\left(t+t_0\right)\right)+\left(\frac{\gamma}{2}\right)\sin\left(2\omega\left(t+t_0\right)+\varphi\right)\right\}. \tag{3.19}$$

and a constant. Thus, the electron can be thought of as a particle that is oscillating around a moving point.

In the following figure (Fig. 3.9), some trajectories of an electron which has started its propagation with zero initial momentum have been plotted. The displacement of the charged particle is measured in ponderomotive length units[6] and the ratio between the electric field amplitude of the 2ω colour and the electric field amplitude of the fundamental is taken to be equal to 0.63 ($\gamma_2 = 0.63$). As it can be seen, depending on the ionization time, the electron can either return to its initial position or not.

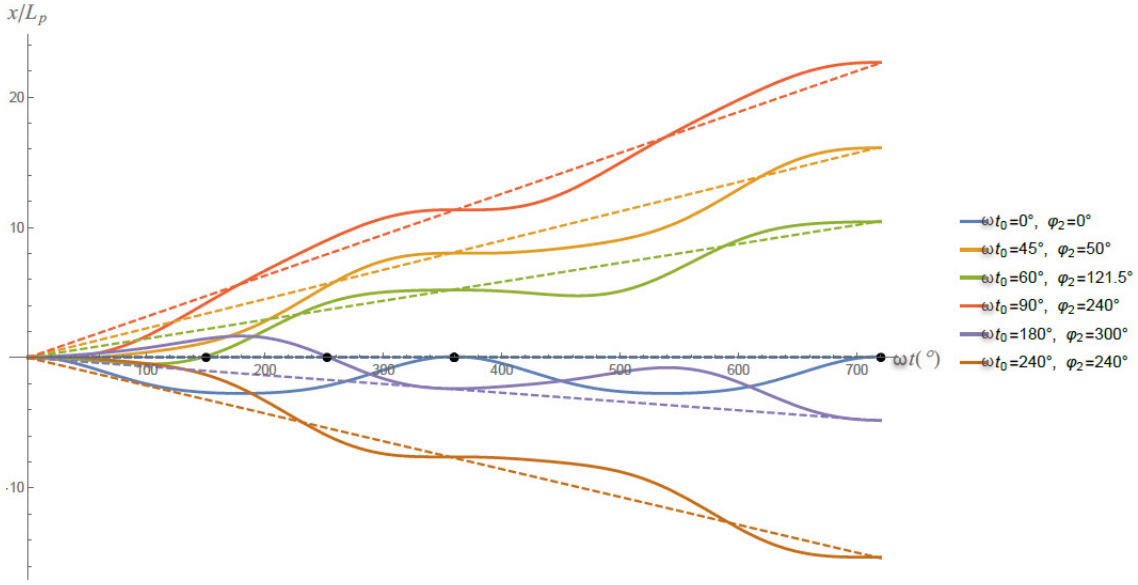

Figure 3.9: Trajectories of electrons, in a two colour field, $\omega/2\omega$, with the relative electric field ratio of the 2ω-field with respect the ω-field, γ, to be equal to 0.63, spawned at different times (t_0) and interacting with different shapes of the electric field (φ_2). The dashed lines indicate the uniform part of the displacement of the electron while the black dots denote the times at which some of the electrons return to their initial position. As an example, for $\mathcal{E}_0 = 10^8 V/cm$ and $\lambda = 1500nm$, $L_p \approx 0.8nm$ and $1^\circ \rightarrow t = 5\times10^{-15}\ s$.

In the case of a two-colour field, composed of the fundamental and the second harmonic of the laser, the cycle averaged kinetic energy of the electron over an optical period time period is equal to:

$$K_{\omega/2\omega} = \frac{1}{2}m\langle\dot{x}^2\rangle\Big|_t = \underbrace{\frac{q^2\mathcal{E}_0^2}{4m\omega^2}\left[1+\left(\frac{\gamma_2}{2}\right)^2\right]}_{U_p\leftarrow\text{Oscillatory term of eq.(3.18)}} + \underbrace{\frac{q^2\mathcal{E}_0^2}{2m\omega^2}\left\{\sin\left(\omega\left(t+t_0\right)\right)+\left(\frac{\gamma}{2}\right)\sin\left(2\omega\left(t+t_0\right)+\varphi\right)\right\}^2}_{\frac{1}{2}mu_{dr}^2\leftarrow\text{Linear term of eq.(3.18}}.^7 \tag{3.20}$$

The charged particle's kinetic energy is composed of two terms. The first term in the equation above,

[6] In the case of a two colour field,

$$L_p^2 \equiv \langle x_{osc}^2\rangle\big|_t = L_p^2(\omega)+L_p^2(2\omega) = \frac{q^2\mathcal{E}_0^2}{2m^2\omega^4}+\gamma_2^2\frac{q^2\mathcal{E}_0^2}{2m^2\left(2\omega\right)^4}.$$

[7] This result coincides to the result given in reference [27].

corresponds to the average kinetic energy due to the oscillating term in the equation of the motion. The second term comes from the linear term of eq. (3.18). This term is the net drift kinetic energy due to the drift momentum (the constant part of the momentum) of the charged particle, and in the case of the two-colour field, it also depends on the phase difference between the two colours, φ_2. This is another characteristic which indicates that the form of the kinetic energy of the returning electrons will depend on the φ_2 parameter

3.2.2 Kinetic energy and of the returning electrons and $E.D.R.E.$

In this paragraph, the form of the kinetic energy of the returning electrons as well as the corresponding energy distributions of the returning electrons will be discussed for a particular shape of a two colour field. The shape of the pulse has been chosen so that some more important qualities of the returning electrons can be clearly explained. For the generation of the data and figures used in this paragraph, the procedures studied in the 3.1.3. 3.1.4 sections of this thesis have been followed. It is important to note, that due to the presence of the additional electromagnetic field with angular frequency 2ω, the kinetic energy of the returning electrons is different from the one attained for the case of a single colour field. The kinetic energy depends heavily on the γ_2 and φ_2 parameters.

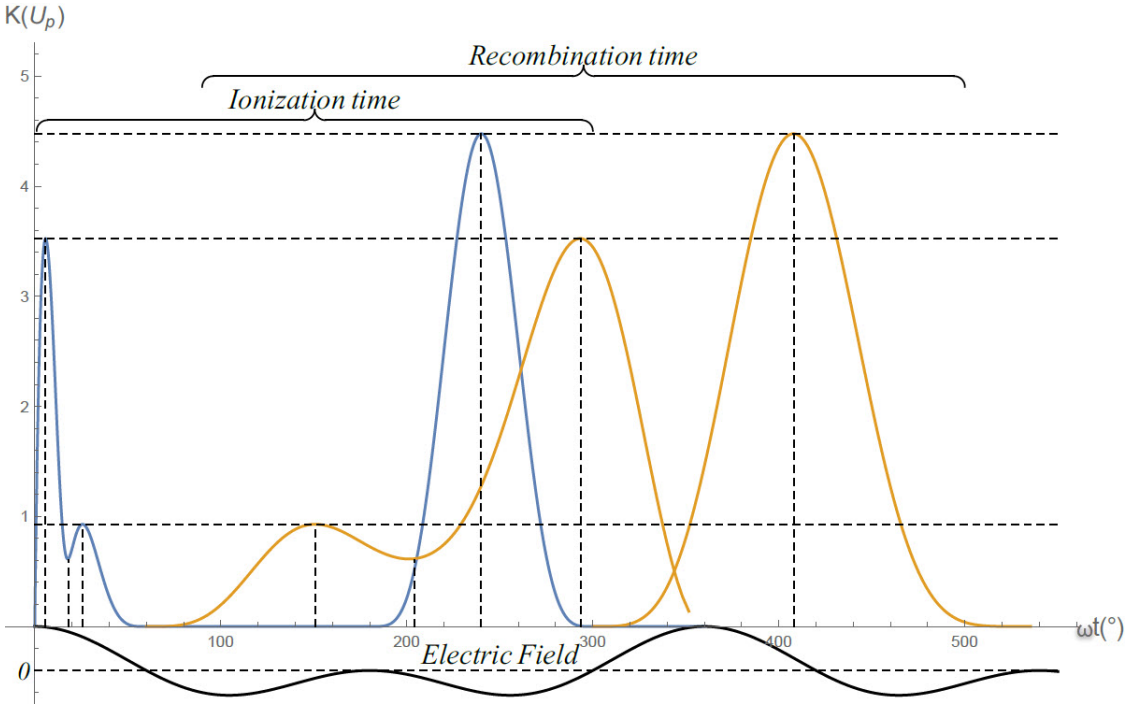

Figure 3.10: Plot of the kinetic energy of the electron when it returns at it's original position (position of the ion) under the influence of a two colour sinusoidal electric field. For this plot, the electric field amplitudes of the two fields are equal $\gamma_2 = 1$ and there is zero phase difference between them, $\varphi_2 = 0$. The graph has been plotted with respect to two parameters, the time in which the electron starts experiencing the electric field (blue curve) and the time on which the electron returned to its parent ion (orange curve). In the same graph, the form of the electric field has been included in order to give a clearer picture of the results. The vertical dashed lines mark the local maxima and minima of the function being plotted whereas the horizontal lines indicates their corresponding returning energy value and the zero value of the electric field. As an example, for $\mathcal{E}_0 = 10^8\ V/cm$ and $\lambda = 1500\ nm$, $K_p \approx 3\ eV$ and $1^\circ \rightarrow t = 5 \times 10^{-15}\ s$.

In Fig. 3.10, the kinetic energy of the returning electrons with respect to the *ionization time* t_0 and the *recombination time* $t_R = t_0 + t_r$, for the values $\gamma_2 = 1$ and $\varphi_2 = 0$, has been plotted. t_r is the

time interval that the electron needed to return to its parent ion. The plot range for the ionization time is twice as large as the corresponding plotting range in the single colour case and this is because of the lack of symmetry in the form of the two-colour field.

In this case, there is not a single local maximum in the kinetic energy of the returning electrons plot. This is a general characteristic in the case of a two colour field which makes the absolute distinction between long and short trajectories impossible. For the shake of completeness, it should be mentioned that the three local maxima appearing for the ionization times $t_0 = 27^\circ,\ 5^\circ$ and 240° are taking the corresponding values $K = 0.9,\ 3.5,\ 4.5 \times U_p$. The local minimum $K = 0.6 \times U_p$ corresponds to the ionization time $t_0 = 18^\circ$.

In the following figure, Fig. 3.11, the *energy distribution of the returning electrons, E.D.R.E.*, has been plotted, for two cases.

1. For the computation of the blue curve, the probability of an electron being liberated at any moment in time was approximated to be given by the formula 2.4 (ADK theory).

2. For the computation of the orange curve, the probability of an electron spawned at any moment was taken to be the same (for example, $\mathcal{W} \to 1$).

By comparison of the two curves, it is clear that the **qualitative** (position of the local maxima in the plot) form of the $E.D.R.E.$ depends on the shape of the ionization field (and not the numerical value of the electric field amplitude), while the magnitude of these peaks also depends on the ionization probability at the time of ionization (i.e. depends on the electric field amplitude at the moment of ionization)

In both cases, the $E.D.R.E.$ of a sinusoidal two colour wave with $\varphi_2 = 0,\ \gamma_2 = 1$ is characterized by four peaks. The peaks appear for those returning kinetic energies that in the $K(t_0)$ and $K(t_r)$ plot there is a local minimum or maximum. Moreover, the maximum values in the $E.D.R.E.$ plot appear for the returning energies $K = 0.6,\ 0.9 \times U_p$. This is happening because, those particular energies correspond to a swallow valley and a non sharp hill, in the $K(t_0)$ plot. Mathematically, the appearance of these local maxima is to be expected due to the denominator in eq. 3.14 in the 3.1.4 paragraph of this thesis. For local minima or maxima in the kinetic energy plot, the denominator goes to zero and thus the $E.D.R.E.(K)$ takes some very large values.

However, in contrast with the case of a simple one colour field (see Fig. 3.7) the ionization probability rate makes significant differences appear between the two $E.D.R.E.$ plots (Fig. 3.11). Even thought the position of the local maxima do not differ, the relative magnitude of them has changed significantly. To understand this different behaviour, in Fig. 3.12 the ionization probability rate , $\mathcal{W}_{ADK}$ has been plotted as a function of the ionization time, t_0. In order to produce this, the 2.4 formula was used, by setting the intensity of the electromagnetic field to be equal with $\mathcal{I} = 10^{14}\ W/cm^2$. The $\mathcal{W}_{ADK}$ has been multiplied with a constant so that the maximum value of the plot in the $t_0 \in [0, 360^\circ]$ to be equal with one. In the following, we are going to use the abbreviations: $K_{min}^{\text{peak}} = 0.6 \times U_p$ and $K_{max}^{\text{peak}} = 4.5 \times U_p$.

In Fig. 3.12 the vertical blue column correspond to the ionization time intervals in which the returning kinetic energy lied in the range $[K_{max}^{\text{spike}} - 0.01 \times U_p, K_{max}^{\text{spike}}]$,while the red vertical columns correspond to the ionization time intervals in which the kinetic energy of the returning electrons lied in the range $[K_{min}^{\text{spike}}, K_{min}^{\text{spike}} + 0.05 \times U_p]$. The horizontal columns show the ionization probability rates for the corresponding ionization time intervals. As you can see, there are five time intervals which contribute to the $E.D.R.E.(K_{min}^{\text{peak}})$ [8]) while there is only one which contributes to the $E.D.R.E.(K_{max}^{\text{peak}})$ [9]. Thus, in the plot of the kinetic energy of the electron which return to the ion's position (see Fig. 3.10), there are five ionization

[8] centred at $1^\circ,\ 16^\circ,\ 33^\circ,\ 205^\circ$ and 275° and denoted by $\Delta t_{min}^{(i)},\ i = 1, \cdots, 5$ respectively

[9] centred at 240° and denoted by Δt_{max}

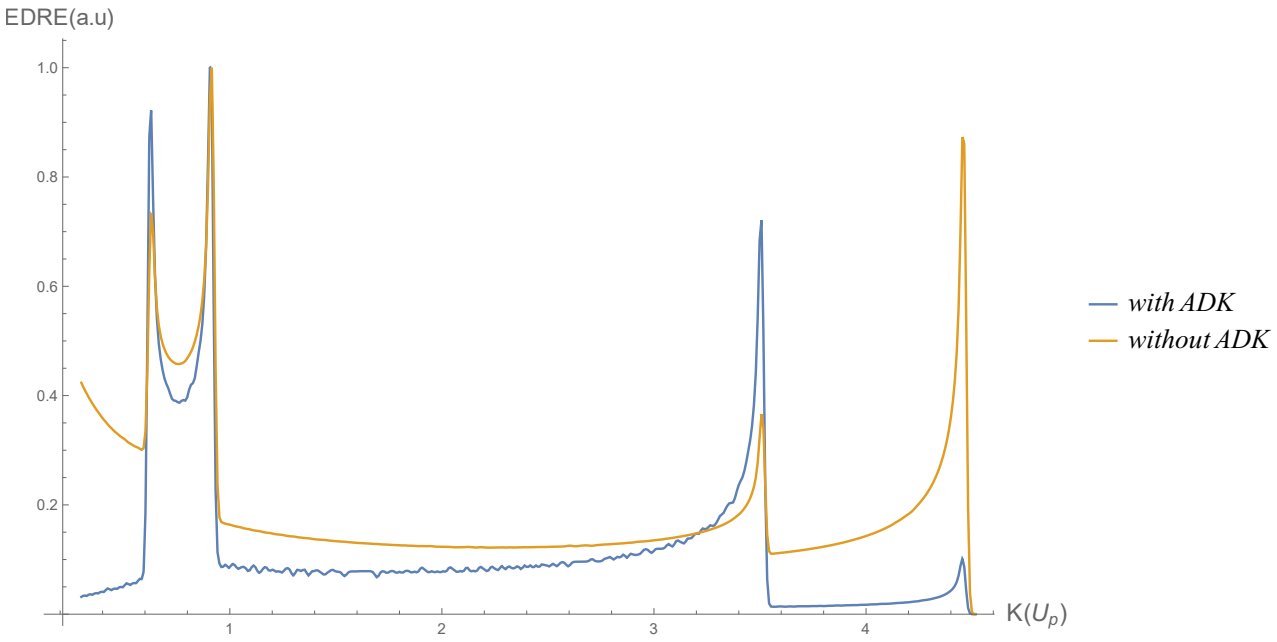

Figure 3.11: Kinetic energy distribution of the returning electron in two- colour field, assuming that α) the probability of an electron being spawned at any given moment is given by the $ADK-$theory (blue curve) and β) the probability of an electron being emitted at any given moment is the same (orange curve). The electric field amplitudes of the two fields are equal $\gamma = 1$ and there is zero phase difference between them, $\varphi = 0$, while the intensity due to the fundamental frequency of the laser field was set to be equal with $\mathcal{I} = 10^4\ W/cm^2$. Comparing the two curves, it is clear that the **qualitative** form (position of peaks) of the $E.D.R.E.$ does not heavily depend on the ionization probability. It is the **quantitative** part of the $E.D.R.E.$ that depends on it. For the evaluation of this distribution, small values of the returning energy have been discarded. The distribution is normalised with respect to its maximum value, $max(EDRE) = EDRE|_{K=0.9\times U_p}$. The four local maxima in the graph correspond to the local maxima and local minimum of the $K(t_0)$ and $K(t_R)$ plots.

moments for which the returning kinetic energy is equal to K_{min}^{peak} while there is only one ionization moment which results in the kinetic energy of the returning electron to be equal with K_{max}^{peak}.

Even though each of the time intervals, which contribute to the $E.D.R.E.(K_{min}^{\text{peak}})$ value, is narrower than the time interval which is responsible for the $E.D.R.E.(K_{max}^{\text{peak}})$ value ($\Delta t_{min}^{(i)} < \Delta t_{max}$), the sum of these intervals is greater. As a matter of fact, the time interval $\Delta t_{min}^{(1)} + \Delta t_{min}^{(2)} + \Delta t_{min}^{(3)}$ is a little longer than the Δt_{max} interval. Moreover, the probability of an electron being liberated in any of the $\Delta t_{min}^{(1)},\ i = 1,\ 2,\ 3$ time intervals is greater than the probability of an electron being liberated in the Δt_{max} interval (in Fig. 3.12, the first time intervals marked with red color have higher ionization probability rates that the time intervals marked with red color). So, the total ionization probability for the first case is greater than the total ionization probability for the second case. As a result, the value of $E.D.R.E.(K_{min}^{\text{peak}})$ is expected to be greater than the $E.D.R.E.(K_{max}^{\text{peak}})$.

The discussion above, has made clear, that the fact, that there are some preferable ionization time moments, has increased the value of the ratio: $E.D.R.E.(K_{min}^{\text{peak}})/E.D.R.E.(K_{max}^{\text{peak}})$. As a result, the relative magnitude of the last local maximum with respect to the first one should be increased (blue line in Fig. 3.11). Overall, we can verify is that the ionization rate cannot alter the positions of the local maxima in the $E.D.R.E.$ plot. Nevertheless, the ionization probability can significantly alter the ratios between the values of the $E.D.R.E.$ at every peak.

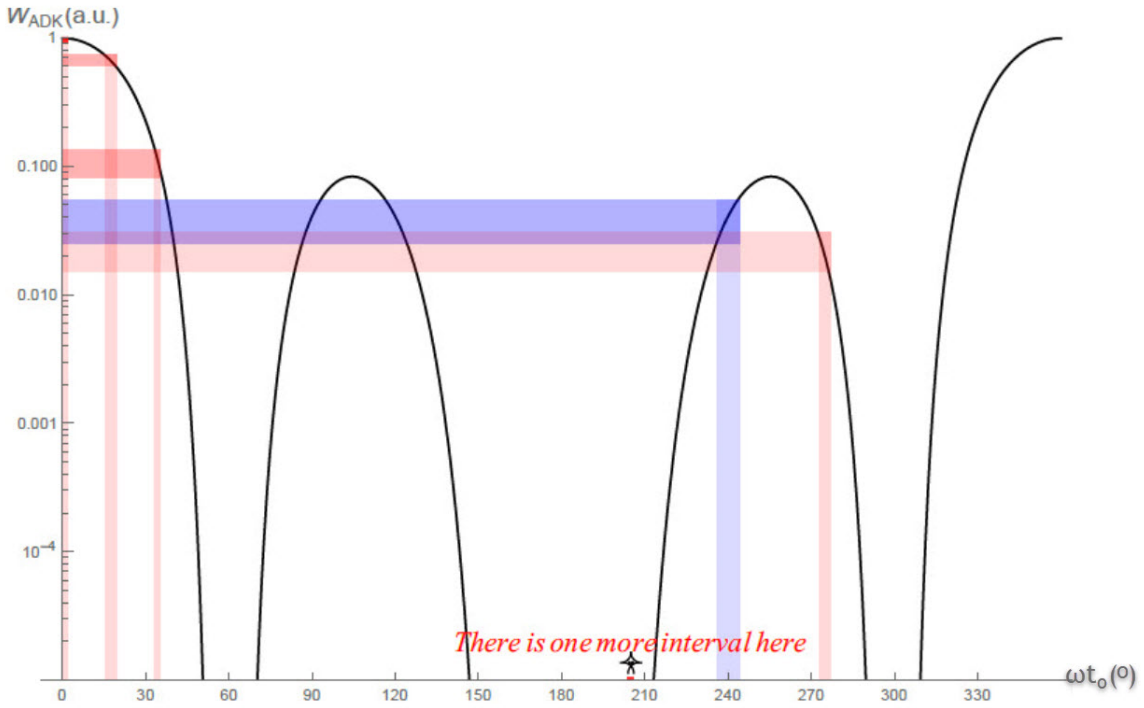

Figure 3.12: Ionization probability rate as a function of the candidate ionization moments t_0 for a two-colour continuous electromagnetic field. For the creation of this graph, the ionization probability rate given by the $ADK-$theory was used, $\mathcal{W}_{ADK}$, by setting the intensity of the fundamental harmonic of the laser field to be equal to $\mathcal{I} = 10^{14}\ W/cm^2$. The electric field amplitudes of the two fields are equal in strength, $\gamma = 1$, and the phase difference between the two of them is equal to zero.

3.2.3 Optimization for generation of the narrowest kinetic energy distribution of the returning electrons distribution

In the last two paragraphs of this chapter, I examine the dynamical behaviour of emitted electrons experiencing the force exerted on them by an external laser field. The trajectories of the electrons heavily depend on the moment in which the system is ionized. Different ionization moments, result in different trajectories of the electrons. While some of the electrons return to their original position there are some other ones that do not.

The two free parameters of the dichromatic pulse, φ and γ, have a strong effect on the dynamics of the problem. Those two parameters were studied in order to examine if a narrow $E.D.R.E.$ can be achieved. In this paragraph, a detailed discussion on a laser pulse which is optimal with respect to the creation of a narrow E.D.R.E. will be made.

With the graphical solving method that was presented in section 3.1.3, we were able to examine a large variety of $\omega/2\omega$ fields and identify fields for generating the narrowest rescattering kinetic energy distribution possible. In Fig. 3.13 the $E.D.R.E.$, is plotted as a function of the phase difference between the two colours. For this figure the intensity of the fundamental harmonic of the laser field was set to be equal with $\mathcal{I}_\omega = 10^{14} W/cm^2$, while $\gamma = 0.45$. For the calculation of the plots for the rescattering energies distributions ($E.D.R.E.$), the probability of an electron being ionized at any moment in time was assumed to be given by the 2.4 formula. As you can see, for two characteristic values of the phase difference between the two colours, the $E.D.R.E.$ presents a single local maximum which makes a distinction. For a single local

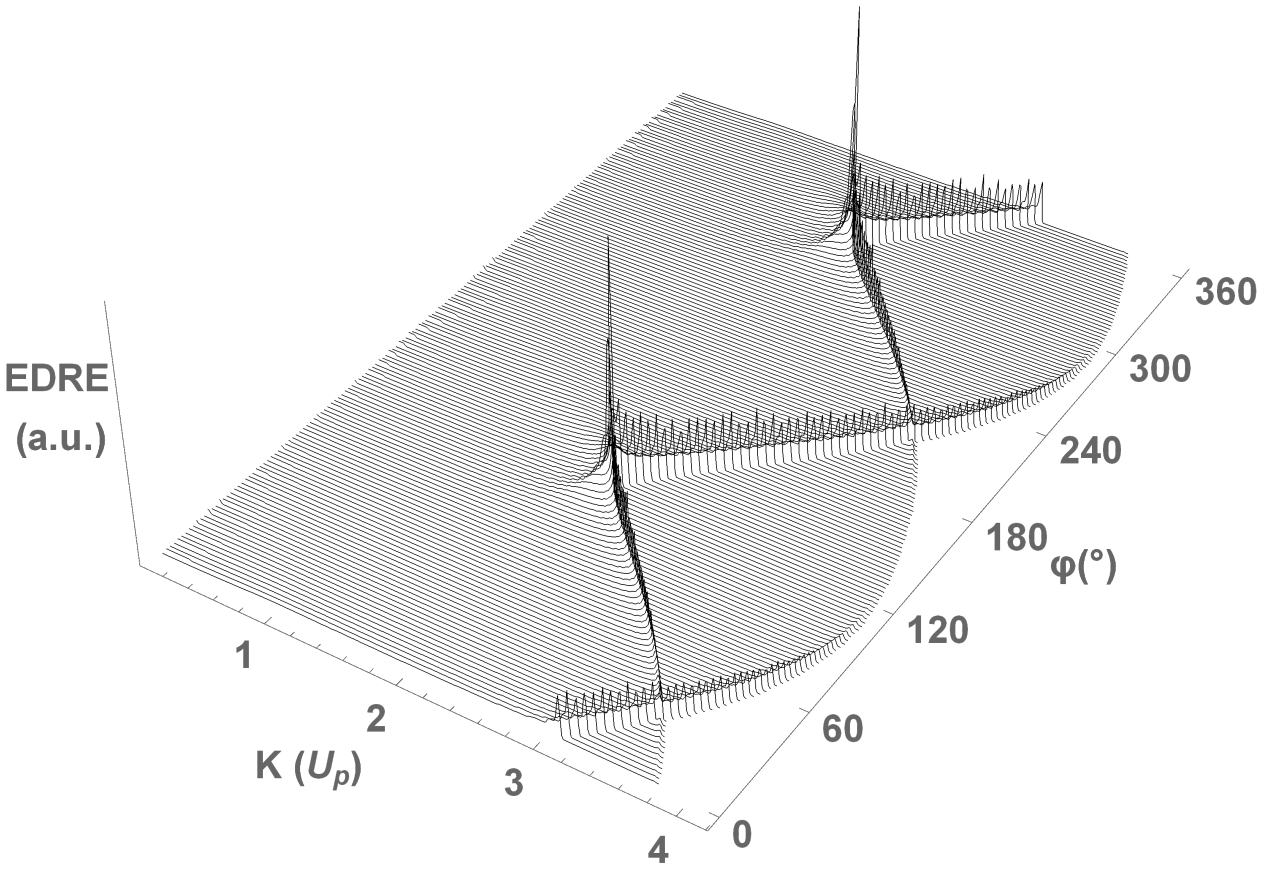

Figure 3.13: $3D$ plot of the Kinetic energy distribution of the returning electron, $E.D.R.E.$, in two colour field as as function of the returning energy and the phase difference between the two colours. To produce this graph, the ratio of the electric field amplitudes of the two fields is set to be equal to $\gamma = 0.45$, while the intensity of the fundamental is $\mathcal{I} = 10^{14} W/cm^2$. For this plot, the ionization probability rate was assumed to be given by the $ADK-$theory, $\mathcal{W}_{ADK}$.

maxima to appear, the phase difference between the two colours is $\varphi = 121.5^\circ$ or $\varphi = 301.5^\circ$.

The reason that the two optimized φ values differ by exactly 180° comes from the form of the continuous electromagnetic field. The electric field form that is used to describe a continuous $\omega/2\omega$, molds the trajectory of the electrons (eq. 3.18) and their corresponding kinetic energy at every moment in time

$$u(t, t_0; \gamma_2, \varphi_2) = -\frac{q\mathcal{E}_0}{m\omega^2}\left\{\cos\left(\omega\left(t + t_0\right)\right) + \sin\left(\omega t_0\right) + \left(\frac{\gamma}{2}\right)\left[\cos\left(2\left(t + t_0\right) + \varphi\right) + \sin\left(2t_0 + \varphi\right)\right]\right\}. \quad (3.21)$$

For the equation above there is an identity,

$$u(t, t_0; \gamma_2, \varphi_2 + 180^\circ) = -u(t, t_0 + 180^\circ; \gamma_2, \varphi_2), \quad (3.22)$$

which tells us that the plot of the kinetic energy s for a given phase difference φ_2, for every value of the γ_2 parameter, is similar with the kinetic energy for a phase difference $\varphi_2 + 180^\circ$. The only difference is that the horizontal axis has been translated by (in SI units) $180/\omega[s]$. In Fig. 3.14, we have plotted the optimized

electric field as a function of time.

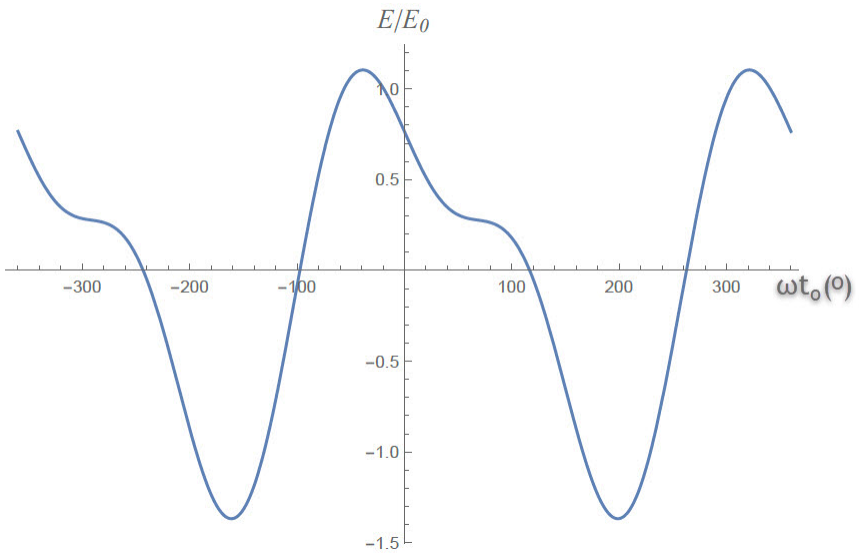

Figure 3.14: Form of the electric field component of the a two colour $\omega/2\omega$ laser field. For this plot, the ratio between the two fields strength is set to be equal with $\mathcal{E}_{2\omega}/\mathcal{E}_{\omega} = \gamma_2 = 0.45$, while their phase difference is equal to $\varphi_2 = 121.5°$.

It should be stressed out that the exact formula which gives the ionization probability rate of an electron from the system is not explicitly needed for discovering the optimized laser pulse to be used in a laboratory. For laser intensities below the saturation level, the ionization probability rate is in general (no matter the model) a function which depends exponentially on the strength of the electric field (another known model is the PPT-model [3]).

3.2.3.1 Kinetic energy and kinetic energy distribution of the returning electrons for the optimized continuous electromagnetic field.

In the remaining section of this chapter, the origin of the results exhibited in Fig 3.13 for the optimized field will be discussed. In Fig. 3.15, we have plotted the Kinetic energy of the returning electrons as a function of the candidate ionization time, t_0 and the electric field amplitude of the optimized field. In order not to plot a discontinuous function, for this graph, we have translated the horizontal axis by 30°. The blue columns depict the the three time intervals in which the kinetic energy of the returning electrons lie in the range $K \in [(2.10 - 0.05) \times U_p,\ 2.10 \times U_p]$, while the red columns depict the time interval in which the kinetic energy of the returning electrons lie in the range $K \in [(4.20 - 0.05) \times U_p,\ 4.20 \times U_p]$. In this plot, we can see that there are three local maxima and one local minimum. The value of the first local maximum is equal with $K = 4.20 \times U_p$ (denoted with K_{max} from now on) and corresponds to the ionization moment $\omega t_0 = 6.0°$. The value of both the second and third local maxima is equal with $2.10 \times U_p$ (denoted with K_{opt} from now on) and correspond to the ionization moments $\omega t_0 = 198.5°$ and $\omega t_0 = 210.5°$ respectively. The Kinetic energy of the returning electrons for $\omega t_0 = 204°$ is equal with $4.15 \times U_p$ and corresponds to the local minimum of the plot. As you can see, the total time interval corresponding to $K \in [K_{opt} - 0.05U_p,\ K_{opt}]$ is much wider than the time interval corresponding to $K \in [K_{max} - 0.05 \times U_p,\ K_{max}]$.

In the following figure, Fig. 3.16, the E.D.R.E. generated by the optimized field-shape has been plotted, for two cases. For the computation of the blue curve, the probability of an electron being liberated

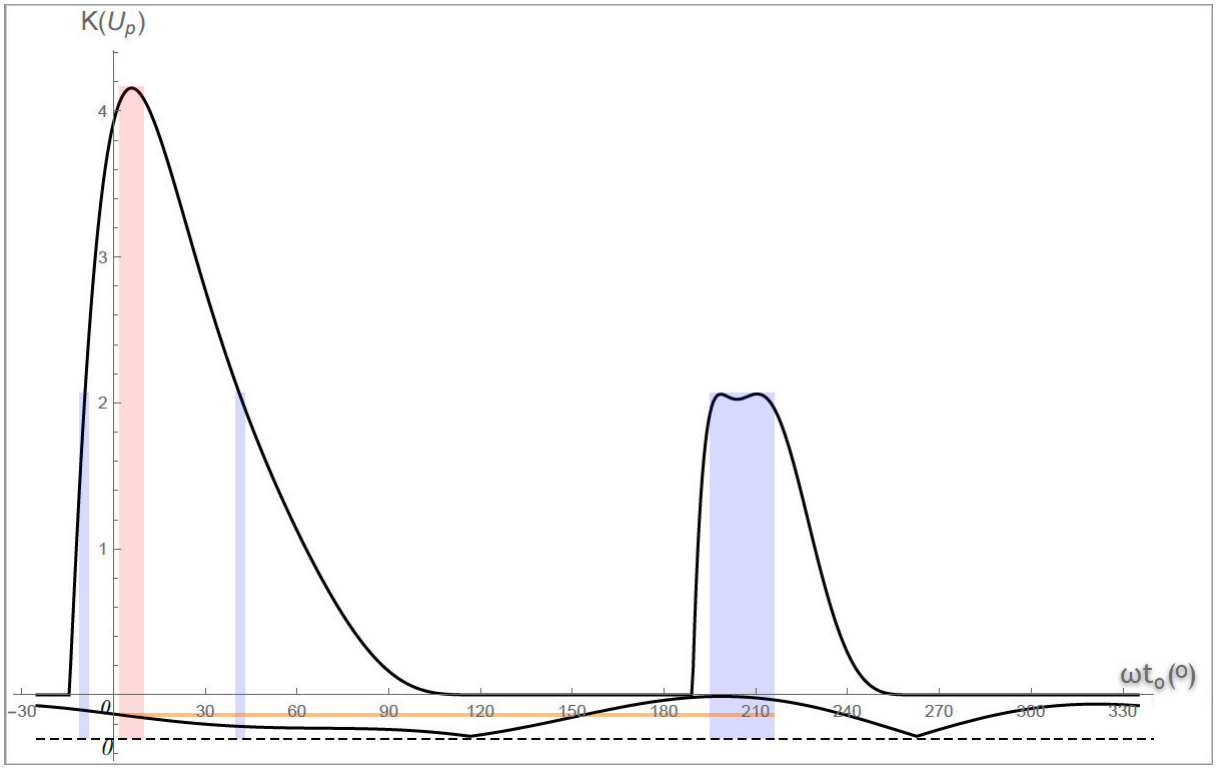

Figure 3.15: Plot of the kinetic energy of the returning electron in the optimized electric field. For the optimized pulse, the ratio of the electric field amplitudes of the two fields is equal to $\gamma = 0.45$ and the phase difference between the colours is equal to, $\varphi = 121.5^{\circ}$. The graph has been plotted with respect to the time in which the electron starts experiencing the electric field, ionization moment t_0. In the same graph, the form of the electric field amplitude has been included to show that the plateau ($K \in [(2.10 - 0.05) \times U_p,\ .10 \times U_p]$ and the ionization time interval $t_0 \in [195^{\circ},\ 216^{\circ}]$), corresponds to an ionization time in which the electric field amplitude was maximum, while for the ionization time interval $t_0 \in [2^{\circ},\ 10^{\circ}]$, with the corresponding returning kinetic energy $K \in [(2.10 - 0.05) \times U_p,\ 2.10 \times U_p]$, the corresponding electric field amplitude takes approximately half of its maximum value (The vertical orange line has been drawn to make it clearer.). The horizontal dashed line depicts the zero value of the electric field amplitude. As an example, for $\mathcal{E}_0 = 2 \times 10^8\ V/cm$ and $\lambda = 1500\ nm$, $U_p \approx 12\ eV$ and $1^{\circ} \approx 5 \times 10^{-15}\ s$.

at any moment in time was approximated to be given by the formula 2.4 while for the computation of the orange curve, the probability of an electron spawned at any moment was taken to be the same ($\mathcal{W} \to 1$).

By comparing the two curves, it is clear that the position of the local maxima in the plot (**qualitative** form of the *E.D.R.E.*) does not heavily depend on the preferable ionization moment of an electron. It is the **quantitative** part of the *E.D.R.E.* that depends on it. Nevertheless, in contrast with the previous cases that have been studied, the probability of an electron being ionized at any moment in the presence of the pulse has significantly altered the form of the *E.D.R.E.*. In a linear scale, the orange curve is characterised by two maxima [10], while blue curve has only one.

In Fig. 3.17 the ionization probability rate, $\mathcal{W}_{ADK}$, has been plotted as a function of the ionization time, t_0. In order to make this, the 2.4 formula was used, by setting the intensity of the fundamental harmonic of the electromagnetic field to be equal with $\mathcal{I} = 10^{14}\ W/cm^2$. The $\mathcal{W}_{ADK}$ has been multiplied with a constant so that the maximum value of the plot in the $t_0 \in [-30, 330^{\circ}]$ to be equal with one. In this figure, the vertical blue columns correspond to the ionization time intervals in which the returning kinetic

[10] This has to do with the step size, used for the discretization of the returning kinetic energy range of values and the calculation of the weighted histogram (*E.D.R.E.* problem), $0.05 \times U_p$. If the step size was even smaller, the first peak in the blue and orange curves would split into two (one corresponding to the two local maxima and one corresponding to the one local minimum.).

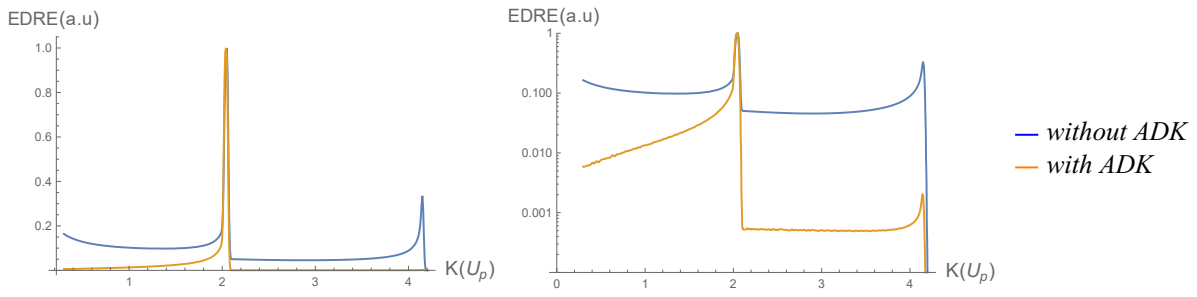

Figure 3.16: Kinetic energy distribution of the returning electron in the optimized two colour field in a linear (left panel) and a logarithmic scale (right panel), assuming that the probability of an electron being spawned at any given moment is given by the $ADK-$theory (blue curve) and the probability of an electron being liberated at any given moment is the same (orange curve). The ratio of the electric field amplitudes of the two fields is equal with $\gamma_2 = 0.45$, the phase difference between the colours is equal to, $\varphi_2 = 121.5°$., while the intensity of the fundamental harmonic of the laser field was set to be equal with $\mathcal{I} = 10^{14} W/cm^2$. For the evaluation of this distribution, small values of the returning energy have been discarded. The distribution is normalised with respect to its maximum value, $max(EDRE) = EDRE|_{K=2.10\times U_p}$.

energy lied in the range $[K_{opt} - 0.05 \times U_p, K_{opt}]$, while the red vertical column correspond to the ionization time intervals in which the kinetic energy of the returning electrons lied in the range $[K_{max} - 0.05 \times U_p, K_{max}]$. The horizontal columns show the ionization probability rates for the corresponding ionization time intervals.

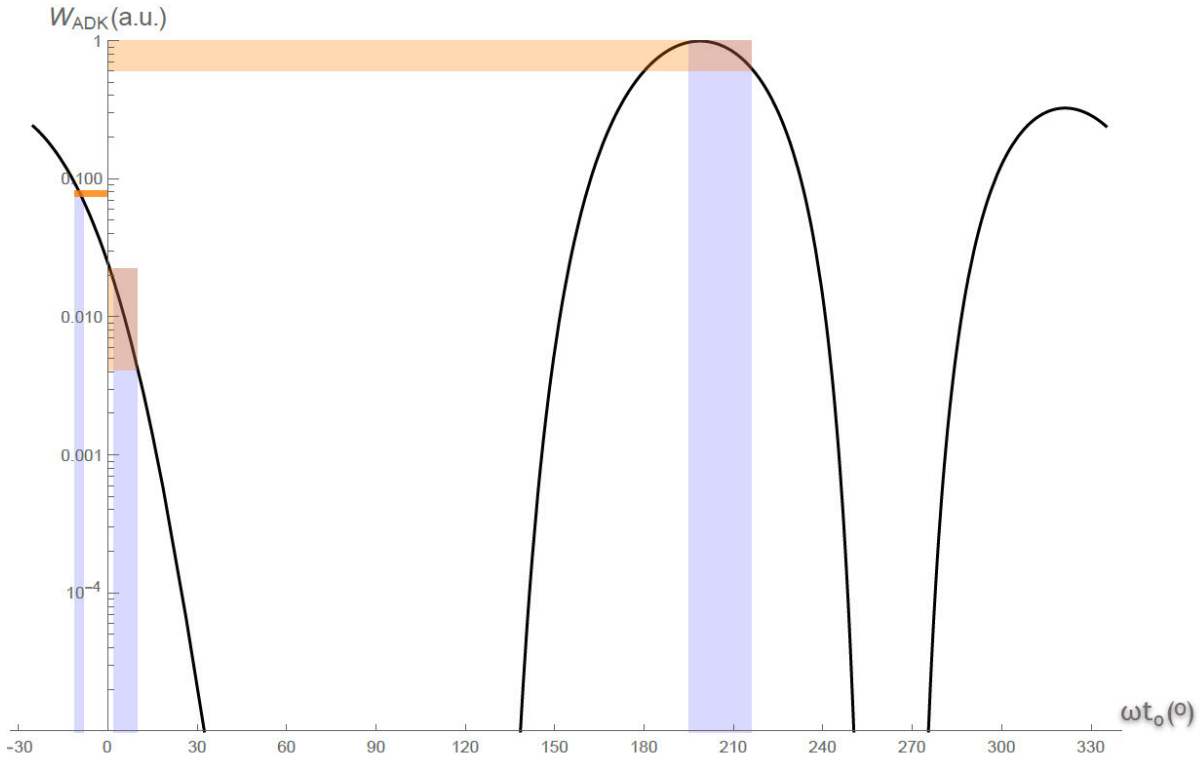

Figure 3.17: Ionization probability rate as a function of the candidate ionization moments t_0 for a two colour optimized electromagnetic field. For the creation of this graph, the ionization probability rate given by the $ADK-$theory was used, $\mathcal{W}_{ADK}$, by setting the intensity of the fundamental harmonic of the laser field to be equal to $\mathcal{I} = 10^4\ W/cm^2$.The ratio of the electric field amplitudes of the two fields is equal with $\gamma_2 = 0.45$, the phase difference between the colours is equal to, $\varphi_2 = 121.5°$..

In the time period which corresponds to the returning kinetic energies around the $K = K_{max}$ value, the ionization probability rate is approximately one hundred times less that the ionization probability rate corresponding to the kinetic energies around the $K = K_{opt}$ value. This means, that the contributions of electron which return to the ion's position to the formation of the $E.D.R.E.$ is not as effective as the contribution form the latterly mentioned ones. As a matter of fact, the ratio of the total ionization probability of an electron being ionized so that its returning kinetic energy lays in the range $K \in [K_{opt} - 0.05 \times U_p, K_{opt}]$ is approximately 400 hundred times greater that the corresponding total ionization probability that results in $K \in [K_{max} - 0.05 \times U_p, K_{max}]$[11]. Thus the $E.D.R.E.(K_{opt})$ value is anticipated to be approximately two order of magnitude greater that the $E.D.R.E.(K_{max})$ value (see right panel in Fig. 3.16).

In conclusion, what makes this fields optimum is not only the form of the kinetic energy of the returning electrons but also the probability of an electron being liberated from the system at any given moment. The kinetic energy of the returning electrons gives the characteristic shape of the the kinetic energy distribution of the returning electrons while the ionization probability rate alters it in such a way so that the $E.D.R.E.$ becomes very sharp.

3.2.4 Advantages and robustness of the optimized fields

In the previous section of this thesis, we have studied the form of the kinetic energy of the returning electrons vs the candidate ionization time plot, for the case of the "optimized pulse" ($\gamma = 0.45,\ \varphi = 121^\circ$) and the corresponding kinetic energy distribution. As it can be seen in Figure 3.19, the value of the $EDRE$ in the peak observed in the kinetic energy spectrum, is maximized for $\gamma = 0.45$. But in order to make clear why we have given the name "optimized" to this field, we have to make a comparison and test its reliability.

In Fig. 3.18, we have plotted the $E.D.R.E.(K)$ for a simple cos-like continuous wave and $E.D.R.E.(K)$ for the optimized laser pulse. For both plots, the intensity of the fundamental harmonic of the laser was fixed to $\mathcal{I} = 10^{14}\ W/cm^2$. Both distributions have been normalized with respect to their maximum values. The horizontal axis has not been plotted because, one of this curves has been translated so that its maximum value coincides with the maximum value of the other. This has been done in order to facilitate the comparison among the two curves. In the case of one colour field, for the $E.D.R.E. \in [0.1, 1]$, the kinetic energy of the returning electrons interval is approximately $0.8 \times U_p$, while for the the optimal field, the kinetic energy of the returning electrons interval is approximately $0.1 \times U_p$.

To test the reliability of the optimized pulse with respect to φ and γ parameters, we mention that the $E.D.R.E.$ is not a fast varying function with respect to them. The robustness of the problem regarding the φ has already been demonstrated in Fig. 3.13 while its robustness with respect to small variations of the gamma parameter is demonstrated in Fig. 3.19

Another test is to consider the case in which the returning electrons do not scatter with the parent ion on their first return to it. In other words we are considering the case in which the returning electron does not interact with the the parent ion. The electrons that are not interacting with the parent ion when they return to their original position, will continue propagating in the laser field and perhaps, at some later time some of them might "re-return" back to it. But having propagated in the laser field after not interacting with the parent ion will result in changing the final kinetic energy of these electrons and thus altering their contribution to the $E.D.R.E.$.

[11] More precisely, the ratio is equal with

$$\frac{\int_{195^\circ}^{216^\circ} \mathcal{W}_{ADK}(t_0) dt_0}{\int_{2^\circ}^{10^\circ} \mathcal{W}_{ADK}(t_0) dt_0} \approx 425$$

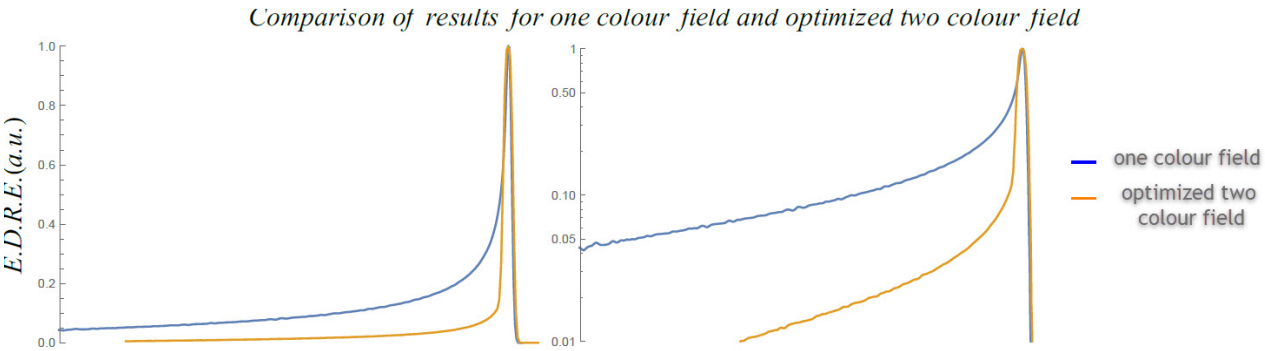

Figure 3.18: Comparison of the $E.D.R.E.$ for one colour field $\gamma = 0$ and the optimized two colour field, $\gamma = 0.45$, $\varphi = 121.5°$, in a linear (left panel) and a logarithmic scale (right panel). For this figure, the horizontal axis is not the same for the two figures but it has been translated, in order to bring the two peaks at the same position. This has been done in order to make the comparison easier and this is also the reason that no horizontal axis is shown.

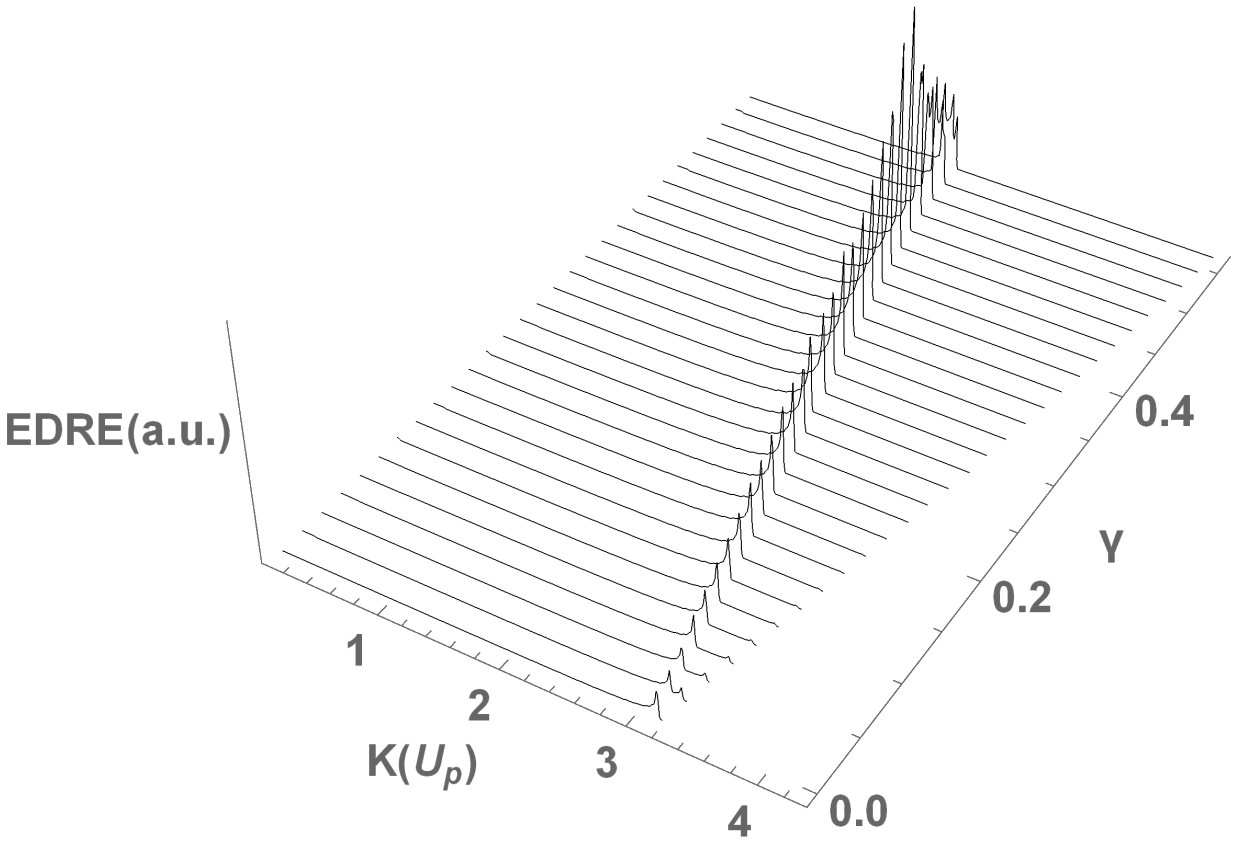

Figure 3.19: $3D$ plot of the Kinetic energy distribution of the returning electron, $E.D.R.E.$, in two colour field as a function of the kinetic energy and the ratio of the electric field amplitudes of the two fields. To produce this graph, the phase difference between the two colours is set to be equal to $\varphi_2 = 121°$, while the intensity of the fundamental is $\mathcal{I} = 10^{14} W/cm^2$. For this plot, the ionization probability rate was assumed to be given by the $ADK-$theory, $\mathcal{W}_{ADK}$.

Yet the duration of the returning time intervals (time intervals Δt in which some electrons return to their original position) is a decreasing function with respect to the number of returns (see Fig. 3.20[12]). As a result the contribution of the kinetic energies of the electrons, that return to the parent ion's location for the second time, to the *E.D.R.E.* is much less than the contribution of the kinetic energies of the electrons that return to the parent ion's location for the first time. All the third passes are much more ineffective than the second ones, all the fourth passes are much more ineffective than the third ones and so on. To make this clear in Fig. 3.20, we have plotted the returning time, t_R, of the electrons vs the candidate ionization moment, t_0. The total time interval between the N-th and the N+1-th return of the electrons to their original position is decreasing. A third pass of the electrons from their original position is corresponding to $\omega\Delta t_3 = 35°$, a possible fifth pass is corresponding to$\omega\Delta t_5 = 21°$ and a possible seventh pass is corresponding to $\omega\Delta t_5 = 14°$.

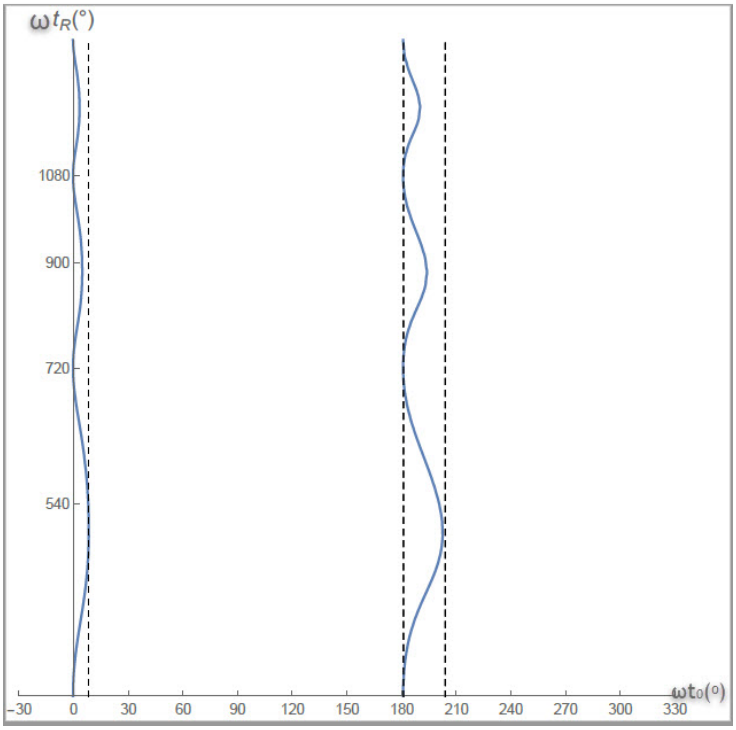

Figure 3.20: Recollision temporal coordinates for the optimized two colour field. After $4 \times 360°$ time propagating in the laser field, the electrons have a non zero probability of returning to their original position for up to seven times.

The possibility of an electron not interacting with the parent ion might not seem as a very likely event, but the probability of interacting is proportional to the total cross section of the rescattering problem. In general, the total cross section is of the order of $\sigma_{tot} = \sigma_{\text{elastic}} + \sigma_{\text{inelastic}} \sim 10^{-16} - 10^{-15} cm^{-2}$ [29] and this means that the probability of an electron interacting with the parent ion is very small. Based on this fact, we can estimate the probability of an electron interacting with the parent ion on its $n-$th return as being uncorrelated with the probability of interacting with it all the previous times. In other words, the kinetic energy of an electron that returned to the parent ion (for example) for the second time has the same effectiveness to the formation of the *E.D.R.E.* as the kinetic energy that the same electron had when it returned to the parent ion for the first time[13].

[12] In Fig. 3.20, the "width" of both blue curves is decreasing as ωt_R increases.

[13] This is not entirely correct, since when a particle is propagating in a laser field, its wavefunction is spreading as time

In the following figure, (Fig. 3.21), we have plotted the $E.D.R.E.$ of one colour field and of the optimized laser pulse, considering that each electron can return to its original position up to a maximum of three times. For this plot, the intensity of the fundamental harmonic of the laser was fixed to $\mathcal{I} = 10^{14}\ W/cm^2$. As you can see, in the plot, the quantitative $E.D.R.E.$ for the case of the one colour field (blue curves) has been altered significantly while for the case of the optimized pulse (orange curves), did not. The changes in the $E.D.R.E.$ for the optimized field make their appearance only for those returning kinetic energies whose corresponding $E.D.R.E.$ values are relatively low.

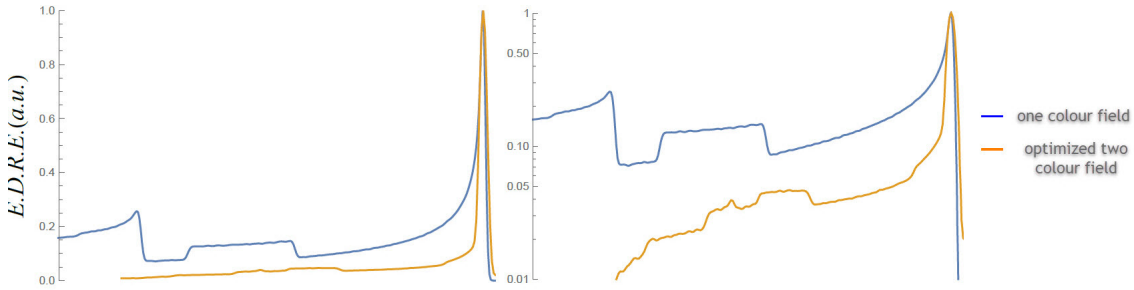

Figure 3.21: Comparison of the $E.D.R.E.$ for one colour field $\gamma = 0$ and the optimized two colour field, $\gamma = 0.45$, $\varphi = 121.5°$, in a linear (left panel) and a logarithmic scale (right panel). Considering that each electron can return to its original position up to a maximum of three times. For this figure, the horizontal axis is not the same for the two figures but it has been translated, in order to bring the two peaks at the same position. This has been done in order to make the comparison easier and this is also the reason that no horizontal axis is shown.

3.2.5 From continuous waves to pulses

In the previous subsections, continuous electromagnetic waves with a relatively high laser intensity were studied. But in most of the laboratories throughout the world, great intensity comes with a cost. The cost of duration. The electromagnetic fields that are used in strong laser field physics are not continuous waves but pulses, brief bursts of electromagnetic energy. So in order for the description of the semi-classical problem of the kinetic energy distribution of the returning electrons (E.D.R.E.) to be complete, the case of particular pulses should be examined as well.

In general, the mathematical formulas describing an electromagnetic pulse can be written as the product of a continuous electromagnetic wave and a smooth function outlining its extremes. This function is referred to as an envelope, $h(t)$, and using it the total electromagnetic field takes the form

$$\mathcal{E}_{tot} = \mathcal{E}_0 \times \underbrace{h(t, t_0; \mathcal{N})}_{\text{envelope form}} \times \underbrace{\{\cos(\omega(t + t_0) + \Phi) + \gamma \cos(2\omega(t + t_0) + \varphi + \Phi)\}}_{\text{carrier wave}}. \tag{3.23}$$

For this thesis, we have chosen to model the temporal envelope as a $\cos^2$-envelope and not as a Gaußian envelope, because a $\cos^2$-envelope becomes zero in a finite amount of time. The Gaußian- envelope, on the other hand, only approaches zero as the time goes to infinity, which complicates numerical calculations.

$$h(t, t_0; \mathcal{N}) = H(\pi\mathcal{N} - \omega|t + t_0|) \cos^2\left(\frac{\omega(t + t_0)}{2\mathcal{N}}\right). \tag{3.24}$$

passes by. As the time duration of an electron's propagation away from and towards the nucleus increases, the dispersion of its wavefunction is increased and the probability of an electron rescattering with its parent ion decreases. This is the phenomenon of quantum diffusion and results in constraining the contributions from long lasting trajectories. This is something that has been theoretically examined in [18]

In the expression above, $\mathcal{N}$ denotes the total number of cycles in the pulse, H is the *Heaviside* step function,

$$H(x) = \begin{cases} 1, & x \geq 0 \\ 0, & x < 0 \end{cases}, \tag{3.25}$$

and the extra phase, Φ in eq. 3.23 defines the relative phase between the envelope and the carrier frequency. This is called Carrier-Envelope-Phase (CEP). The CEP becomes relevant for few cycle pulses where its variation has a large influence on the shape of the field below the envelope. It decides, for example, whether the maximum of the field is reached twice, $\Phi = 180°$ or only once $\Phi = 0°$.

In Fig. 3.22 the forms of the pulses that are going to be examined in this subsection are presented. In the left panel, the enveloped wave is a simple, one colour field and in the right panel, the enveloped wave is the optimized continuous wave. For both graphs, the total number of cycles of the ω component of the field is equal with six. It is important to note that in all of the following figures, the ponderomotive energy has been defined with respect to the maximum value of the electric field, i.e. as if there is had no envelope.

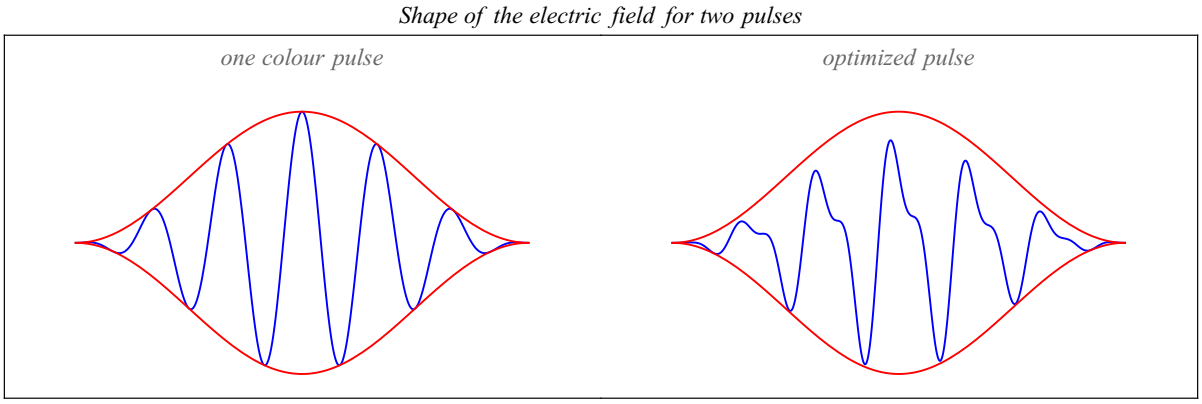

Figure 3.22: Shapes of the electric field components of two laser pulses. In the left panel, the enveloped wave is a simple cos-like wave, $\gamma_2 = 0$ while on the right panel the enveloped wave is the optimized continuous two colour field with $\gamma_2 = 0.45$, $\varphi_2 = 121.5°$ and $\Phi = 0°$.

To begin with, we are considering the case of a few cycle pulse. In Fig. 3.23 and in Fig. 3.24, the $E.D.R.E.$ for two laser pulses are presented, assuming that α) the probability of an electron being spawned at any given moment is given by the $ADK-$theory (blue curve) and β) the probability of an electron being liberated at any given moment is equal (orange curve). In both figures, the number of cycles of the ω harmonic component are equal with $\mathcal{N} = 4$, the number of maximum returns of each electron to its original position has not been bounded, and CEP has been set equal with zero, $\Phi = 0$. In Fig. 3.23, the carrier wave is a simple cos-like field (see left panel 3.22) while in Fig. 3.24, the carrier wave is the optimized continuous wave (see right panel 3.22).

As you can see, for both field shapes, the ionization probability rate has greatly altered the form of the $E.D.R.E.$. For the simple cos-like carrier wave, the $E.D.R.E.$ is characterized by multiple local maxima. From all of them, only two are important ones. One which corresponds to the $K \approx 3.2 \times U_p$ and one which corresponds to $K \approx 2.2 \times U_p$. Both of these local maxima correspond to returning kinetic energies which come from the eq. (3.15)[14]. For the first local maximum, the envelope has not affected the magnitude of the electric field, and thus $K \approx 3.2 \times U_p$. On the contrary for the second local maximum,

[14] $K_{max} = 3.17 \times U_p$

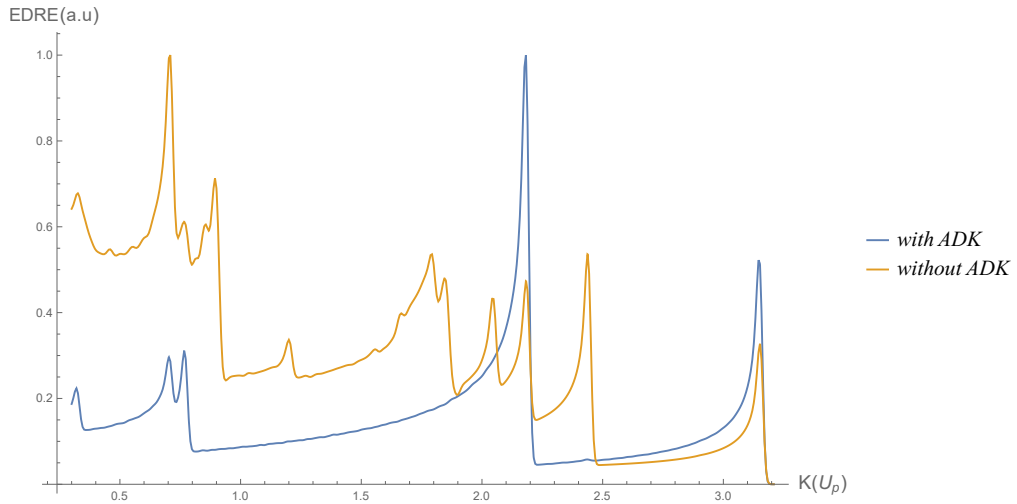

Figure 3.23: Kinetic energy distribution of the returning electron in an enveloped one colour field, assuming that α) the probability of an electron being spawned at any given moment is given by the $ADK-$theory (blue curve) and β) the probability of an electron being liberated at any given moment is the same (orange curve). The envelope contains 4 cycles of the carrier wave, the carrier-envelope-phase is set to zero, $\Phi = 0$ and the maximum intensity of the fundamental harmonic of the laser field was set to be equal with $\mathcal{I} = 10^{14}\ W/cm^2$.

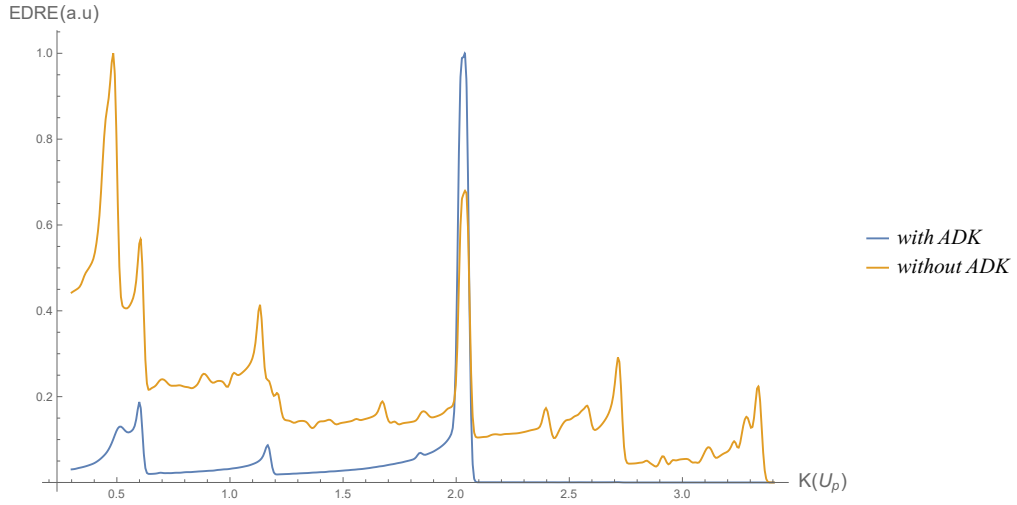

Figure 3.24: Kinetic energy distribution of the returning electron in an enveloped two colour optimized field, assuming that α) the probability of an electron being spawned at any given moment is given by the $ADK-$theory (blue curve) and β) the probability of an electron being liberated at any given moment is the same (orange curve). The envelope contains 4 cycles of the ω carrier wave and 4 cycles of the 2ω carrier wave. For this figure, the carrier-envelope-phase is set to zero, $\Phi = 0$ and the maximum intensity due to the fundamental harmonic of the laser field was set to be equal with $\mathcal{I} = 10^{14}\ W/cm^2$.

the envelope has changed the electric field amplitude significantly. Thus, $K \approx 3.2 \times U_p(\mathcal{I} < \mathcal{I}_max) = 3.2 \times \left(\frac{U_p(\mathcal{I}<\mathcal{I}_max)}{U_p(\mathcal{I}=\mathcal{I}_max)}\right) U_p(I = I_max) \neq 3.2 \times U_p(\mathcal{I} = \mathcal{I}_max)$. Comparing this figure with Fig. 3.7, we can see that the envelope has resulted in altering the form of the $E.D.R.E.$. Instead of a single local maximum, there are two. Moreover, the maximum value of the $E.D.R.E.$ does not correspond to the first peak but to the second one.

On the contrary, in the case of the optimized pulse, the complete $E.D.R.E.$ (blue curve) is characterized by a single, important (with great values of $E.D.R.E.$) local maximum. The form of the $E.D.R.E.$ has not been significantly changed (compare with Fig. 3.11) and the local maximum corresponds

to the $K \approx 2 \times U_p$ value just like in the case of a continuous wave. Another advantage is the width of the spike which corresponds to the maximum value of $E.D.R.E.$. $K \approx 2 \times U_p$, corresponds to a local maximum with a narrow width; $\delta K \approx 2 \times U_p$.

Next, we are going to consider a relatively many-cycle-pulse. In Fig. 3.25 and in Fig. 3.26, the $E.D.R.E.$ for two laser pulses are presented, assuming that α) the probability of an electron being spawned at any given moment is given by the $ADK-$theory (blue curve) and β) the probability of an electron being liberated at any given moment is the same (orange curve). In both figures, the number of cycles of the ω harmonic component is equal with $\mathcal{N} = 8$, the number of maximum returns of each electron to its original position has not been bounded, and CEP has been set equal to zero, $\Phi = 0$. In Fig. 3.25, the carrier wave is a simple cos-like field (see left panel 3.22) while in Fig. 3.26, the carrier wave is the optimized continuous wave (see right panel 3.22).

In both figures, the ionization probability rate has greatly altered the form of the $E.D.R.E.$. For the simple cos-like carrier wave, the complete $E.D.R.E.$ (blue curve) is characterized by multiple local maxima, many of which take significant $E.D.R.E.$ values. The positions of the local maxima are relatively close to one another, $K = 3.2,\ 2.9,\ 2.8 \times U_p$ and also the maximum value of the $E.D.R.E.$ does not correspond to the first but to the third peak [15]. Comparing this figure with Fig. 3.7 and Fig. 3.23, we can see that the envelope has resulted in altering the form of the $E.D.R.E.$. More importantly, we can deduce that in the case of a simple $\cos-$like pulse the form of the $E.D.R.E.$ greatly depends on the number of cycles that are contained in the envelope.

On the contrary, in the case of the optimized pulse, the complete $E.D.R.E.$ (blue curve) is characterized by two, important (with great values of $E.D.R.E.$) local maxima. Nevertheless, the form of the $E.D.R.E.$ has not been significantly changed (compare with Fig. 3.11 and Fig. 3.26) and the $K \approx 2 \times U_p$ is still the returning kinetic energy value for which $E.D.R.E.$ takes the maximum value; just like in the case of a continuous wave. Moreover, the width of this local maximum remains to be very narrow, $\delta K \approx 0.1 \times U_p$. This is another characteristic which makes this electromagnetic wave form interesting. The maximum value of the $E.D.R.E.$ always corresponds to the returning kinetic energy $K \approx 2 \times U_p$ (blue and orange curve) and it has a spectrum width which is very narrow.

Overall, we can deduce that the "optimized" pulse has an electric waveform which exhibits some very interesting characteristics. The "optimized" pulse is stable under some small variations of the phase difference and the ratio of the field amplitudes between the two colours. The form of its kinetic energy distribution is getting significantly altered only for a many-cycle-pulse and even though every possible return of the electron was taken into account (multiple passes) the maximum value of $E.D.R.E.$ is peaked around the $K \approx 2 \times U_p$ value. This is happening because of the particular characteristics of its profile; i.e. the shape of the electromagnetic wave.

Given these characteristics, we think that the "optimized" pulse can be a good candidate for experimentally investigating several processes related to electron rescattering, such as high-harmonic generation non-sequential double ionization and more. The fact that the maximum value of the $E.D.R.E.$ corresponds to a sharp peak means that most of the returning electrons have the same retuning kinetic energy. By increasing the intensity of the laser source, the U_p value and thus the local maximum of the $E.D.R.E.$ correspond to greater kinetic values as well. After some "critical" intensity value, the energy level needed for a particular transition in the system can be reached. As a result, with the use of the optimized pulse, the returning electrons can be used, for studying certain collisionally induced resonant transitions.

[15] not the spike which corresponds to the highest kinetic energy

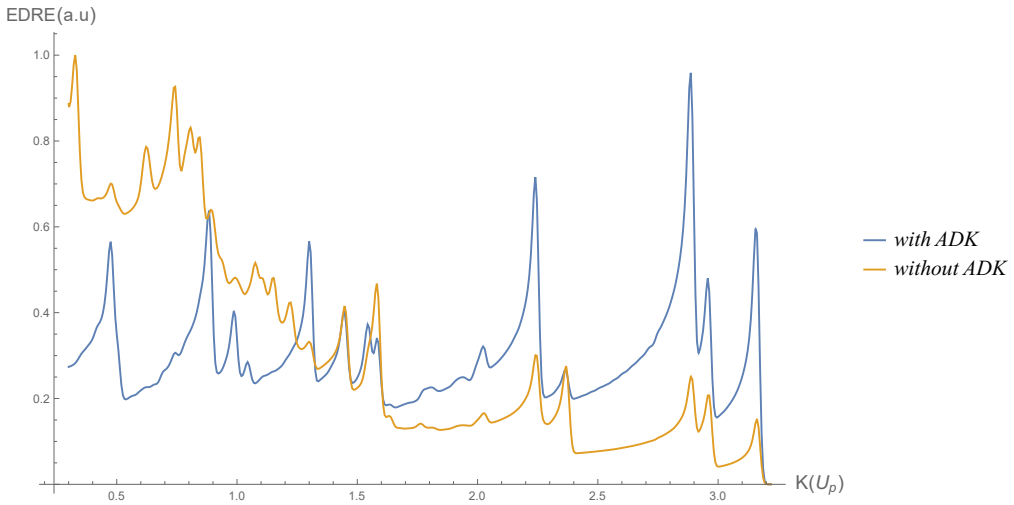

Figure 3.25: Kinetic energy distribution of the returning electron in an enveloped one colour field, assuming that α) the probability of an electron being spawned at any given moment is given by the $ADK-$theory (blue curve) and β) the probability of an electron being liberated at any given moment is the same (orange curve). The envelope contains 8 cycles of the carrier wave, the carrier-envelope-phase is set to zero, $\Phi = 0$ and the maximum intensity due to the fundamental harmonic of the laser field was set to be equal with $\mathcal{I} = 10^{14}\ W/cm^2$.

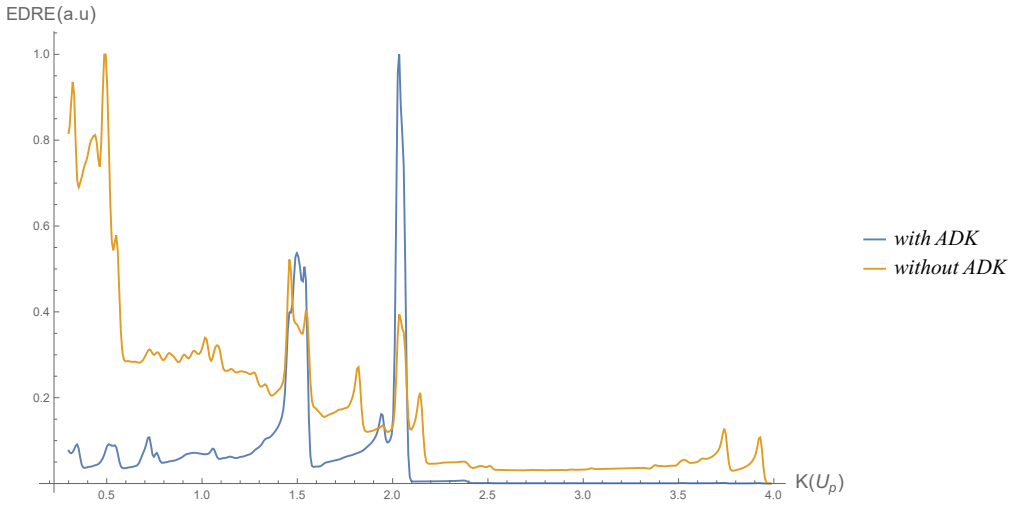

Figure 3.26: Kinetic energy distribution of the returning electron in an enveloped two colour field, assuming that α) the probability of an electron being spawned at any given moment is given by the $ADK-$theory (blue curve) and β) the probability of an electron being liberated at any given moment is the same (orange curve). The envelope contains 4 cycles of the ω carrier wave and 8 cycles of the 2ω carrier wave. For this figure, the carrier-envelope-phase is set to zero, $\Phi = 0$ and the maximum intensity of the fundamental harmonic of the laser field was set to be equal with $\mathcal{I} = 10^{14}\ W/cm^2$.

Chapter 4

High (-order) Harmonic Generation

High (-order) Harmonic Generation (HHG) is one of the major topics of laser physics. When an atom is exposed to an intense electromagnetic field, there is a high chance of ionization. Some of the electrons that are liberated from the atom are accelerated by the field and acquire high velocities and momenta. These electrons can then recombine with the ionic core and release energetic photons, the so called harmonics. As the intensity of the driving field increases, so does the energy of the produced photons.

When a simple, sinusoidal continuous wave is used for the harmonic generation, the harmonic spectrum has a very characteristic and universal shape. The emitted photons are generated in multiples of the energy of the photon of the driving field $\hbar\omega$, each of the multiple called harmonic order. After the first few high intensity orders for the relative low to mid orders, the intensity of all the harmonic components is roughly equal in strength and in the bibliography this region is referred to as a *plateau*. Following the *plateau*, the spectrum's intensity is exponentially decreasing and this region is the so called *cutoff* region. The cutoff sets the limit for the highest frequency that can be efficiently generated. In the most common case, where a symmetric sinusoidal pulse has been used to generate the harmonics, only harmonics of odd order can be generated, since the atomic and (non-oriented) molecular gases have inversion symmetry [19]. If however, an asymmetric pulse is use to excite the gas, harmonics of both odd and even order can be generated.

But is there a way in which these harmonic spectra can be qualitatively explained? In the case of a monochromatic laser field of linear polarization, the maximum energy at the end of the plateau can be approximated by the formula $E_{max} \approx I_p + 3.2 \times U_p$, so that the maximum harmonic which is being efficiently produced is of the order:

$$\mathcal{N}_{max} \approx \frac{I_p + 3.2 \times U_p}{\omega} \tag{4.1}$$

This can be easily explained using the *simple man's* and its numerical results presented in Chapter 2 of this thesis. Historically, this approach was also firstly used by *Corkum* to explain the empirical formula eq. 4.1 [16]. Using this method, he managed to give an insight into the physical picture of the problem using his quasi-classical approach.

The electrons tunneled through the atomic barrier, appear in the continuum with nearly zero velocity. In the continuum, for a narrow, sinusoidal field, the maximum kinetic energy of the returning electrons is approximately 3.2 U_p. In this step of the process, the electrons that return to the nucleus can then emit harmonics by recombining to the ground state and thus emitting photons with maximal photonic energy.

A simple theory to qualitatively describe and examine this phenomenon was formulated by *Lewenstein et al* in their work [18]. The theory agrees well with the predictions of other single-atom theories and in particular with the cutoff law. It justifies the semiclassical interpretation of harmonic generation in low-frequency domain by using the so called *Strong Field Approximation*.

The intuitive picture of this problem suggests that in order to control the process of HHG, the classical motion of the electrons should be studied in the laser field while neglecting the influence of the atomic potential.

In this Chapter, *Lewenstein's* theory for the production of high order harmonics is presented, together with the so called *Strong Field Approximation, SFA*. Both of these theories will be used to calculate the *time-dependent dipole moment* of the series, from it its *Fourier* series expansion and from it the harmonic spectra. Furthermore, the correlation between the harmonic spectrum and the simple man's model will be demonstrated, using the saddle point approximation.

Lewenstein's model will be used for the numerical calculation of the harmonic spectra for one and two colour $\omega/2\omega$ fields. For the case of an incident one colour continuous field there is a plateau and a cutoff region that can be explained qualitatively using the previously mentioned semi-classical law. However, in the spectra generated by two colour fields, there are two plateau and two cutoff regions. In order to qualitatively explain this characteristic of the harmonic spectra, a *modified cut-off law* will be presented.

Finally, I examine the high harmonic generation spectra for the "optimized" field (presented in Chapter 3). The spectra for the optimized field contain a few harmonics of increased value which form a "peak" at the end of the plateau (see Fig. 4.3) (just like in the corresponding *kinetic energy distribution of the returning electrons*) and an interesting characteristic with respect to the intrinsic phases of the harmonics.

4.1 HHG theory

Consider an atom in a *single-electron approximation* under the influence of the laser field $\vec{\mathcal{E}}(t)$ of linear polarization in the x direction, in the case where the atomic system can be ionized by the minimum absorption of $10-20$ laser photons and where the ponderomotive energy U_p is comparable or even larger than the ionization potential I_p, and yet still below the saturation level U_{sat} of the system (above which we enter the "over the barrier ionization" regime 2.1.2). The first condition is being chosen in order to make the contribution of phenomena such as multi-photon ionization insignificant since the n-photon ionization rate decreases exponentially fast with n.[1] [28]. The second condition ensures that in this regime of parameters the tunneling or over-the-barrier ionization theory becomes valid (the Keldysh parameter $\gamma_k = \sqrt{I_p/2U_p} < 1$) [2].

In the *length or Coulomb gauge* with the use of the dipole approximation the time-dependent Schröndinger equation $TDSE$ takes the form:

$$i\frac{\partial}{\partial t}\left|\psi(\vec{r},t)\right\rangle = \hat{\mathcal{H}}(t)\left|\psi(\vec{r},t)\right\rangle = \left[-\frac{1}{2}\nabla^2 + V(\vec{r}\,) - \mathcal{E}(t)x\right]\left|\psi(\vec{r},t)\right\rangle, \tag{4.2}$$

where $V(\vec{r}\,)$ denotes the atomic potential. Even though in this section of the thesis atomic units are being used, all energies are measured in terms of the photon energy. Assuming that the system was initially in the ground state, $|g\rangle$, which we will assume to have spherical symmetry, and only after a bit of time has passed since the laser was activated, the electron's wavefunction is expected to have slightly been deformed:

$$\left|\psi(\vec{r},t)\right\rangle = e^{-iI_p t}\left|g\right\rangle + \left|\delta\psi\right\rangle. \tag{4.3}$$

As a result the valence electron is no longer in a stable, bound state. Direct substitution into the $TDSE$ eq.

[1] The n-photon ionization rate W is given by $W = \sigma_n \mathcal{I}^n$, where σ_n is the generalized n-photon ionization cross section and $\mathcal{I}$ is the intensity of the incident electromagnetic wave. σ_n is decreasing very fast with respect to n.

(4.2) shows that the "deformation" term, $|\delta\psi\rangle$ can be written as:

$$|\delta\psi(t)\rangle = i\int_{t_0}^{t} e^{-i\int_{t_1}^{t}\hat{\mathcal{H}}(\tau)d\tau}\mathcal{E}(t_1)xe^{iI_pt_1}\,|g\rangle\,dt_1 \tag{4.4a}$$

$$= i\int_{t_0}^{t}\sum\!\!\!\!\!\!\int_{j} \underbrace{e^{-i\int_{t_1}^{t}\hat{\mathcal{H}}(\tau)d\tau}\,|j\rangle}_{III}\ \underbrace{\langle j|\,\mathcal{E}(t_1)x}_{II}\ \underbrace{e^{iI_pt_1}\,|g\rangle}_{I}\,dt_1. \tag{4.4b}$$

[2] Even though this equation does not look very appealing, it can be translated into a beautiful and easy to grasp picture. The system starts its journey in the stable state $|g\rangle$. Being in the ground state, the electron's ground state amplitude is oscillating with frequency I_p[3] until some later time t_1 ($I-$factor in eq.(4.4b)), when it suddenly starts experiencing the force due to the laser ($II-$factor in eq.(4.4b)). At that moment, the electron immediately makes a transition to another state $|i\rangle$, the evolution of which, is afterwards affected by both the parent's ion and the laser's potential ($III-$factor in eq.(4.4b)).

4.1.1 *Strong Field Approximation* (SFA)

As we have discussed in previous sections of this thesis, 1.1.1,2.1 under these conditions, the system is ionized by the laser field. Having escaped from the atom, the liberated electron propagates in the electric field of the laser. In this stage of the process, the effects of the force of the parent ion: $-\vec{\nabla}V(\vec{r}\,)$ is assumed to be negligible. This can be justified based on two facts. First and foremost the electron leaves the atoms typically when the field reaches its peak value. Secondly, the liberated electron has probably escaped when "its distance from the nucleus is long enough". As the electron is accelerated in the field, it acquires a high velocity and momentum, and is driven further from the parent ion, so that the role of $V(\vec{r})$ is even less pronounced[4]. This argument is particularly valid if the electron returns to the nucleus with a large kinetic energy. In the literature, this approximation is referred to as the *Strong Field Approximation* (SFA).

All the above considerations suggest that two approximations can be used.

1. The chance of an the electron making a transition to an excited state is very low. The electrons lean towards a transition to the continuum, so that all the contributions to the evolution of the system of all the bound states except for the initial state of the system, i.e. the ground state $|g\rangle$ can be neglected[5]. Generally speaking, this assumption holds when there are no intermediate resonances.

2. Since in the continuum the electron can be treated as a free particle that experiences only the effect of the electric field of laser, it can be assumed that the $|j\rangle$ states can be described as plane waves with initial momentum $|\vec{p}_0\rangle$.

[2] The completeness equation that I have used ,$\sum\!\!\!\!\!\!\int_j |j\rangle\langle j| = \mathbb{1}$, assures that there is no basis vector "missing". The energy spectrum of the problem is composed of discrete ($\sum$-part of the $\sum\!\!\!\!\!\!\int$-symbol) **and** continuous ($\int$-part of the $\sum\!\!\!\!\!\!\int$-symbol) energy levels.

[3] $I_p/\hbar$ in SI

[4] One could argue that there are several major problems with these two approximations, which are stemming from the neglection of the effect of the parent's ion potential. Firstly, during the transition to the continuum the process of ionization will be different if we include its interaction with the atomic core. Since the electron has to tunnel through the barrier, the tunneling probability is strongly affected by the shape of the barrier ($\langle j|\,x\,|g\rangle$ depends on the $|g\rangle$ and $|j\rangle$ state). This is a good argument and this problem can, in general, be corrected by incorporating the effect of the Coulomb tail into the electron action or by treating the atomic potential as a first order perturbation.

[5] Since we are talking about a transition from a single initially bound state into the continuum spectrum, the completeness relation is simplified: $\sum\!\!\!\!\!\!\int \to \int$

So that in the end, the "distorted" part of the wavefunction can be written as:

$$|\delta\psi(t_2)\rangle \approx i\int_{t_0}^{t_2}\int d\vec{p_0}^3\mathcal{E}(t_1)e^{-i\int_{t_1}^{t_2}\hat{\mathcal{H}}_f(\tau)d\tau}\,|\vec{p_0}\rangle\,\langle\vec{p_0}|x|g\rangle\,e^{iI_pt_1}dt_1, \qquad \hat{\mathcal{H}}_f=-\frac{1}{2}\nabla^2-\mathcal{E}(t)x, \tag{4.5}$$

where the "f" subscript stands for the word "free".

4.1.2 Time dependent-dipole moment

One of the main reasons to make such an approximation i.e. to completely neglect the parent's ion potential in the continuum, is that the action of the $e^{-i\int_{t_1}^{t_2}\hat{\mathcal{H}}_f(\tau)d\tau}$ operator on a plane wave state $|p_0\rangle$ results in:

$$e^{-i\int_{t_1}^{t_2}\hat{\mathcal{H}}_f(\tau)dt}\,|\vec{p_0}\,\rangle = e^{-i\int_{t_1}^{t_2}E_{kin}(t_1;\tau)d\tau}\left|\vec{p_0}+\vec{A}(t_1)-\vec{A}(t_2)\right\rangle, \tag{4.6}$$

$$E_{kin}(t_1;t_2)=\frac{1}{2}\left(\vec{p_0}+\vec{A}(t_1)-\vec{A}(t_2)\right)^2, \qquad \vec{A}(t)=\int_{t^*}^{t}\mathcal{E}(\tau)d\tau, \tag{4.7}$$

where t^* can take an arbitrary value. To make things as simple as possible, the t^* parameter is chosen in such a way so that the evaluation of the primitive function of the electric field at that moment yields zero. The derivation of this result can be found in the Appendix 5.2 The exponential operator is known in the bibliography as the *Volkov propagator* and its action on a plane wave $|\vec{p_0}\rangle$ results in the generation of the so called *Volkov state*:

$$\left\langle\vec{r}\left|e^{-i\int_{t_1}^{t_2}E_{kin}(t_1;\tau)dt}\right|\vec{p_0}+\vec{A}(t_1)-\vec{A}(t_2)\right\rangle=\frac{1}{(2\pi)^{3/2}}e^{i\left[\vec{p_0}-\int_{t_1}^{t_2}\mathcal{E}(\tau)d\tau\right]\cdot\vec{r}-i\int_{t_1}^{t_2}E_{kin}(t_1;\tau)d\tau}, \tag{4.8}$$

where, $\langle\vec{r}\,|i\rangle$ corresponds to the position representation of the $|i\rangle$ state: $\psi_i(\vec{r})$. Eqs. (4.6,4.7,4.8) describe plane waves with time varying momenta. The momentum of an electron, that initiated its oscillation in the laser filed at time t_0, is given by *Newton's equations of motion* (since $\vec{A}(t_1)-\vec{A}(t_2)=-\int_{t_1}^{t_2}\mathcal{E}(\tau)d\tau$). The E_{kin} term corresponds to the instantaneous kinetic energy of the electron.

By factoring out the free oscillations of the ground-state amplitude with the frequency I_p, the wavefunction takes the form:

$$|\psi(t_2)\rangle = e^{iI_pt_2}\left(|g\rangle+\int d\vec{p_0}^3\beta(\vec{p_0},t_2)\,|\vec{p_0}\rangle\right), \tag{4.9a}$$

$$\beta(\vec{p_0},t_2)=i\int_{t_0}^{t_2}\mathcal{E}(t_1)\left\langle\vec{p_0}+\vec{A}(t_2)-\vec{A}(t_1)\middle|x\middle|g\right\rangle e^{i\mathcal{S}(\vec{p_0},t_1,t_2)}, \tag{4.9b}$$

$$\mathcal{S}(\vec{p_0},t_1,t_2)=-\int_{t_1}^{t_2}\left[\left(\vec{p_0}+\vec{A}(t_2)-\vec{A}(\tau)\right)^2/2+I_p\right]d\tau. \tag{4.9c}$$

Eqs. (4.9) are eqs. (3,5) used in [18] to explain the HHG spectra.

The rate of generated photons is proportional to the time dependent dipole moment and thus the time-dependent dipole moment is the next quantity that needs to be evaluated. In order to calculate the x component of the time-dependent dipole moment (the other two components are equal to zero) we have to evaluate:

$$\langle x\rangle_{t_2} = \langle\psi(t_2)|x|\psi(t_2)\rangle \tag{4.10a}$$

$$= \langle g|x|g\rangle+\int d\vec{p_0}^3\left(\beta(\vec{p_0},t_2)\,\langle g|x|\vec{p_0}\,\rangle+c.c.\right)+\int d\vec{p_0}^3d\vec{p_0}'^3\beta(\vec{p_0},t_2)\beta(\vec{p_0}',t_2)^*\,\langle\vec{p_0}'\big|x\big|\vec{p_0}\rangle\,. \tag{4.10b}$$

The first factor in eq. (4.10b), $\langle g|x|g\rangle$ is nothing but a constant and since we are interested in the *Fourier* components of the time-dependent dipole moment, this factor is insignificant and will be omitted. The second factor corresponds to all the possible bound-free transitions and vise versa, while the last factor, corresponds to all the possible *continuum-continuum* transitions. Nevertheless, the amplitude of any *continuum-continuum* transition between free states has been proved to be zero [20].

By introducing the momentum $\vec{p}$[6]

$$\vec{p} = \vec{p_0} + \vec{A}(t_2), \tag{4.11}$$

the time dependent dipole moment can be brought into a more symmetric and compact form. This is done by removing a factor that depends on the moment of measurement t_2, in the τ integral in eq. (4.9c), so that

$$\boxed{\begin{array}{c}\langle x\rangle_{t_2} \approx 2\mathcal{R}e\left\{i\int_{t_0}^{t_2} dt_1 \int d\vec{p}^{\,3}\mathcal{E}(t_1)\left\langle g\middle|x\middle|\vec{p}-\vec{A}(t_2)\right\rangle\left\langle \vec{p}-\vec{A}(t_1)\middle|x\middle|g\right\rangle e^{-i\mathcal{S}(\vec{p},t_1,t_2)}\right\}, \\ \mathcal{S}(\vec{p},t_1,t_2) = \int_{t_1}^{t_2}\left[\frac{1}{2}\left(\vec{p}-\vec{A}(\tau)\right)^2 + I_p\right]d\tau\end{array}}. \tag{4.12}$$

[18] The equations above are intuitive and clear. The electron stays in the ground state until t_1 when it makes transition to the continuum, with probability amplitude: $\left\langle \vec{p}-\vec{A}(t_1)\middle|\mathcal{E}(t_1)x\middle|g\right\rangle = \mathcal{E}(t_1)\left\langle \vec{p}-\vec{A}(t_1)\middle|x\middle|g\right\rangle$. Then the electron moves in the laser field where it is oscillating and accumulating the phase: $\mathcal{S}(\vec{p},t_1,t_2)$ given by the integral of its instantaneous kinetic energy: $\int(\vec{p}-\vec{A}(\tau))^2/2d\tau$ (see eq. 4.6) performed between the moment it was spawned t_1[7] and the moment t_2 when it recombines with the parent ion. The effects of the atomic potential are assumed to be small between t_1 and t_2, so that $\mathcal{S}(\vec{p},t_1,t_2)$ actually describes the motion of an electron freely moving in the laser field with a constant momentum $\vec{p}$. Note, however, that $\mathcal{S}(\vec{p},t_1,t_2)$ does incorporate some effects of the binding potential through its dependence on I_p. The form in which the ionization potential appears in the equation comes from the factorization of the free oscillations of the ground-state amplitude. The electron then recombines with an amplitude equal to $\left\langle g\middle|x\middle|\vec{p}-\vec{A}(t_2)\right\rangle$, which gives the last remaining factor.

Let's take a look on eq.(4.12). In general the instantaneous kinetic energy $(\vec{p}-\vec{A}(\tau))^2/2$ is large (compared with the energy of the photons), so that the $\mathcal{S}(\vec{p},t_1,t_2)$ corresponds to some very large angle. The real or imaginary part of the $e^{-i\mathcal{S}(\vec{p},t_1,t_2)}$ term, i.e. the cosine and sine of this angle is just as likely to have a positive or negative sign. By changing the $\vec{p}$ variable by a small amount $\delta\vec{p}$, the change of the instantaneous kinetic energy is likewise small on the laser field's energy scale, but not when it is measured in terms of the photon energy. These small changes in the $\vec{p}$ variable will, in general, make enormous changes in the $\mathcal{S}(\vec{p},t_1,t_2)$ phase and the cosine and sine will oscillate exceedingly rapidly between plus and minus values. The total contribution will then add to zero for if a momentum $\vec{p}$ makes a positive contribution, another infinitesimally close makes an equal negative contribution so that no net contribution arises. Therefore, not every $\vec{p}$ momentum needs to be considered if the neighboring momentums have a different $\mathcal{S}(\vec{p},t_1,t_2)$ phase; for the momentums in the neighborhood cancel out the contribution. But for the special momentum, for which the $\mathcal{S}(\vec{p},t_1,t_2)$ phase is an extremum, a small change in the momentum produces, in first order at

[6] Actually, the variable being introduced, is a *canonical momentum* (see Appendix 5.2). But eq.(4.11) is also the solution of *Newton's equations of motion* in the case of an electromagnetic field and since the (kinetic-) momentum is better known and understandable quantity compared with the canonical momentum, I choose to refer to it as the (kinetic-) momentum.

[7] In the previous chapters, t_0 was used to denote the time that the electrons were spawned, while in this chapter t_1 denotes the time that the electron has spawned.

least, no change in the $\mathcal{S}(\vec{p}, t_1, t_2)$ phase. All the contributions from the momenta in this region are nearly in phase and do not cancel out. Therefore, only the momenta in the vicinity of the $\vec{p}_{stationary}$ can we get important contributions, and we need only consider the particular momentum as being of importance.

In the end, the major contribution to the integral over p in eq. (4.12) comes from the stationary points of the classical action [18],

$$\vec{\nabla}_{\vec{p}}\, \mathcal{S}(\vec{p}, t_1, t_2) = 0. \tag{4.13}$$

On the other hand, the gradient of the classical action with respect to the momentum $\vec{\nabla}_{\vec{p}}\, \mathcal{S}$ term is equal to the difference between the position of the free electron at time t_2 and time t_1, so that

$$\vec{\nabla}_{\vec{p}}\, \mathcal{S}(\vec{p}, t_1, t_2) = \vec{r}(t_2) - \vec{r}(t_1) = 0. \tag{4.14}$$

The physical meaning of the result expressed by eq. (4.14): the dominant contribution to the harmonic emission comes from the electrons which tunnel away from the nucleus at some position $\vec{r}$ but then re-encounter it, while oscillating in the laser field, in the same position $\vec{r}$. This was one of the major assumptions made by the semiclassical Simple Man's Model, which as we see, is justified by the quantum mechanical SFA description.

Introducing a new variable $t_r = t_2 - t_1$, which corresponds to the time duration of the electrons trajectory, extending the integration to infinity (since there is no restriction for it) and according to the considerations above, using the saddle-point approximation[8] I derive for the time-dependent dipole moment the following formula:

$$\langle x \rangle_{t_2} \approx 2\mathcal{R}e\Bigg\{ i \int_0^{\infty} dt_r \left(\frac{2\pi}{\epsilon + it_r} \right)^{3/2} \mathcal{E}(t_2 - t_r) \left\langle g \middle| x \middle| \vec{p}_{st}(t_2, t_r) - \vec{A}(t_2) \right\rangle \times \\ \times \left\langle \vec{p}_{st}(t_2, t_r) - \vec{A}(t_2 - t_r) \middle| x \middle| g \right\rangle e^{-i\mathcal{S}(\vec{p}_{st}, t_2, t_r)} \Bigg\}, \tag{4.15}$$

where

$$\vec{p}_{st}(t_2, t_r) = \frac{1}{t_r} \int_{t_2 - t_r}^{t_2} \vec{A}(\tau) d\tau. \tag{4.16}$$

The stationary value of the canonical momentum $\vec{p}_{st}(t_2, t_r)$, allows the electron trajectory that lasts for a time period t_r to return to the same position at some later time t_2.

Last but not least, the first factor in the integral over t_1 in eq. (4.15), $[2\pi/(\epsilon + it_r)]^{3/2}$ comes from the regularized Gaussian integration over p around the saddle-point while the infinitesimal ϵ has been put in by hand to handle the expression numerically. Lewenstein and his collaborators translated it as the term which expresses the effects of *quantum diffusion* of the electronic wavepacket [18]. This can be seen by its effect on the integral. All it does is to constrain the contributions from long lasting trajectories. This is exactly the same effect as the dispersion of an electron's wavefunction. As the time duration of an electron's propagation away from and towards the nucleus increases, the dispersion of its wavefunction is increased and the probability of an electron's rehabilitation of the ground state decreases.

As the electron is oscillating in the laser field, there is also non-negligible probability of it being scattered off by the parent's ion potential. This is happening even in the case where the electrons "appeared" in a distance far from the nucleus. Since the $\vec{\mathcal{E}}$ laser field is homogeneous in space and an

[8] The method is discussed in one of the appendices 5.3

electron's "preferable" direction lies along the $x-$axis, it is reasonable to expect that the evolution of the electron's wavepacket will be characterized by its oscillation along the x direction. During the time the electron is initially drawn away from the nucleus and is then drawn towards it, the electronic wavepacket will *diffuse*, i.e. the electronic wavepacket will be spread out. As a result, parts of the initially localized electron's wavefunction have reached the region of the nucleus with significant amplitudes. But it has to be noted that there are also those electrons whose wavefunction's quantum diffusion has led to the dispersion of the wavefunction in regions far away from the nucleus.[9].

4.1.3 Expansion of the time dependent dipole moment as a *Fourier series*

Since the time dependent dipole moment is assumed to be a periodic function with respect to time (the electric field which is responsible for this quantity is periodic and no depletion effect of the ground state is taken into account), it can be expanded in terms of an infinite sum of harmonically related sinusoids

$$\langle x(t)\rangle = \sum_{q=-\infty}^{\infty} \tilde{x}_q e^{-iqt} \tag{4.17}$$

$$= \tilde{x}_0 + 2\sum_{q=1}^{\infty} |\tilde{x}_q| \cos\left(qt + \underline{\angle \tilde{x}_q}\right). \tag{4.18}$$

This expansion is called the *Fourier series expansion*, $\tilde{x}_q$ denotes the $q-$th harmonic components and $\underline{\angle \tilde{x}_q}$ denotes its principle argument or its *intrinsic phase*. The $q-$th harmonic component, is given by the *Fourier transform* of the time dependent dipole moment

$$\tilde{x}_q = \frac{1}{2\pi}\int_t^{t+2\pi} \langle x(t_2)\rangle e^{iqt_2} dt_2 \tag{4.19a}$$

$$= 2\mathcal{R}e\Bigg\{ \frac{i}{2\pi}\int_t^{t+2\pi}\int_0^{\infty} dt_r \left(\frac{2\pi}{\epsilon + it_r}\right)^{3/2} \mathcal{E}(t_2 - t_r) \left\langle g\middle| x\middle| \vec{p}_{st}(t_2, t_r) - \vec{A}(t_2)\right\rangle \times$$

$$\times \left\langle \vec{p}_{st}(t_2, t_r) - \vec{A}(t_2 - t_r)\middle| x\middle| g\right\rangle e^{-i\mathcal{S}(\vec{p}_{st}, t_2, t_r) + iqt_2} dt_2 \Bigg\}. \tag{4.19b}$$

The harmonic spectrum is proportional to the plot of the squares of the harmonic amplitudes $|\tilde{x}_q|^2$ versus q.

4.1.4 Relation to the simple man's model

Just for the sake of completeness, it should be mentioned that eq. (4.15) shows a further relation between our quantum theory and the semiclassical *simple man's model*. In the limit $I_p \ll U_p$ the saddle point of the integral over t_r in eq. (4.15) tends to the stationary point of the classical action: $\mathcal{S}(\vec{p}, t_2, t_r)$, which corresponds to the zero value of the initial velocity, $\vec{p}(t_1) = \vec{p}(t_2 - t_r) = 0$. Thus, the second basic assumption of the semiclassical two-step model used in this thesis is also justified: the electrons which contribute most to harmonic generation are not only those which return to the nucleus, but also those which are liberated with zero initial velocity.

Nonetheless in this thesis eq.(4.15) will be evaluated using numerical methods in order to attain the time dependent dipole momentum of the system as a function of time. The main reason for choosing the numerical evaluation is to have a unified approach that can treat excitation from both a symmetric sinusoidal

[9]In scattering processes the main quantity that needs to be examined is the cross section which in general has a very small value $\sigma_{tot} \lll 1$. As a result, the re-scattering processes should be treated as a perturbation.

field, which is commonly studied in the literature, and excitation from an asymmetric $\omega/2\omega$ pulse. In any case, the results of the numerical evaluation (for the symmetric pulse) coincide with the results produced in reference [18].

The close relationship between our quantum mechanical theory and the semiclassical picture becomes even more striking when the harmonic emission spectrum is calculated (eq.4.19a) using the saddle point method for the t_r and t_2 integrals as well. This is done in order to attain a picture of the physical process. The saddle-point equations come from the t_r and t_2 integrals and take the form

$$\vec{\nabla}_{\vec{p}}\, \mathcal{S}(\vec{p}_{st}, t_2, t_r) = \vec{r}(t_2) - \vec{r}(t_2 - t_r) = 0 \tag{4.20}$$

$$\frac{\partial}{\partial t_r}\mathcal{S}(\vec{p}_{st}, t_2, t_r) = \frac{1}{2}\left(\vec{p} - \vec{A}(t_2 - t_r)\right)^2 + I_p = 0 \tag{4.21}$$

$$\frac{\partial}{\partial t_2}\mathcal{S}(\vec{p}_{st}, t_2, t_r) = \frac{1}{2}\left(\vec{p} - \vec{A}(t_2)\right)^2 - \frac{1}{2}\left(\vec{p} - \vec{A}(t_2 - t_r)\right)^2 = q \tag{4.22}$$

The first one of these equations indicates that the trajectories which contribute the most are those where the electron's initial spawn position is also the position on which the electron's recombination with the parent ion takes place. The electron spawned at some position $\vec{r}(t_2 - t_t)$ at some time $t_2 - t_r$ and later returned to it at t_2. Eq. (4.21) has an interesting and more complicated interpretation. If the ionization potential I_p was zero it would simply state that the electron being liberated at time $t_2 - t_r$ should have a velocity equal to zero. Nevertheless, the ionization potential is not equal to zero (after all if it was zero then there would be no point in speaking for tunneling ionization) and in order for the electron to pass through the Coulomb's barrier it must have a negative kinetic energy the moment of its liberation. This condition can only be fulfilled when t_r is a complex valued. The imaginary part of t_r can then be interpreted as the tunneling time. i.e. the time the electron spend under the barrier in order to be set free. The meaning of the complex t_r parameter in this way, was firstly being done in the seminal papers of *Ammosov et al.* [21–23]. Last but not least, using eq. (4.21), eq. (4.22) takes the form

$$\frac{1}{2}\left(\vec{p} - \vec{A}(t_2)\right)^2 + I_p = E_{kin} + I_p = q, \tag{4.23}$$

which is simply the fundamental physical law regarding energy conservation. The equation above states that the final kinetic energy of the recombining electron together with the energy that was needed in order to ionize the atom generates the q-th harmonic. This equation is the reason that the maximum emitted harmonic frequency is given by the maximum possible kinetic energy of the returning electron at the moment of its recollision with the nucleus. Qualitatively, this conclusion is fully consistent with the semiclassical argument that was presented in the beginning of this chapter in order to derive eq.(4.1).

4.2 Generation of spectra with the use of Lewenstein's model

The simplest case scenario in which the theory can be applied to is the case in which the electromagnetic field $\vec{\mathcal{E}}$ is generated by a continuous monochromatic laser of linear polarization. In this case the electric field amplitude and its corresponding vector potential at any moment in time can be expressed as:

$$\vec{\mathcal{E}}(t) = \mathcal{E}_0 \cos(t)\hat{x}, \qquad \vec{A}(\tau) = \mathcal{E}_0 \sin(\tau)\hat{x}, \tag{4.24}$$

the stationary momentum as

$$\vec{p}_{st}(t_2, t_r) = \mathcal{E}_0 \left(\frac{\cos(t_2) - \cos(t_2 - t_r)}{t_r} \right), \tag{4.25}$$

and by making use of the eqs. (4.7) the time dependent dipole moment (eq.(4.15)) takes the form:

$$\langle x \rangle_{t_2} \approx 2\mathcal{R}e \Bigg\{ i \int_0^\infty dt_r \left(\frac{2\pi}{\epsilon + it_r} \right)^{3/2} \mathcal{E}_0 \cos(t_2 - t_r) \left\langle g \middle| x \middle| \vec{p}_{st}(t_2, t_r) - \vec{A}(t_2) \right\rangle \times$$
$$\times \left\langle \vec{p}_{st}(t_2, t_r) - \vec{A}(t_2 - t_r) \middle| x \middle| g \right\rangle e^{-i\mathcal{S}(\vec{p}_{st}, t_2, t_r)} \Bigg\}, \tag{4.26}$$

where the classical action is equal to

$$\mathcal{S}(\vec{p}_{st}, t_2, t_r) = \int_{t_2 - t_r}^{t_2} \left[\frac{1}{2} \left(\vec{p} - \vec{A}(\tau) \right)^2 + I_p \right] d\tau. \tag{4.27}$$

To examine the harmonic spectrum, in this subsection, we have assumed that the ground's state wavefunction can be approximated by the wavefunction of a harmonic oscillator. We have used the wavefunction of the harmonic oscillator because we want to make the resemblance between the form of the HHG with the *kinetic energy density of the returning electrons* depicted more clearly. [10]

$$\psi = \left(\frac{a}{\pi} \right)^{3/4} e^{-ar^2/2}, \qquad a = 2I_p, \tag{4.28}$$

with the corresponding dipole matrix elements being proportional to

$$\langle \vec{p} \, | x | g \rangle = i \left(\frac{1}{\sqrt{\pi a}} \right)^{3/4} \frac{\vec{p}}{a} e^{-p^2/2a}. \tag{4.29}$$

The resemblance of the form of the HHG with the *kinetic energy density of the returning electrons*, is a general characteristic and does not depend strongly on the dipole matrix elements. As being discussed in [18], the spectrum of the HHG is not strongly affected by the wavefunction being used.

4.2.1 Simple sinusoidal field

The results in the case of a neon atom $I_p = 14.4$ (measured in photon energy) exposed to a 825 nm wavelength radiation of a simple monochromatic sinusoidal electromagnetic wave at intensity equal to $5 \times 10^{14} W/cm^2$ is shown in Fig.4.1. As you can see for the intensity being presented the harmonic spectrum has the characteristic shape being mentioned in the literature [18, 24, 25]. There is a large number of harmonic components with roughly the same amplitude (plateau) followed by a sharp cutoff. In the *plateau* region, there is a relatively small fluctuation of the harmonics strength around a mean value.

Given the intensity and its corresponding ponderomotive energy, the cutoff law eq.(4.1) predicts that after the 85th harmonic order, will the amplitude of the harmonic spectra start decreasing exponentially fast. The cutoff low is approximately correct and its disability in predicting the exact cutoff harmonic order can be attributed to the fact that in the semiclassical method described here, no interference phenomena are taken into account. The probability of an electron passing through the barrier as well as the effect of the

[10] For an alternative description of the HHG spectra, the wavefunction of a hydrogen-like atom can be used. For more information, check the Appendix 5.4.1

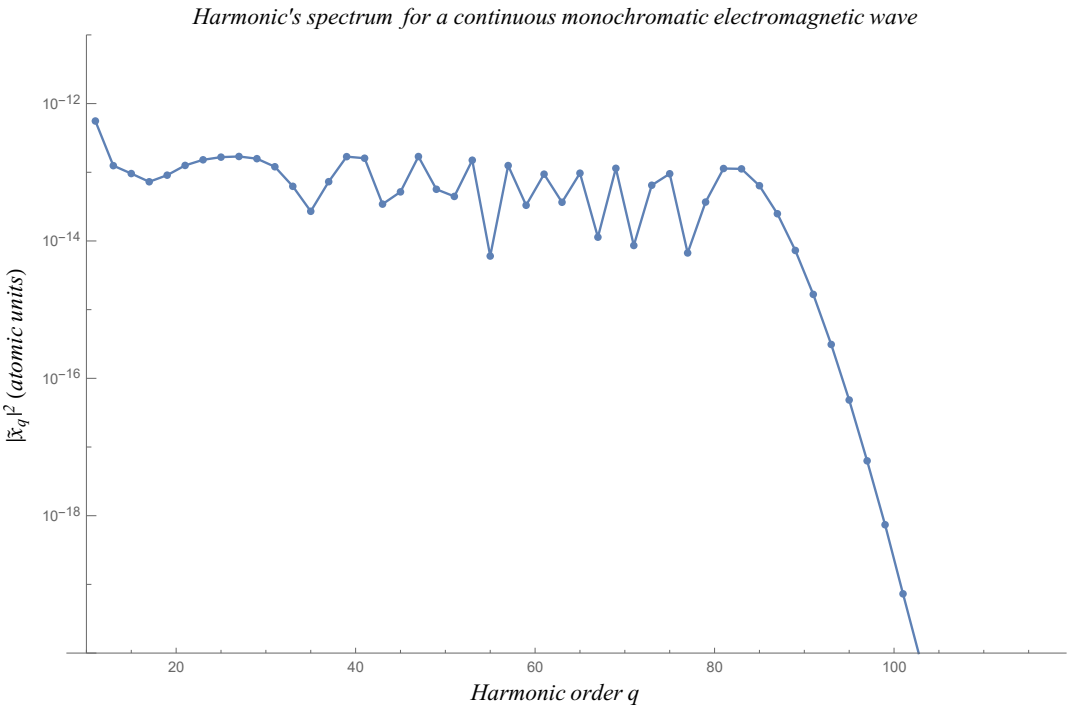

Figure 4.1: Harmonic spectra in the case of a Neon atom $I_p = 14.4\hbar\omega$ exposed to a continuous monochromatic electromagnetic wave of wavelength $\lambda = 825nm$ ($\hbar\omega \approx 1.5eV$) for the intensity $\mathcal{I} = 5 \times 10^{14} W/cm^2$.

quantum diffusion phenomenon of the electronic wavepacket have a strong influence on the contribution of each one of the classical trajectories which are the main contributors in the interference.

4.2.2 $\omega/2\omega$ asymmetric pulse

So far the HHG spectrum created by a simple sinusoidal field have been calculated. In doing so the results of my calculations have been verified by comparing with well known results form the bibliography, and in particular with reference [18][11].

In the following we will proceed to study the HHG spectrum that can be generated using an $\omega/2\omega$ asymmetric pulse. The aim is to explore the effect of the rescattering electron kinetic energy on the HHG spectra. In particular, in the previous section 3.2.3 I have pointed out that when the $\omega/2\omega$ phase difference φ and intensity ratio γ have the particular values of 121.5° and 0.45 respectively, the vast majority of the rescattering electrons return to the ionic core with similar kinetic energies, i.e. 'monochromatic' rescattering electrons are produced. The aim of this paragraph is to explore whether this narrow distribution of the returning kinetic energies will have any effect in the HHG spectrum. This is a reasonable question and its answer is expected to be positive since it is the energy of the rescattering electrons that control the energy of the harmonics. The aim of this study is twofold: first, a clear effect of these $\omega/2\omega$ parameters in the HHG spectrum will verify the results of the classical calculations presented in section 3.2.3 using a quantum theory. Second, this study will explore the application of such asymmetric pulses in controlling the spectrum of high harmonics as well as in the generation of short (as) pulses.

Lewenstein's model describing the HHG can also be used to examine the HHG of a two colour laser field. Generally speaking, in the case of a continuous two colour electromagnetic field with linear

[11] See Appendix 5.4

polarization, the field amplitude at any moment in time, using the dipole approximation, can be expressed in the following way

$$\vec{\mathcal{E}}(t) = \mathcal{E}_0 \left(\cos(t) + \gamma \cos(2t + \varphi)\right) \hat{x} \tag{4.30}$$

where φ corresponds to the phase difference between the two colours at $t = 0$ and γ is the ratio of the electric field strengths. Given these two parameters the "vector potential" and the stationary momentum take the form

$$\vec{A}(\tau) = \mathcal{E}_0 \left(\sin(\tau) + \frac{\gamma}{2} \sin(2\tau + \varphi)\right) \hat{x}, \tag{4.31}$$

and

$$\vec{p}_{st}(t_2, t_r) = \frac{\mathcal{E}_0}{t_r} \left[(\cos(t_2) - \cos(t_2 - t_r)) + \frac{\gamma}{4} \left(\cos(2t_2 + \varphi) - \cos(2t_2 - 2t_r + \varphi)\right)\right], \tag{4.32}$$

respectively. By inputting these expressions in eqs.(4.15),(4.19a) and following the same procedure as was described above, the HHG spectra for an arbitrarily asymmetric two colour field can be obtained.

More specifically, the laser fields to be considered, correspond to the asymmetric electromagnetic waves for which the ratio of the electric field strengths lies in the range from 0.45 to 0.55 and φ parameter is approximately equal to 121.5°.

First of all, in Fig.4.2, you can see the important role the γ and φ parameters play. The harmonic spectrum in the case of a two color field are characterized by the appearance of two *plateaus* and *cutoffs* regions. The plateaus are 2 for any value of φ and for many values of the γ parameter. In each one of the plateaus, there is a large number of harmonic components with roughly the same amplitude followed by a cutoff region. For the harmonic orders following the first plateau, there is a sharp decrease in the intensity, by almost two orders of magnitude, while for the harmonic orders following the second cutoff region, the intensity is decreased to such an extend that there was no point in plotting them.

On the left panel in Fig. 4.3, a zoom in the plateau of the HHG spectrum produced using a simple symmetric, sinusoidal continuous field is depicted (same as graph 4.1 with linear scale in the vertical axis). As we see the intensity of the harmonics is roughly the same, with small fluctuations. On the right panel in Fig. 4.3, a similar plot of the plateau of the HHG spectrum which is now produced using an asymmetric pulse with $\gamma = 0.5$ and $\varphi = 121.5°$ is depicted. This asymmetric continuous field results to monochromatic rescattering electrons (section 3.2.3) and we see immediately, that this narrow shape of the $EDRE$ is "transferred" to the HHG spectrum, as the last few harmonics of the plateau have distinctively higher intensity than all others.

It is important to note that this characteristic is robust under small deviations around the $\gamma = 0.5$ and $\varphi = 121.5°$ values. In Fig. 4.4 this robustness is demonstrated. The stability of the form of the spectra, regarding the γ parameter must be noted since in a modern laboratory the ratio of the electric field strengths cannot be measured to arbitrary precision. The stability around the φ parameter has been included, in order to encourage the conduction of an experiment.

4.2.3 Energy density of the returning electrons in the high harmonics generation spectra and the modified semiclassical cutoff law

All of the characteristics that have been discussed above were also seen when the *energy density of the returning electrons* ($EDRE$) was examined in the 3.2.3 section using the ADK theory. The influence of the γ and φ parameters in the harmonic spectra is similar to the influence they had on the $EDRE$ in the classical limit. This is something to be expected. After all, when the dominant contribution to the

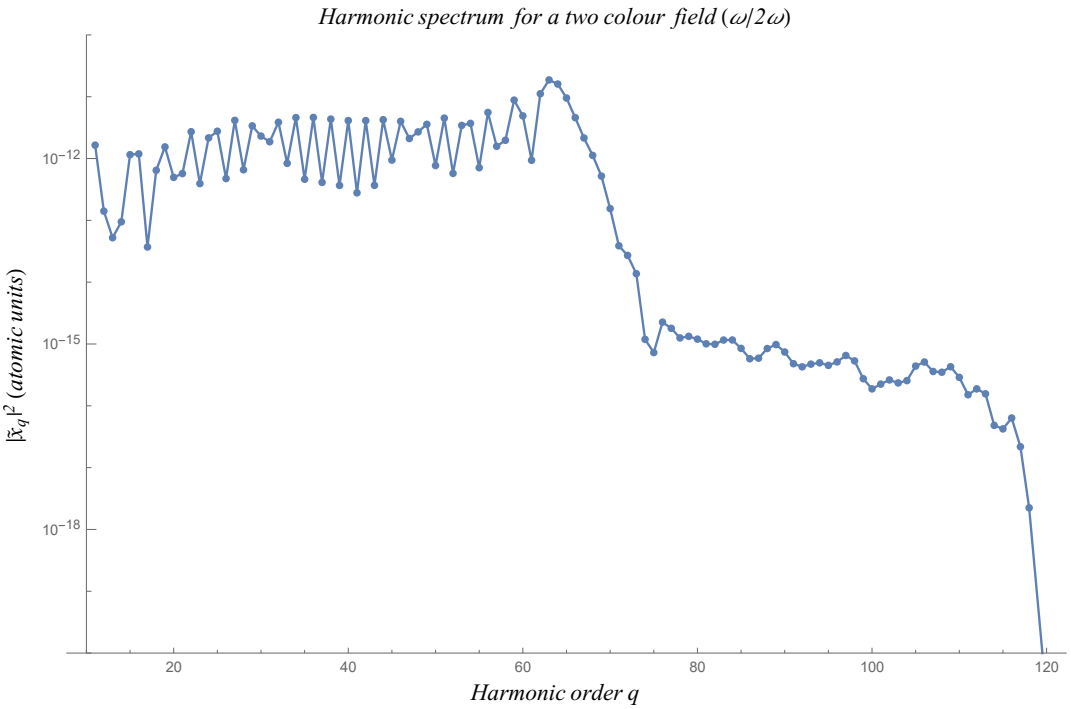

Figure 4.2: Harmonic spectra in the case of a Neon atom $I_p = 14.4\hbar\omega$ exposed to a continuous two colour asymmetric electromagnetic field $\omega/2\omega$ $(825nm/412.5nm)$ $(\hbar\omega \approx 1.5eV)$, with phase difference $\varphi = 121.5°$, the ratio of the electric fields strength $\gamma = 0.5$ and for the intensity of the fundamental frequency ω to be equal to $\mathcal{I} = 5 \times 10^{14} W/cm^2$.

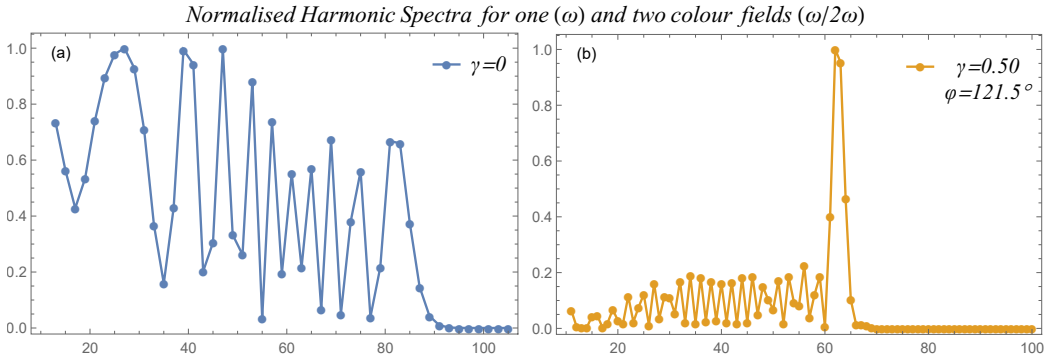

Figure 4.3: Comparison of the harmonic spectra obtain from the exposure of a Neon atom $(I_p = 14.4\hbar\omega)$ in a mono- (ω) and a bi-chromatic $(\omega/2\omega)$ continuous field. The fundamental frequency of the laser field corresponds to $(825nm)$ $(\hbar\omega \approx 1.5eV)$ and its intensity $\mathcal{I} = 5 \times 10^{14} W/cm^2$. Panel a) coincides with Fig.4.1 in a linear scale, while panel b). coincides with Fig.4.2 in a linear scale.

harmonic spectrum comes from the classical trajectories for which the initial momentum is equal to zero, the corresponding kinetic energy density profile is expected to play the most important role. To make this statement clearer, in Fig. 4.5, the HHG spectra Fig. 4.5.a and the $EDRE$ Fig.4.5.b in the case of $\gamma = 0.45$ have been plotted with respect to the phase difference between the two colours of the laser field φ. As you can see, in the harmonic spectra a vague image of the $EDRE$ in the classical limit is depicted. In particular, both the HHG and the $EDRE$ spectra are quite spread when the phase difference φ has values very different from the value 121.5°. As the phase difference approaches 121.5°, both the HHG and the $EDRE$ spectra are being 'focused' around an energy value close to $2 \times U_p$. Therefore it is easy to conclude that the narrow

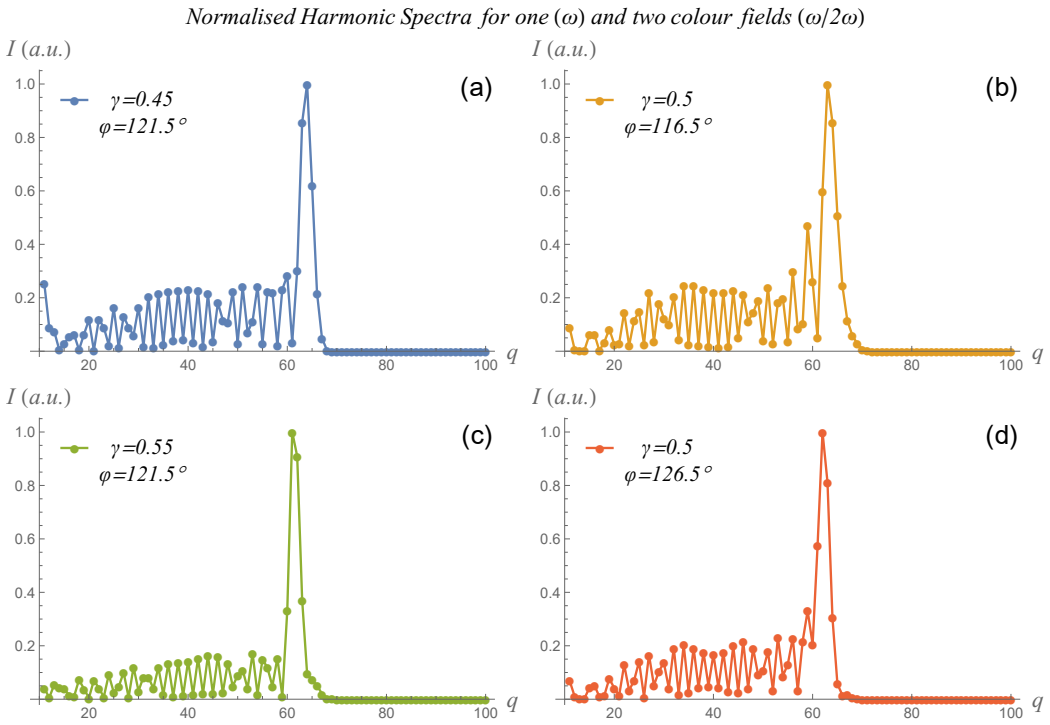

Figure 4.4: Plot of the normalized harmonic spectra obtain from the exposure of a Neon atom ($I_p = 14.4\hbar\omega$) in two colour field ($\omega/2\omega$). γ is the ratio of the electric field strengths $\mathcal{E}_{2\omega}/\mathcal{E}_{\omega}$ and φ is the phase difference of the two colours in the moment $t = 0$. The fundamental frequency of the laser field corresponds to ($825nm$) ($\hbar\omega \approx 1.5eV$) and its intensity for all of the cases is equal to $\mathcal{I} = 5 \times 10^{14} W/cm^2$.

distribution of the kinetic energy of the rescattering electrons is the cause of the pronounced peak in the HHG spectra at the end of the plateau.

It should be noted that this result, produced using a completely different calculation (SFA) to what was used in the 3.2.3 chapter (Newton's equation of motion), supports the validity of the results of this section (chapter 4).

Moreover, by plotting the $EDRE$ in a logarithmic scale, the plateau characteristic of the two cutoff regions of the HHG in the case of two colour fields can be explained. To make this clear, let us examine the representative $EDRE$ for $\gamma = 0.5$ and $\varphi = 121.5°$, see Fig. 4.6. In this case, the $EDRE$ is characterized by two peaks occurring when the kinetic energy of the returning electrons is equal to approximately $2.0 \times U_p$ and $4.1 \times U_p$ respectively albeit the peak at $4.1 \times Up$ is much smaller than the peak at $2.0 \times Up$, where U_p denotes the total ponderomotive energy[12]. For the corresponding harmonic spectrum shown in Fig. 4.6, the cutoff regions can roughly be approximated by the *modified semi-classical cutoff law* in which the maximum kinetic energy of the returning electrons. E_{max} in eq. 4.1 has been replaced with the kinetic energy for which the $EDRE$ shows a peak followed by a step-like decrease in intensity (see Fig. 4.6).

$$\mathcal{N}_1 \approx \frac{I_p + 2.0 \times U_P}{\omega}, \qquad \mathcal{N}_2 \approx \frac{I_p + 4.1 \times U_P}{\omega}, \tag{4.33}$$

Taking into account the given intensity and the corresponding ponderomotive energy, the *modified cutoff law* eq. (4.33) predicts that after the 61th harmonic order, will the amplitude of the spectrum start decreasing very rapidly for the first time and after the 106th harmonics order, will the amplitude of the

[12] $U_p = U_p^{(\omega)} + U_p^{(2\omega)} = U_p^{(\omega)} \left(1 + \frac{\gamma^2}{4}\right) = \frac{\mathcal{E}^2}{4} \left(1 + \frac{\gamma^2}{4}\right)$

harmonic spectra be diminished.

The modified cutoffs law is approximately correct (mean deviation is around 10 harmonic orders) and its disability in predicting the exact cutoff harmonic order can be attributed to the fact that in the semi-classical picture the *quantum diffusion* of the electronic wavepacket is not taken into account.

4.3 Phases of the Harmonic Component

Another interesting question raised almost immediately, after the first spectra had been observed [17], was whether or not the harmonics were *phase-locked*. To put it in another way, is the phase difference between two consecutive harmonics a constant? If the phase of the harmonics can be kept constant then they can be constructively interfered to create trains of short pulses of increased intensity.

Consider the simplest case scenario where N different harmonic components, with the same amplitude, are in a phase locked mode. The intensity $\mathcal{I}(t)$ of the total signal emitted by these harmonics is proportional to:

$$\mathcal{I}(t) \propto \left| \sum_{n=q_i}^{q_i+N-1} e^{-i(qt+q\varphi_0)} \right|^2 = \left| \sum_{q=1}^{N-1} e^{-i(qt+q\varphi_0)} \right|^2 = \left| \frac{e^{iN(t+\varphi_0)/2}-1}{e^{i(t+\varphi_0)/2}-1} \right|^2 = \frac{\sin^2\left(\frac{N(t+\varphi_0)}{2}\right)}{\sin^2\left(\frac{t+\varphi_0}{2}\right)}, \tag{4.34}$$

where φ_0 denotes the phase difference between two consecutive harmonics. Due to the constructive interference between the various harmonics (within a spectrum obtained for particular values of ϕ and γ), the maximum value of the intensity is constructively amplified[13]. Its time profile is a periodic function with periodicity $T/2 = 2\pi/\omega$, half the period of the laser and consists of sharp peaks, with full width at half maximum $\Delta T \approx T/2N$, shown by the blue line in Fig. 4.7. In contrast, when the phase difference between them appears to be completely random, yet constant, the effectiveness of the amplification of the total intensity signal $\mathcal{I}(t)$ is decreased since no interference occurs, shown by the orange line.

Unfortunately the simple man's model cannot be used to examine the phases of the various harmonic components. To do so one has to turn to an analytic and fully quantum mechanical theory of harmonics generation; valid in the tunneling region. In this section, the phases of the various harmonic components will be evaluated using the *Strong Field Approximation* (SFA) presented in the previous subsections.

Given the *Fourier transform* of the time dependent dipole moment, the phases of the various harmonic components corresponds to the arguments of them when being written in a polar form. In order to make a better approximation with respect to the intrinsic phases, the dipole matrix element corresponding a hydrogen atom (eq. 5.17) will be used for the calculation of the time dependent dipole moment, as was done in 4.1.2 . The phase differences between them can be evaluated by subtracting from the phase of each order of harmonics, the phase of the subsequent or preceding order (in this thesis, $\Delta\varphi_q = \underline{/\tilde{x}_{q+1}} - \underline{/\tilde{x}_q}$).

In the simplest case scenario of a simple monochromatic sinusoidal electromagnetic wave, the intrinsic phases ($\underline{/\tilde{x}_q}$)and the phase differences between the intrinsic phases of two consecutive harmonics components ($\Delta\varphi_q$) are shown in Fig. 4.8 and Fig. 4.9 respectively. As you can see, it seems that the intrinsic phases of the harmonics are completely random in the plateau, while after the cutoff region (harmonic order, $q = 81$) the phase locking mode exhibited by the harmonics is not very interesting, because the harmonic amplitude decreases very rapidly with the process order (in agreement with the results in [24]). As a consequence the contribution of only one or two harmonics is significant for the intensity $\mathcal{I}(t)$, leading to temporarily broad light pulses with a relatively small amplitude.

[13] This is happening for any given value of φ_0

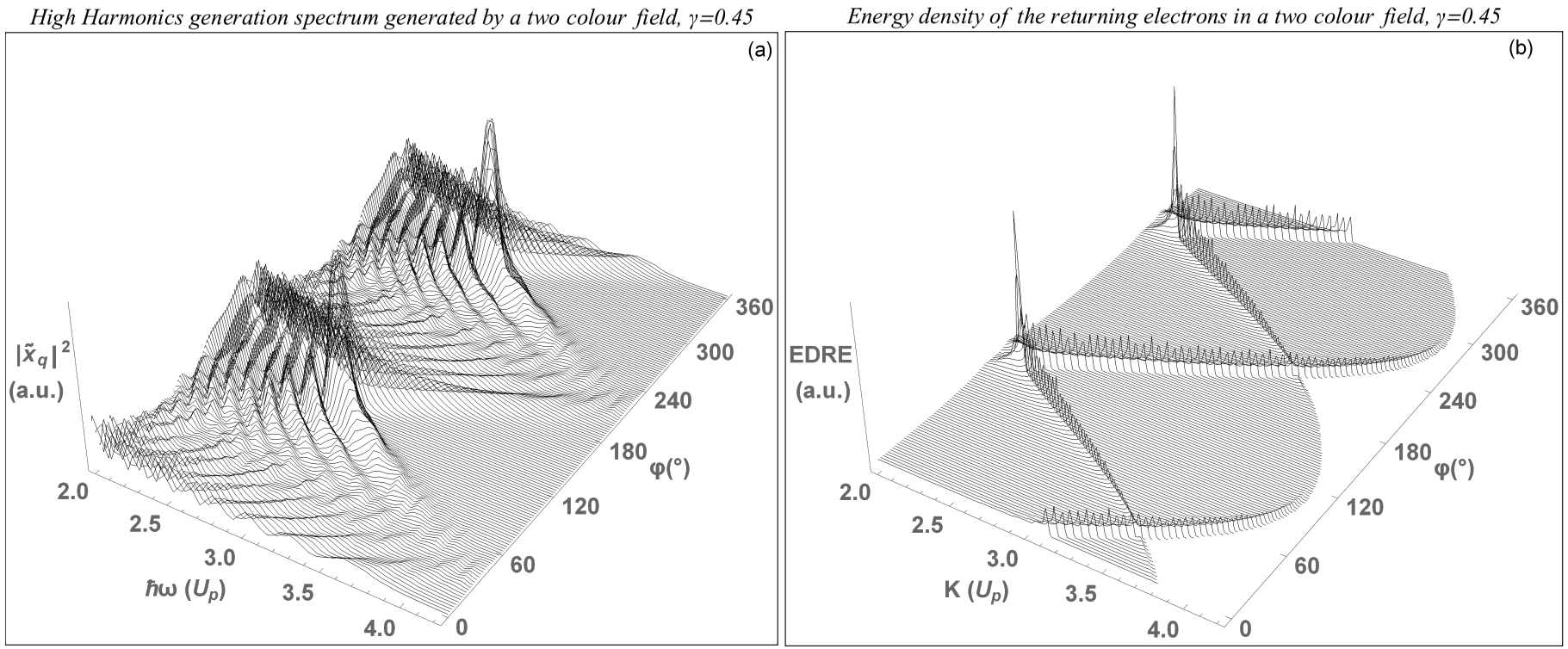

Figure 4.5: Comparison of the high (order) harmonic generation spectra obtained from the exposure of a Neon atom ($I_p = 14.4\hbar\omega \approx 0.65U_p$) in a a bichromatic ($\omega/2\omega$) laser field, with $\gamma = 0.45$ with the electron energy density of the returning electrons, when the initial velocity of the electrons is set to be equal to zero. The fundamental frequency of the laser field corresponds to ($825nm$) ($\hbar\omega \approx 1.5eV$) and its intensity $\mathcal{I} = 5 \times 10^{14} W/cm^2$.

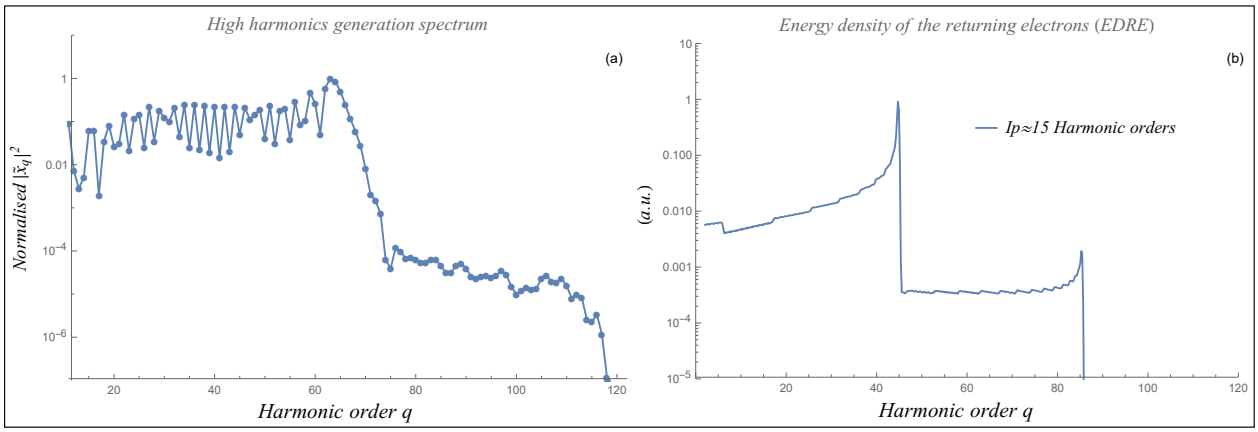

Figure 4.6: Comparison of the harmonic spectra obtain from the exposure of a Neon atom ($I_p = 14.4\hbar\omega$) in a a bichromatic ($\omega/2\omega$) laser field, with $\gamma = 0.5$ and $\varphi = 121.5^\circ$ with the electron energy density of the returning electron, when the initial velocity of the electrons is set to be equal to zero. The fundamental frequency of the laser field corresponds to ($825nm$) ($\hbar\omega \approx 1.5eV$) and its intensity $\mathcal{I} = 5 \times 10^{14} W/cm^2$.

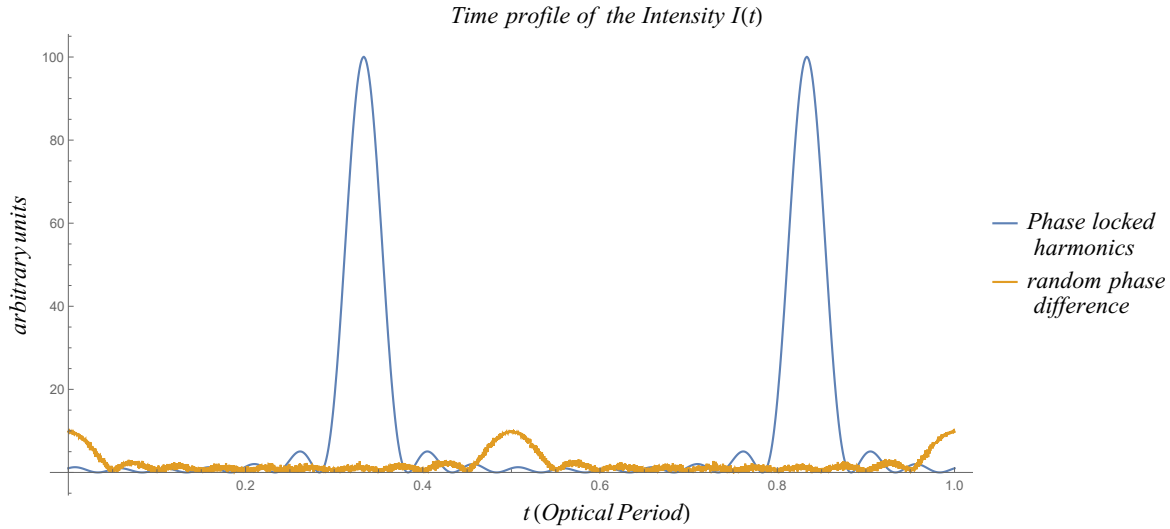

Figure 4.7: Time profile of the intensity as a function of time $\mathcal{I}(t)$ for the case of $N = 10$ harmonics. The blue line depicts the intensity of the total signal of a series of phase locked harmonics. The orange line depicts the intensity of the total signal of a series of harmonics whose phase difference varies around the phase locked mode by the maximum value of 30°.

In the cases of the previously mentioned asymmetric two colour laser fields, the phases of the various harmonics also present an interesting result. For a number of harmonic components before the first cutoff region (harmonic order $q = 61$), the intrinsic phases are not completely random (see left panel of Fig. 4.8). On the contrary, a valley/local minimum is present and in it the phase differences are close to zero. On the left of the local minimum, a steadily decreasing behaviour of the harmonics is observed with a relatively small step. On the contrary, after the cutoff region (61-th harmonic component), the phases of the harmonics seem to increase with a higher rate and away from the valley the intrinsic phases appear to be completely random. Last but not least, for harmonics orders beyond the second cutoff region (harmonic order, $q = 120$), the oscillations of the intrinsic phases seems to stop[14].

[14]It is important to note that in order to plot clearly the small fluctuations around the mean value, for each case of the

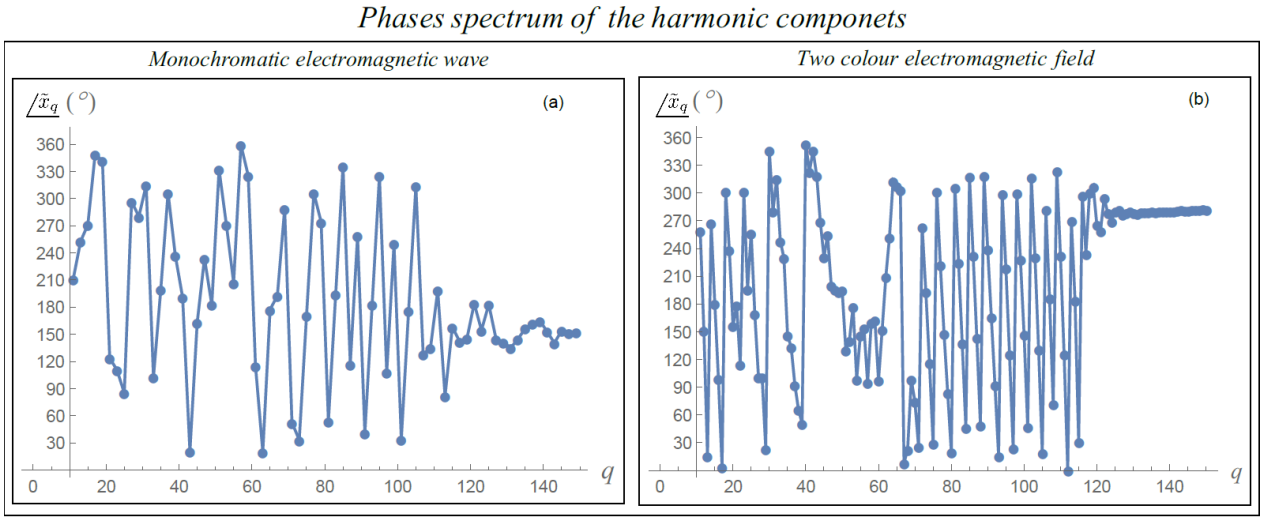

Figure 4.8: Intrinsic phases, $\angle\tilde{x}_q$, of the harmonic components in the case of a Neon atom $I_p = 14.4\hbar\omega$ exposed to a continuous one (ω) and two colour electromagnetic field ($\omega/2\omega$), with $\gamma = 0.45$ and $\varphi = 121.5^\circ$, with the fundamental wavelength $\lambda = 825nm$ ($\hbar\omega \approx 1.5eV$) and the intensity of the ω component $\mathcal{I} = 5 \times 10^{14} W/cm^2$.

In the right panel in Fig. 4.9, the phase differences for the asymmetric pulse, seem to increase very slowly with respect to the harmonic order, q, and the fluctuations around the mean value are not as strong as in the case of the symmetric pulse. Beyond the first cutoff region, the fluctuations of the phase differences are getting weaker (with some exceptions) but on a different value of the phase difference. Nevertheless, given that an appropriate filtering mechanism can be used to filter out the low order harmonic components, and the fact that after the first cutoff region the amplitude of the harmonic components has fallen off by four to six orders of magnitude, the generation of trains of attosecond pulses with with higher intensities (for a given amplitude) is assumed to be possible.

For the same reasons discussed in the previous subsection, the stability of this approximate phase locking mode needs to be tested under small deviation of the γ and φ parameter around their preferable values. In Fig. 4.10 four different cases has been plotted. In the left column, small deviation of the γ parameter around the value $\gamma = 0.5$ has been plotted while on the right column, small deviation of the φ parameter around the value $\varphi = 121.5^\circ$ has been plotted. In all four of these cases it seems that the phase differences follow the behaviour discussed previously and in general the phases do not seem to have been significantly altered.

The intensity of the total signal for the asymmetric cases is also expected to be greater than the total signal of a monochromatic electromagnetic wave, since in the former case not only a somewhat phase locked mode is presented but also the amplitude of the harmonics components is, by (approximately) two order of magnitude greater compared with the latter case (see Fig. 4.1, 4.2).

parameters in Fig. 4.9, an appropriate constant phase φ_0 has been added to all the phase difference φ, $\angle\tilde{x}_q \to \angle\tilde{x}_q + \varphi_0$. The constant phase φ_0 does not have a physical meaning. It has been used in order to translate all the phase differences by a constant amount upwards or downwards to make the the phase differences in the best way depicted. If, for example, the phases have been translated upwards, the phases whose value is greater than 360° will disappear from the top of the graph and reappear in the bottom of it. This is because I have plotted the principle phase differences value, $\mod(\angle\tilde{x}_q, 360)$[15]. What this operation is basically implying is that the top and the bottom of the graphs are connected in a cyclic manner, in a similar way the numbers 1 and 12 are connected in an analogue clock.

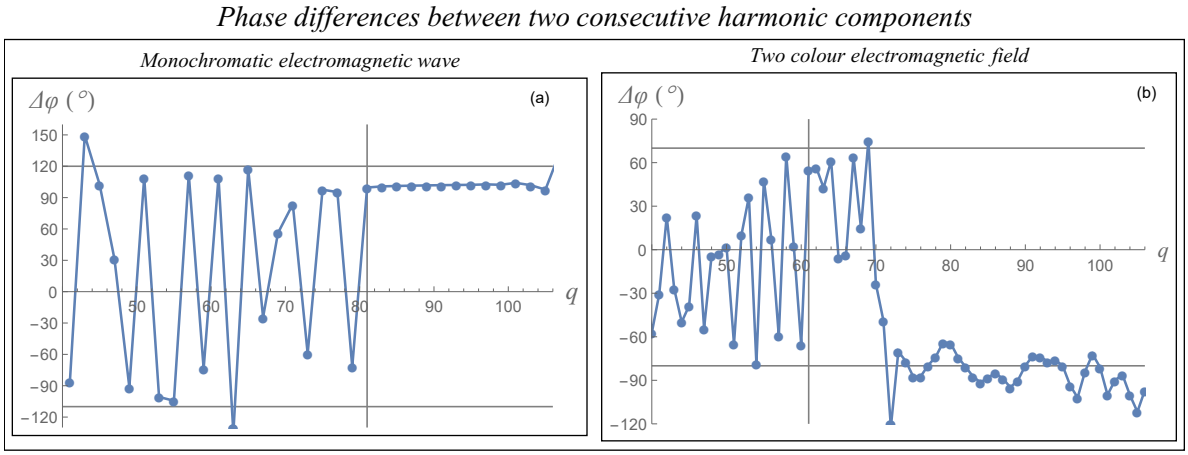

Figure 4.9: Phases differences of two consecutive harmonic components, $\Delta\varphi_q = \overline{/\tilde{x}_{q+1}} - \overline{/\tilde{x}_q}$, in the case of a Neon atom $I_p = 14.4\hbar\omega$ exposed to a continuous one (ω) and two colour electromagnetic field ($\omega/2\omega$), with the fundamental wavelength $\lambda = 825nm$ ($\hbar\omega \approx 1.5eV$) and the intensity of the ω component $\mathcal{I} = 5 \times 10^{14} W/cm^2$. In both panels, the grid-lines are used to distinguish the phase differences of the harmonic component with significant amplitude from the ones with insignificant amplitudes.

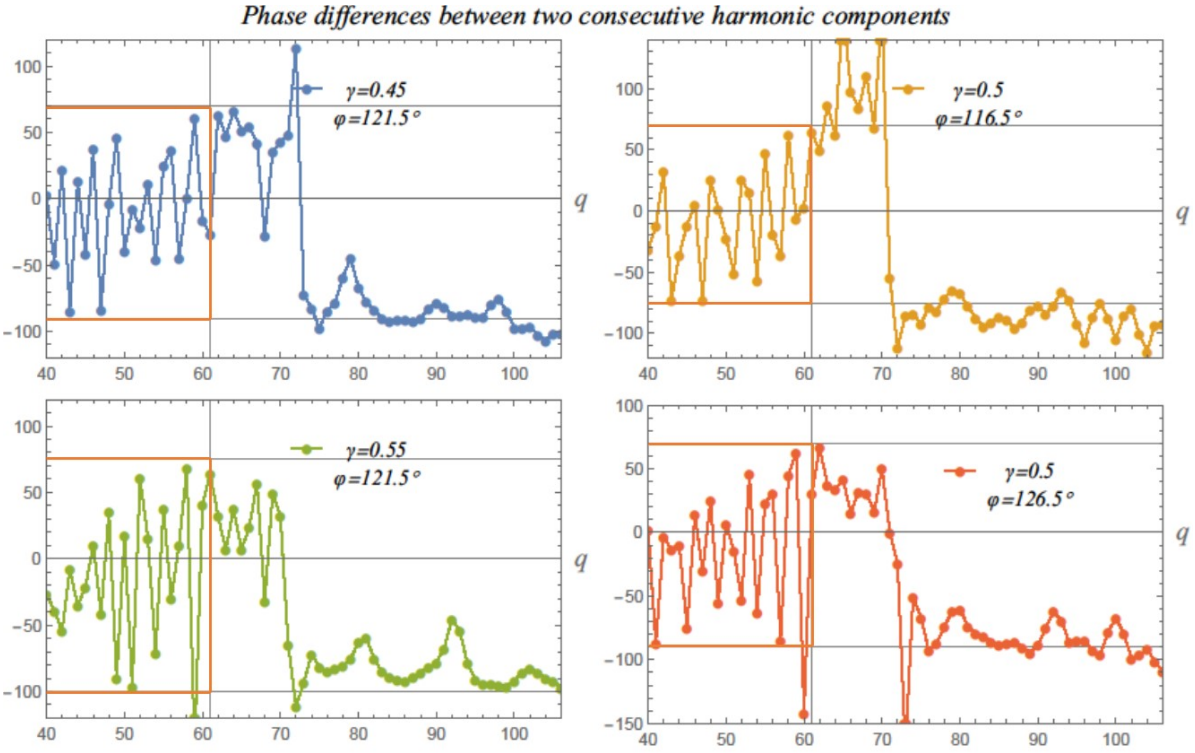

Figure 4.10: Phases differences of two consecutive harmonic components obtained from the exposure of a Neon atom $I_p = 14.4\hbar\omega$ in a two colour laser field $\omega/2\omega$. In all of the cases, the intensity of the fundamental harmonic of the laser is equal to $\mathcal{I} = 5 \times 10^{14} W/cm^2$ and its corresponding wavelength is equal to $\lambda = 825nm$ ($\hbar\omega \approx 1.5eV$). In all panels, the red grid-line square is used to distinguish the phase differences of the harmonic component with significant amplitude from the ones with insignificant amplitudes.

4.3.0.1 Interference of the harmonic components of the time dependent dipole moment

By filtering out some of the low order harmonic components of the time dependent dipole moment (eq. 4.17) and given the fact that after the first cutoff regions the amplitudes of the harmonic components are

weaker by approximately four to six orders of magnitude, the *effective time dependent dipole moment* can be approximated by

$$x_{eff}(t) = 2\sum_{q=q_i}^{q=q_f} |\tilde{x}_q| \cos\left(qt + \underline{/\tilde{x}_q}\right), \tag{4.35}$$

where $\tilde{x}_q$ denotes the $q-$th harmonic component and $\underline{/\tilde{x}_q}$ denotes its principle argument or its *intrinsic phase*.

The harmonic components of the x_{eff} are fast oscillating on the time scale of the fundamental harmonic $q = 1$ and we wish to examine whether it is significantly different from zero only in a limited time interval. To do so, we assume that we can approximate the basic characteristics of the $x_{eff}(t)$ function just by expressing it in the form of an almost harmonic oscillator,

$$x_{eff}(t) \sim A(t)\cos(\langle q\rangle t), \tag{4.36}$$

with a single fast oscillation frequency

$$\langle q\rangle = \sum_{q=q_i}^{q_f} \frac{q}{q_f - q_i + 1} = \frac{q_i + q_f}{2}, \tag{4.37}$$

having a slowly time varying (on the time scale of the fast oscillations) amplitude $A(t)$

$$A(t) = \left|\sum_{q=q_i}^{q=q_f} \tilde{x}_q e^{-iqt}\right|. \tag{4.38}$$

,

just like it is done in [31] The cosine term is oscillating very rapidly compared with the time varying amplitude because the $\langle q\rangle$ quantity has a relatively large value. So, in the time period of the cosine term $T = 2\pi/\langle q\rangle$, the amplitude $A(t)$ has not changed significantly and the mean value of the effective time dependent dipole moment $\langle x_{eff}\rangle$ in this time period can be approximated as

$$\langle x_{eff}\rangle \sim A(t). \tag{4.39}$$

Therefore, the mean intensity of the total signal emitted by the harmonic orders from q_i to q_f over one optical cycle of the average harmonic $\langle q\rangle$ is approximately equal to

$$\mathcal{I}(t) = NA^2(t) = N\left|\sum_{q=q_i}^{q=q_f} \tilde{x}_q e^{-iqt}\right|^2 = N\left|\sum_{q=q_i}^{q=q_f} |\tilde{x}_q| \exp\{i\underline{/\tilde{x}_q}\}\, e^{-iqt}\right|^2, \tag{4.40}$$

where N serves as a normalization constant in order to set the maximum value of the $\mathcal{I}(t)$ function in the case of a monochromatic sinusoidal electromagnetic wave to be equal to one.

In Fig. 4.11, I have plotted the $\mathcal{I}(t)$ function with respect to time, using the harmonic components that had been evaluated in the previous subsection, regarding the exposure of a Neon atom in the laser field of a mono- and bi-chromatic laser field.

In all cases, the number of components being used are 11 (even + odd= 11) and the intensity of the ω colour of the laser is equal to $\mathcal{I} = 5\times10^{14} W/cm^2$. This was done in order to compare the effectiveness of the generation of trains of attosecond pulses between the three cases. Nevertheless, the harmonic components, generated by the symmetric continuous field, span a range containing 22 harmonic orders whereas, in the

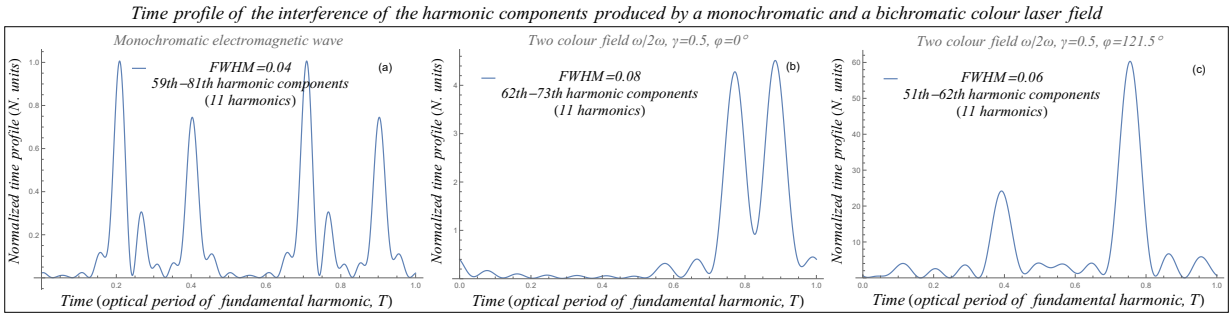

Figure 4.11: Time profiles of the filtered signal due to the interference of high harmonic orders emitted by a neon atom. In all panels, the horizontal axis correspond to the time period of the fundamental harmonic, $T = 2\pi/\omega \approx 2.75fs$, and the vertical axes corresponds to the relative intensity of the signal. The relative intensity is with respect to the minimum value of the two maximum values of the two time profiles. Laser parameters are the same as in the previous Figure 5.2, i.e. $I_p = 14.4\hbar\omega$, $\omega/2\omega$ $(825nm/412.5nm)$ $(\hbar\omega \approx 1.5eV)$, and the intensity of the fundamental harmonic component is equal to $\mathcal{I} = 5 \times 10^{14} W/cm^2$

case of the asymmetric field the harmonic components being used cover a range containing 11 harmonics . This is happening because, due to an inversion symmetry, only odd harmonic order are emitted in the former case. In the one colour field scenario, the harmonic components taken into account range from the 59-th to the 81-th harmonic components . In the cases of the asymmetric field, the harmonic components taken into account range from the 62-th to the 73-th order for $\varphi = 0°$ and from the 51-th to the 62-th order for $\varphi = 121.5°$. The harmonic components are not the same since the cutoff regions in these three do not coincide. In other words, the time profiles, have been plotted by taking into account only the last eleven harmonic components, whose amplitudes take significant values. In the former case,the cutoff region is presented in the $\mathcal{N} \approx 81$-th harmonic order (see, eq.(4.1)) while in the $\gamma = 0.5$ cases, the first cutoff regions, are presented in the $\mathcal{N}_1 \approx 61$-th and $\mathcal{N}_1 \approx 73$ harmonic orders (see eq.(4.33).

The time profile for these cases, is quantitatively characterized by narrow peak pulses with the *Full Width Half Maximum* $FWHM$, being approximately equal to six percent of the time period of the fundamental harmonic of the laser, $12\pi/100\omega$. The maximum intensity in the case of the asymmetric pulse with $\varphi = 121.5°$, is sixty times greater than the maximum intensity of the simple sinusoidal electromagnetic field while for $\varphi = 0°$, the maximum intensity is only four times greater. These results can be attributed to the higher values of the spectrum of the asymmetric pulse compared to the spectrum obtained from the one colour field (see Fig.4.1, 4.2 and 5.2), as well as to the form of the phase spectrum of the two colour fields (see Fig.4.8).

To examine whether solely, one of the aforementioned reasons is responsible for the increased short pulse intensity, in Fig.4.12, a modified $\mathcal{I}$ function is shown. The $\mathcal{I}$ function has been modified by replacing all the harmonic amplitudes with unity, $|\tilde{x}_q| \to 1$, so that the magnitude of the amplitudes of the various harmonics will play no significant role. Basically, I have replaced the characteristic form of the Harmonic spectrum, with a square/uniform frequency spectrum form.

In all three panels in Fig. 4.12, we can see that the form of the time profiles have changed. On the left panel, for the case of the simple sinusoidal electromagnetic wave, there has not been a significant change. The two main peaks have swapped their places and the $FWHM$ of the maximum peak has increased by a small amount. In the cases of the asymmetric pulses (middle and right panel), it is shown that the form of the time profile has been significantly changed. In the middle panel, in the case of $\gamma = 0.5$ and $\varphi = 0°$, the two main peaks have become three and the relative amplitude has been decreased by approximately 75%. In

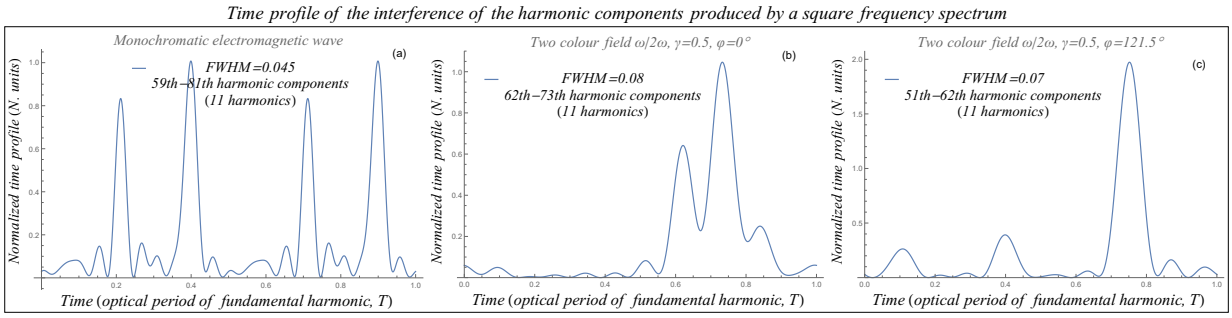

Figure 4.12: Time profiles due to the interference of harmonic orders with a square frequency spectrum. The intrinsic phases used in both panels were evaluated from the exposure of a Neon atom to a bichromatic laser field. In both panels, the horizontal axis correspond to the time period of the fundamental harmonic, $T = 2\pi/\omega \approx 2.75fs$, and the vertical axes corresponds to the relative intensity of the signal. The relative intensity is with respect to the minimum value of the two maximum values of the two time profiles. Laser parameters are the same as in the previous Figure 5.2, i.e. $I_p = 14.4\hbar\omega$, $\omega/2\omega$ $(825nm/412.5nm)$ $(\hbar\omega \approx 1.5eV)$, and the intensity of the fundamental harmonic component is equal to $\mathcal{I} = 5 \times 10^{14} W/cm^2$

the right panel, in the case of $\gamma = 0.5$ and $\varphi = 0121.5°$, the previously two main peaks have become three, the maximum intensity is approximately two times greater than the maximum intensity of the ω field (the relative intensity has decreased by approximately 97%) and the $FWHM$ has slightly been increased.

Based on the ratio of the maximum Intensity of the asymmetric to the symmetric electromagnetic fields, we can deduce that the phase differences in the case of the $\omega/2\omega$ electromagnetic fields are slightly more effective than the ω electromagnetic field when it comes to the maximum intensity of the total signal. Therefore the intensity enhancement of the time profile for $\gamma = 0.5$ and $\varphi = 121.5°$ in Fig. 4.11 does not come from the intrinsic phases of the harmonic components but comes from their corresponding relative magnitude which is strongly related with the phase difference of the two colours of the laser field.

Qualitatively, the two graphs in Fig. 4.11 seem to differ with respect to the periodicity of the plotted function and the form of the main peaks. The main difference is the periodicity of the two functions. The number of the dominant peaks comes from the interference of various harmonic components with different amplitudes and the periodicity comes from the type of the harmonic orders that interfere. In the left panel, the plot of the $\mathcal{I}(t)$ quantity depicts a function which has twice the frequency of optical period of the fundamental harmonic of the laser. This double frequency characteristic comes from the fact that in the amplitude function $A(t)$, the even harmonics do not contribute,

$$A_\omega(t+\pi) = \left| \sum_{q=q_i}^{q_f} \tilde{x}_{2q+1} e^{-i(2q+1)(t+\pi)} \right|, \qquad q \in \mathbb{N} \tag{4.41a}$$

$$= \left| \sum_{q=q_i}^{q_f} \tilde{x}_{2q+1} e^{-i(2q+1)t} \right| = A_\omega(t) \Longrightarrow \boxed{A_\omega(t+\pi) = A_\omega(t)}. \tag{4.41b}$$

On the contrary, in the case of the asymmetric two colour field, both, even and odd harmonic components contribute to the Amplitude $A(t)$ and therefore, the period of the $\mathcal{I}(t)$ function is the same as the optical periodicity of the ω colour.

Chapter 5

Conclusions

This thesis presents the theory and method with which, the kinetic energy of the rescattering electrons can be evaluated. The method is general and can be used to examine the interaction of an atomic system with an arbitrary asymmetric pulse. The study was based on two main features:

1. the possibility of an electron starting experiencing the effect of the external field (ionization of the system) and

2. the effect that the light source had on the liberated electrons.

Using the theory and the numerical methods described in this text, the kinetic energy distributions of the rescattering electrons were examined and a exquisitely narrow peak in the kinetic energy distribution was found. The narrow width comes from the form of the "optimized" two colour $\omega/2\omega$ laser field. The "optimized" laser field's was found to be reliable and robust. The kinetic energy distribution of the rescattering electrons generated by the optimized field is not significantly affected by small variations of the laser parameters (phase difference between the two colour pulses and the ratio between the two colour amplitudes), the pulse's duration (number of cycles of the ω and 2ω carriers in the envelope) or by the number of candidate interaction events of the rescattering electrons with its parent ion.

To explore some candidate applications of the optimized field, the theory behind the generation of high harmonics was studied. For two colour fields, the spectra of high order harmonics are characterized by the existence of two different plateaus, where the intensity of all the harmonic components is roughly a constant. Following the first plateau, the spectrum's intensity is substantially decreased, and after the second plateau, the spectrum's intensity is negligible (cutoff regions). The location of the plateau and the cutoff regions were found to have a great resemblance with the kinetic energy distributions of the rescattering electrons and ultimately a modified cutoff law was introduced.

In the study of the high orders harmonic generation, the optimized field presented another interesting characteristic. (At least theoretically) the difference between the intrinsic phases of two consecutive harmonics component reduced. As a result, the interference of its harmonics components is constructive and thus the optimized field could be used for the preparation of attosecond pulses of increased intensity.

Appendices

5.1 Deformation of the initial wavefunction of a particle

Consider a particle whose wavefunction is obtained by solving the Time-Dependent Schröndinger Equation ($TDSE$):

$$i\frac{\partial}{\partial t}\left|\psi(\vec{r},t)\right\rangle = \hat{\mathcal{H}}(t)\left|\psi(\vec{r},t)\right\rangle = \left(\hat{\mathcal{H}}_0 + V_{ex}\right)\left|\psi(\vec{r},t)\right\rangle. \tag{5.1}$$

The energy spectrum of the $\hat{\mathcal{H}}_0$ operator is assumed to be known and the V_{ex} denotes the potential energy of the particle which comes from the interaction of it with an external source. Assuming that the electron was initially in a bound $|i\rangle = e^{-i\hat{\mathcal{H}}_0 t}|b\rangle = e^{iI_p t}|b\rangle$ state, with ionization potential I_p and only after just a moment has passed since the electron interacted with the external source, the electron's wavefunction is expected to have slightly been deformed:

$$\left|\psi(\vec{r},t)\right\rangle = |i\rangle + |\delta\psi\rangle. \tag{5.2}$$

As a result the valence electron is no longer in the initial stable, bound state. The term which is responsible for the deformation of the initial $|i\rangle$ state can be evaluated by directly substituting the wavefunction of the electron into the $TDSE$ eq. (5.1):

$$i\frac{\partial}{\partial t}\left|\psi(\vec{r},t)\right\rangle = \left(\hat{\mathcal{H}}_0 + V_{ex}\right)\left|\psi(\vec{r},t)\right\rangle \Longrightarrow \tag{5.3a}$$

$$\left(i\frac{\partial}{\partial t} - \hat{\mathcal{H}}\right)|\delta\psi\rangle = V_{ex}(t)\,|i\rangle \Longrightarrow \tag{5.3b}$$

$$e^{i\int_{t_0}^{t}\hat{\mathcal{H}}(\tau)d\tau}\left(i\frac{\partial}{\partial t} - \hat{\mathcal{H}}\right)|\delta\psi\rangle = e^{i\int_{t_0}^{t}\hat{\mathcal{H}}(\tau)d\tau}V_{ex}(t)\,|i\rangle \Longrightarrow \tag{5.3c}$$

$$i\int_{t_0}^{t_2}\frac{\partial}{\partial t}\left(e^{i\int_{t_0}^{t}\hat{\mathcal{H}}(\tau)d\tau}|\delta\psi\rangle\right)dt = \int_{t_0}^{t_2} e^{i\int_{t_0}^{t}\hat{\mathcal{H}}(\tau)d\tau}V_{ex}(t)\,|i\rangle\,dt \overset{t\to t_1}{\Longrightarrow} \tag{5.3d}$$

$$e^{i\int_{t_0}^{t_2}\hat{\mathcal{H}}(\tau)d\tau}|\delta\psi(t_2)\rangle - \cancelto{0}{|\delta\psi(t_0)\rangle} = \int_{t_0}^{t_2} e^{i\int_{t_0}^{t_1}\hat{\mathcal{H}}(\tau)d\tau}V_{ex}(t_1)\,|i\rangle\,dt_1 \Longrightarrow \tag{5.3e}$$

$$|\delta\psi(t_2)\rangle = -i\int_{t_0}^{t_2} e^{-i\int_{t_1}^{t_2}\hat{\mathcal{H}}(\tau)d\tau}V_{ex}(t_1)\,|i\rangle\,dt_1 \tag{5.3f}$$

And using a *completeness equation* $\sum\!\!\!\!\!\!\int_j |j\rangle\langle j| = \mathbb{1}$ (which assures that there is no basis vector "missing"), the expression above is brought to the form

$$|\delta\psi(t_2)\rangle = -i\int_{t_0}^{t}\sum\!\!\!\!\!\!\int_j \underbrace{e^{-i\int_{t_1}^{t}\hat{\mathcal{H}}(\tau)d\tau}|j\rangle}_{III}\,\underbrace{\langle j|\,V_{ex}}_{II}\,\underbrace{e^{-i\hat{\mathcal{H}}_0 t}|b\rangle}_{I}\,dt_1. \tag{5.4}$$

The symbol $\sum\!\!\!\!\!\!\int$ is meant to indicate the summation over the discrete ($\sum$) and continuous ($\int$) energy levels of the complete Hamiltonian, $\hat{\mathcal{H}}$ [1]. Even though eq. (5.4) does not look very appealing, it can be translated into a

[1] In a mathematical form, the $\sum\!\!\!\!\!\!\int_j |j\rangle\langle j|$ is equivalent to: $\sum\!\!\!\!\!\!\int_j |j\rangle\langle j| \equiv \sum_n |n\rangle\langle n| + \int d\vec{\kappa}^3\,|\vec{\kappa}\rangle\langle\vec{\kappa}|$

beautiful and easy to grasp picture: The system starts its journey in the $|i\rangle$ state. Being in a bound/stationary state $|b\rangle$, the electron's bound state amplitude is oscillating with bare frequency ${I_p}^2$ until some later time t_1 ($I-$factor in eq.(5.4)), when it suddenly starts interacting with the external source ($II-$factor in eq.(5.4)). At that moment, the electron immediately makes a transition to another state $|j\rangle$, the evolution of which, is afterwards affected by the complete Hamiltonian ($III-$factor in eq.(5.4).

In the fourth line of the above equation (5.3d), I have chosen to set the upper limit equal to t_2 and replace t with t_1 in order for the $|\delta\psi\rangle$ component's interpretation to be broken down using consecutive time moments.

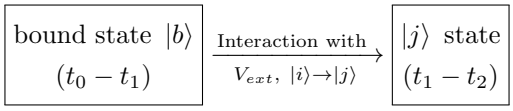

5.2 Volkov states

In this Appendix, the exact solution of the *Time Dependent Schröndinger equation* ($TDSE$) in the case of a continuous electromagnetic wave in the dipole approximation will be deviated, i.e. the solution to an equation of the form

$$\left[-\frac{\hbar^2}{2m}\nabla^2 - \vec{\mathcal{E}}(t)\cdot\vec{r}\right]\psi = i\hbar\frac{\partial\psi}{\partial t} \tag{5.5}$$

The solution of this $TDSE$ is used in the 4.1.1 subsection in order to describe the behaviour of an electron in the presence of a laser field.

The derivation which I am going to present[3] is not the simplest but it gives a very clear feeling for the quantum-classical connection, by managing to correspond some variables, in an understandable and none unintuitive way, to classical known quantities. The method is general, and therefore I am going to replace the $-\vec{\mathcal{E}}(t)\cdot\vec{r}$ potential by V:

$$\left[-\frac{\hbar^2}{2m}\nabla^2 + V\right]\psi = i\hbar\frac{\partial\psi}{\partial t} \tag{5.6}$$

To solve this equation I rewrite the wavefunction in the form: $\psi = \psi_0 e^{iS/\hbar}$, where ψ_0 is a contact and $\mathcal{S}$ is a function, which from now on I will refer to as the action, as a function of position and time. Substituting this expression into the $TDSE$ above the exact equation for the action takes the form:

$$\frac{1}{2m}\left(\vec{\nabla}S\right)^2 + V + \frac{\partial S}{\partial t} = \frac{i\hbar}{2m}\nabla^2 S \tag{5.7}$$

This equation differs from the classical *Hamilton-Jacobi (HJ) equation* (an alternative formulation of classical mechanics, equivalent to other formulations such as Newton's laws of motion, Lagrangian etc.[4]) for the action due to the presence of the last term, which involves the second-order spatial derivative. It coincides with the HJ equation if this term is equal to zero. This is precisely the case for the potentials that depend on the position $\vec{r}$ in physical space linearly ($V(\vec{r},t) = \alpha(t) - \vec{\beta}(t)\cdot\vec{r}$), which allows for solutions to also be linearly

[2] $I_p/\hbar$ in SI

[3] It is based on: M. Yu Ivanov, M. Spanner and O. Smirnova, Journal of Modern Optics 52, pp. 165 – 184, 200. `https://ulp.ethz.ch/education/lectures/laser-atom-interactions.html`

[4] For more information I highly suggest: H. Goldstein, C. P. Poole, J. L. Safko, Classical Mechanics 3rd edition, Pearson Education (2002)

dependent on the position $S = \gamma(t) + \vec{\delta}(t) \cdot \vec{r}$:

$$\frac{\delta^2}{2m} + \alpha - \vec{\beta} \cdot \vec{r} + \dot{\gamma} + \dot{\vec{\delta}} \cdot \vec{r} = 0 \Longrightarrow \tag{5.8a}$$

$$\vec{\delta}(t) = \vec{\delta}_0 + \int_{t_0}^{t} \vec{\beta}(\tau) d\tau \tag{5.8b}$$

$$\gamma(t) = -\int_{t_0}^{t} \left(\frac{1}{2m} \delta(\tau)^2 + \alpha(\tau) \right) d\tau \tag{5.8c}$$

The solution of the HJ equation then corresponds to the classical action, i.e. the least action which corresponds to the time integral of the *Lagrangian* around the physical path of the system: $\mathcal{S} = \int \mathcal{L}(\vec{r}_{cl}(t), \vec{p}_{cl}(t)) dt$. The $\vec{r}_{cl}(t), \vec{p}_{cl}(t)$ are obtained after having solved the *Euler-Lagrange equations*. In the HJ theory, the canonical momentum of the particle is evaluated by the differentiation of the classical action with respect to the position[4]:

$$\vec{\wp} \equiv \vec{\nabla} \mathcal{S} = \vec{\wp}_0 + \int_{t_0}^{t} \vec{\beta}(\tau) d\tau, \tag{5.9}$$

where I have set $\vec{\delta}_0 = \vec{\wp}_0$ so that I can reduce the amount of letters being used. So, overall, in the case of a potential which is linear in time, the solution can be expressed in the following, compact form:

$$\mathcal{S} = -\int_{t_0}^{t} \frac{\wp^2}{2m} d\tau - \vec{\wp} \cdot \vec{r} \tag{5.10}$$

In the case of an electromagnetic wave, working in the length gauge and in the dipole approximation regime, the $TDSE$ takes the form

$$\hat{\mathcal{H}}_f \psi = \left[-\frac{1}{2} \nabla^2 - e \vec{\mathcal{E}} \cdot \vec{r} \right] \psi = i\hbar \frac{\partial \psi}{\partial t}. \tag{5.11}$$

By direct substitution of the potential energy of the particle into eq. (5.9), the canonical momentum is given by $\vec{\wp} = \vec{\wp}_0 - e \int_{t_0}^{t} \vec{\mathcal{E}}(\tau) d\tau$. This solution is identical to the solution obtained by solving *Newton's equations of motions* in the presence of an electric field and thus we can interpret the $\vec{\wp}$ variable as the (classic-)momentum. So, $\vec{\wp}_0$ corresponds to the initial momentum of the particle and $\wp^2/2m$ to its instantaneous kinetic energy. Overall, by setting the proportionality constant ψ_0 to be equal to $(2\pi)^{-3/2}$ the solution to eq. (5.5) takes the form:

$$\psi(t; \vec{p}_0) = \frac{1}{(2\pi)^{3/2}} e^{i\mathcal{S}(t; \vec{p}_0)/\hbar}, \tag{5.12a}$$

$$\mathcal{S} = \vec{p} \cdot \vec{r} - \int_{t_0}^{t} E_{kin} dt, \tag{5.12b}$$

$$E_{kin}(t; \vec{p}_0) = \frac{p^2}{2m}, \tag{5.12c}$$

$$\vec{p}(t; \vec{p}_0) = \vec{p}_0 - e \int_{t_0}^{t} \vec{\mathcal{E}}(\tau) d\tau, \tag{5.12d}$$

and is referred to in the literature as the *Volkov* wavefunction[5].

In the solution there is a degree of freedom regarding the t_0 parameter that needs to be stressed out, since it greatly affects the way in which the terms in eq. (5.12d) can be interpreted. In the case in which t_0 is set to correspond to the first moment in time when the electron experienced the influence of the electric

[5]From now on, in order to avoid any possible misunderstandings, I will replace the canonical momentum with the (kinematic/classical-)momentum $\vec{\wp} \to \vec{p}$.

field, then the $\vec{p}_0$ term can be interpreted as the momentum of the initially "free" electron and the constant term coming from the evaluation of the lower integral limit can be thought of as the drift attained from the electron in the laser field[6]. If t_0 corresponds to a moment in time when the calculation of the lower integral limit yields zero, then the $\vec{p}_0$ term can be seen as the sum of the initial and drift momentum of the particle.

For the easiest understanding in the applications of the equations written above, I believe that the preferable interpretation is the one in which the t_0 corresponds to the moment in when the electron felt the presence of the laser field for the first time.

For the Volkov states, there is another useful identity that I need to mention because it is used to derive the *time dependent dipole moment* in the 4.1.2.

$$e^{-i\int_{t_0}^{t}\hat{\mathcal{H}}_f(\tau)d\tau/\hbar}\psi(t_0;\vec{p}_0)=\psi(t;\vec{p}_0)=\psi\left(t_0;\vec{p}_0-e\int_{t_0}^{t}\vec{\mathcal{E}}(\tau)d\tau\right) \tag{5.13}$$

5.3 Saddle Point Approximation

5.4 Construction of the discrete dipole function

In order to calculate these results, the time dependent dipole moment is the first quantity that needs to be calculated. The time dependent dipole moment was calculated not as a function but as list. By breaking down the time period of the laser in N equally separated time intervals

$$t_2=0,\ \Delta t,\ 2\Delta t,\ 3\Delta t,\ \cdots,\ (N-2)\Delta t,\ (N-1)\Delta t,\ 2\pi,\qquad \Delta t=2\pi/N \tag{5.14}$$

a two dimensional list was created with the first argument of each row being equal to the value of t_2 and the second element being equal to the numeric value of the obtain from the numerical integration of eq. 4.26, i.e. (in a matrix representation)

$$\begin{pmatrix} 0 & \langle x\rangle_0 \\ \Delta t & \langle x\rangle_{\Delta t} \\ 2\Delta t & \langle x\rangle_{2\Delta t} \\ \vdots & \vdots \\ (N-2)\Delta t & \langle x\rangle_{(N-2)\Delta t} \\ (N-2)\Delta t & \langle x\rangle_{(N-1)\Delta t} \\ 2\pi t & \langle x\rangle_{2\pi} \end{pmatrix}. \tag{5.15}$$

The time interval Δt was chosen to be equal to one-hundredth of a radian $0.01rad$, and the initial value of t_2 was arbitrarily chosen to be equal to zero. The time interval must be as small as possible, but the time needed in order to for the integral to be converging to a value was lengthy enough to restrict Δt from getting an even smaller value. Furthermore, the upper limit of integration in the formula was not equal to infinity but set to be equal to 4π since the value of the adjacent interval $t_r \in [4\pi,\infty)$ proved to be negligible. Responsible for this was the diffusion term $1/(\epsilon+it_r)^{3/2}$ in the integral. At this point of the process, it should be stressed out that the regularization constant ϵ was set to be equal $1/2I_p$ and was used in order to prevent a false overestimation of the integration. In the limit $t_r\to 0$, $\langle x\rangle_0\to 0$ (analytically) but in a numerical calculation process the limiting cases are not easily dealt with.

[6]For example, if $\vec{\mathcal{E}}=\vec{\mathcal{E}}_0\cos(\omega t)$, $\vec{p}(t;\vec{p}_0)=\vec{p}_0-(e\vec{\mathcal{E}}/\omega)\sin(\omega t)+(e\vec{\mathcal{E}}/\omega)\sin(\omega t_0)$. The last term corresponds to the drift momentum component which comes from the electric field.

After calculating the time dependent dipole moment list, I had to calculate its Fourier transform. This was done with the numerical integration of the interpolated dipole moment list multiplied with the complex exponential $e^{iq\tau}$ over the time interval $\tau \in [0, 2\pi]$. The data points of the list were connected/fitted with polynomials of first degree. In this way, we managed to have a continues approximation for the function of the time dependent dipole moment but not for its derivatives.

In order to test whether or not the results were reliable or not two tests were performed. The first one was whether the spectra were similar with the ones presented in the bibliography, [18], while the second one was to check whether the amplitudes of the even harmonics were negligible. Both of these tests had a positive answer and their results are presented below.

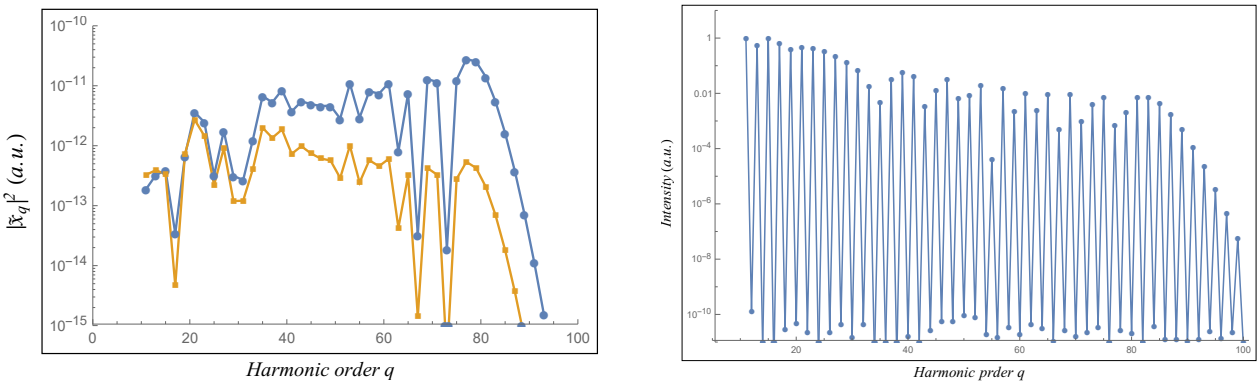

Figure 5.1: On the left panel, the harmonic spectra obtained for $I_p = 13.6$, $U_p = 20$, *and* $a = 2I_p$ for a simple sinusoidal pulse are presented. This spectrum is shown so that its comparison with the second Figure in reference [18] can verify the reliability of all the results presented in this thesis. For this panel only the odd harmonic components that have been evaluated and have been presented. On the right panel, the harmonic spectra obtained for $I_p = 14.4$, $U_p \approx 21$, *and* $a = 2I_p$ for a simple sinusoidal pulse are presented. This spectrum has been plotted, in order to demonstrate that the numerical evaluation of the harmonic amplitudes of even harmonics are negligible.

5.4.1 High (order) harmonic generation with the use of hydrogen like wavefunctions

The description of the HHG using a Gaussian wavefunction (eq. 4.28) was made in order to make the characteristics of the HHG easier to be distinguished. For a better description of the HHG spectra, the wavefunction of the harmonic oscillator can be replaced by the ground state's wavefunction of a hydrogen-like atom[7]

$$\psi = \left(\frac{a^{3/4}}{\sqrt{\pi}}\right) e^{-\sqrt{a}r}, \qquad a = 2I_p. \tag{5.16}$$

with the corresponding dipole matrix elements being proportional to

$$\langle \vec{p} \,|x|g\rangle = i\left(\frac{2^{7/2}a^{5/4}}{\pi}\right)\frac{\vec{p}}{(p^2+a)^3}. \tag{5.17}$$

In Fig. 5.2 the harmonic spectra using the dipole matrix elements corresponding to a ground hydrogen-like wavefunction, for the cases of $\gamma = 0$, $\gamma = 0.5$ with $\varphi = 0°$ and $\varphi = 121.5°$ are shown. In all spectra,

[7] In S.I. units, the Bohr radius and the *Rydberg* constant are equal to $a_0 = \frac{4\pi\varepsilon_0\hbar^2}{m_e e^2}$ and $Ryd = \frac{m_e e^4}{8\varepsilon_0^2 h^2}$ respectively. So $a_0^2 = \frac{\hbar^2}{2m_e}\frac{1}{Ryd} = \frac{\hbar^2}{2m_e}\frac{1}{I_p^{(H)}} \xrightarrow[\hbar=m_e=1]{\text{A.U.}} \frac{1}{2I_p^{(H)}} \xrightarrow[\text{ionization potential}]{\text{Generalizing for any}} \frac{1}{2I_p}$. Thus $\psi_{100}^{(H)} \propto e^{-r/a_0} \xrightarrow[\text{Generalization}]{\text{A.U.}} e^{-\sqrt{2I_p}r}$

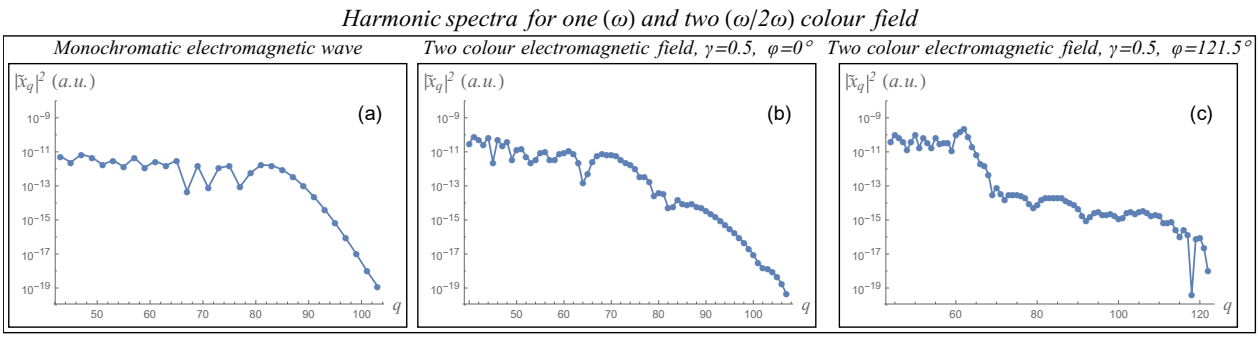

Figure 5.2: Plot of the normalized harmonic spectra obtain from the exposure of a Neon atom ($I_p = 14.4\hbar\omega$) in two colour field ($\omega/2\omega$). γ is the ratio of the electric field strengths $\mathcal{E}_{2\omega}/\mathcal{E}_{\omega}$ and φ is the phase difference of the two colours in the moment $t = 0$. The fundamental frequency of the laser field corresponds to ($825nm$) ($\hbar\omega \approx 1.5eV$) and its intensity for both cases is equal to $\mathcal{I} = 5 \times 10^{14} W/cm^2$.

the characteristics discussed above are present. However, due to the different form of the dipole matrix elements, the interferences have changed, the intensity magnitude has been increased by almost an order and a decreasing term seems to have been added to the mean value of the spectra in each plateau. This is happening because, in this case, the region in which the dipole matrix element takes significant values is strongly localized around the $p = \sqrt{a/5}$ value, resulting in a limited probability amplitude of a returning electron with high kinetic energy to recombine with the parent ion (III term in eq. 4.4b and eq. 4.15). It should also be emphasized that in both cases of $\gamma = 0.5$, the mean value of the intensity in the first plateau is greater than the mean value in the plateau of the harmonic spectra produced solely by the ω laser field, which is something not so unexpectable since the total intensity in the case of $\gamma = 0.5$ ($\mathcal{I} \propto \mathcal{E}^2(1 + 0.45^2)$) is greater that the intensity of in the case of $\gamma = 0$ ($\mathcal{I} \propto \mathcal{E}^2$). Nevertheless, it should also be noted that the intensity in the case of $\varphi = 121.5°$ is greater than the intensity on the case of $\varphi = 0°$. This quantitative characteristic, is something that cannot be attributed to the total intensity of the laser but to the phase difference φ between the two colours of the laser at $t = 0$.

Bibliography

[1] L. V. Keldysh, "Ionization in the field of a strong electromagnetic wave", Sov. Phys. JETP, vol. 20, pp. 1307, 1965

[2] F. A. Ilkov, J. E. Decker, and S. L. Chin, "Ionization of atoms in the tunnelling regime with experimental evidence using Hg atoms", J. Phys. B, vol. 25, pp. 4005, 1992.

[3] A. M. Perelomov, V. S. Popov, and M. V. Terentev, Zh. Eksp. Teor. Fiz. 50, 1393 (1966) [Sov. Phys. JETP 23, 924 (1966)].

[4] P. B. Corkum, "Plasma Perspective on Strong-Field Multiphoton Ionization", PACS numbers: 32.80.Rm

[5] D. N. Fittinghoff et al. , Phys. Rev. Lett. 69, 2642 (1992).

[6] M. V. Ammosov, N. B. Delone, and V. P. Krainov, Zh. Eksp. Teor. Fiz. 91, 2008 (1986) [Sov. Phys. JETP B4, 1191 (1986)].

[7] L. D. Landau and E. M. Lifshitz, Quantum Mechanics, 3rd. Ed. Pergamon, 1978

[8] McPherson, A. et al. Studies of multiphoton production of vacuum-ultraviolet radiation in the rare gases. J. Opt. Soc. Am. B 4, 595 (1987).

[9] Kenichi L. Ishikawa, "High-Harmonic Generation", The University of Tokyo

[10] G G Paulus, W Becker, W Nicklich and H Walther, "Rescattering effects in above threshold ionization: a classical model", Journal of Physics B: Atomic, Molecular and Optical Physics

[11] T. Endo, H. Fujise, Y. Kawachi "Selective bond breaking of CO2 in phase-locked twocolor intense laser fields: laser field intensity dependence, PCCP Issue 5, 2017

[12] E. Kechaoglou, S. Kaziannis and C. Kosmidis, "Controlling intramolecular hydrogen migration by asymmetric laser fields: the water case" Issue 21, 2019, PCCP

[13] Li, X. F.; L'Huillier, A.; Ferray, M.; Lompre, L. A.; Mainfray, G. (1989). "Multiple-harmonic generation in rare gases at high laser intensity". Physical Review A. 39 (11): 5751–5761.

[14] Burnett, N. H.; et al. (1977). "Harmonic generation in CO2 laser target interaction". Appl. Phys. Lett. 31 (3): 172–174.

[15] Tong X. M. and Lin C. D. 2005 J. Phys. B 38 2593

[16] P. B. Corkum, Phys. Rev. Lett. '7l, 1995 (1993).

[17] S. E. Harris *et al.*, Opt. Commun. 100, 487 (1993); G. Farkas and C. Toth, Phys. Lett. A 168, 447 (1992).

[18] M. Lewenstein, Ph. Balcou, M. Yu. Ivanov, Anne L' Huillier and P. B. Corkum Phys. Rev. A 49, 2117 (1994)

[19] J. Marcus Dahlström, *Strong Field Approximation for High Order Harmonic Generation with $\omega/2\omega$ Laser Fields*, Lund Reports on Atomic Physics, LRAP-381 Lund, June 2007

[20] M. Y. Ivanov and K. Rzazewski, J. Mod. Phys. 39, 2377 (1992).

[21] M. V. Ammosov, N. B. Delone, and V. P. Krainov, Zh. Eksp. Teor. Fiz. 91, 2008 (1986) [Sov. Phys. JETP B4, 1191 (1986)].

[22] N. B. Delone and V. P. Krainov, J. Opt. Soc. Am. B 8, 1207 (1991).

[23] V. P. Krainov and V. M. Risfic, Zh. Eksp. Teor. Fiz. 101, 1479 (1992) [Sov. Phys. JETP 74, 789 (1992)].

[24] P. Antoine, A. L'Huillier, and M. Lewenstein, Phys. Rev. Lett. 77, 1234 (1996)

[25] A. L'Huillier, M. Lewenstein, P. Salieres, and Ph. Balcou, Phys. Rev. A 48 R3433 (1993)

[26] A. Iqbal, K. Humayun, S. Maqsood, S. Jawaid, A. Ahmad2 , A. Ur Rahman , B. A. Bacha Chin. Phys. B 28, 023201 (2019)

[27] D. W. Schumacher, P. H. Bucksbaum Phys. Rev. A 54, 5 (1996)

[28] S. L. CHIN and P. LAMBROPOULOS, Multiphoton Ionization of Atoms, ACADEMIC PRESS, 1984

[29] Carelli, F.; Fedus, K.; Karwasz, G. Total Cross Sections for Electron and Positron Scattering on Molecules: In Search of the Dispersion Relation. Atoms 2021, 9, 97. https://doi.org/10.3390/atoms9040097

[30] C. Z. Bisgaard and L. B. Madsen, "Tunneling ionization of atoms", American Journal of Physics 72, 249 (2004).

[31] F. S. CRAWFORD Jr., Prof. of Physics, Univ. of California,Berkley